Volcanisme intraplaque

Point chaud
OIB / LIP / RIFT

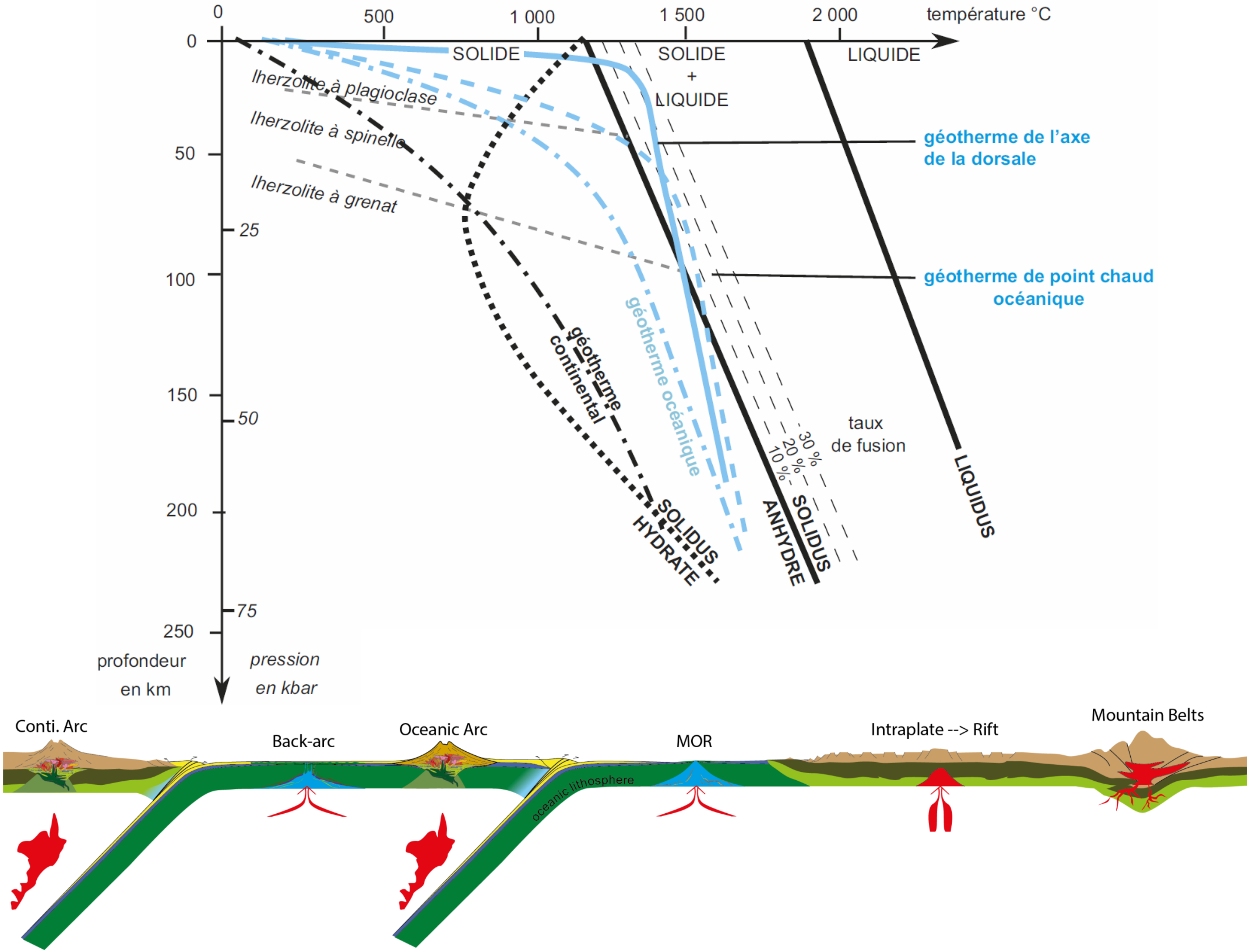

température °C
0
500
1 000
1 500
2 000
SOLIDE
SOLIDE + LIQUIDE
LIQUIDE
lherzolite à plagioclase
lherzolite à spinelle
lherzolite à grenat
géotherme de l'axe de la dorsale
géotherme de point chaud océanique
géotherme continental
géotherme océanique
SOLIDUS HYDRATE
SOLIDUS ANHYDRE
LIQUIDUS
taux de fusion
10 %
20 %
30 %
0
50
100
150
200
250
25
50
75
profondeur en km
pression en kbar
Conti. Arc
Back-arc
Oceanic Arc
MOR
Intraplate --> Rift
Mountain Belts
oceanic lithosphere

French 2015

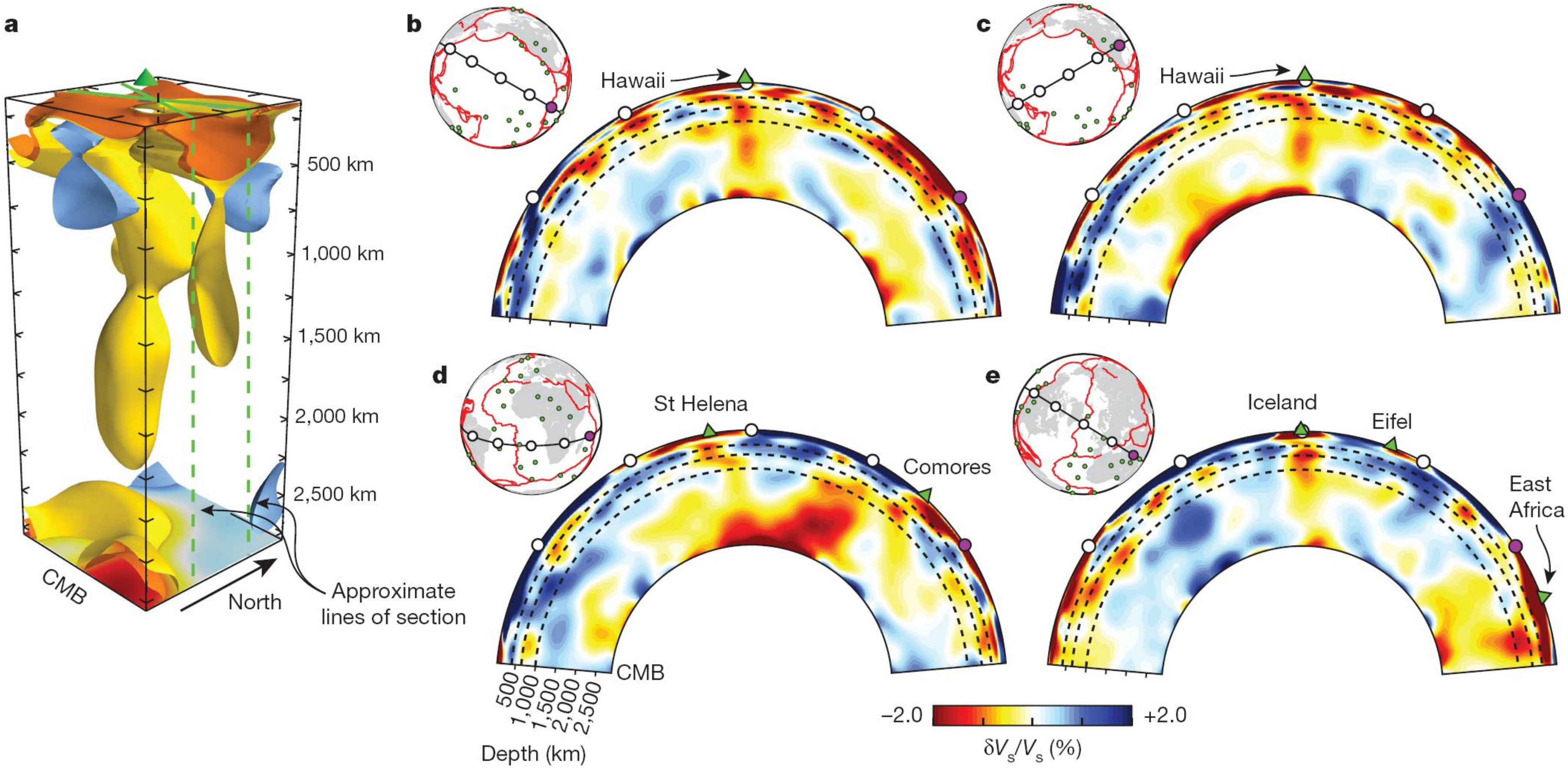

Figure 3 | Hawaii, Iceland, St Helena and the African superplume. a, Three-dimensional rendering of the Hawaiian plume, viewed from the southeast. In the lower mantle, the plume conduit is vertically oriented, rooted in a patch of very low V_s at the base of the mantle, with a weak zone in the depth range 2,300–2,600 km. Above approximately 1,000 km, the conduit is deflected towards the west into the transition zone, and appears to interact with the low-velocity finger oriented in the Pacific plate absolute plate motion direction[21] visible in cross-section above a depth of 500 km. **b**–**e**, Two-dimensional vertical cross-sections along planes as indicated in the inset maps and corresponding broken green lines in **a**, represented in the same way as in Fig. 1. In **c**, in the lowermost mantle between the two westernmost reference white dots, we see the edge of the plume associated with the Caroline hotspot. Subduction zones are well imaged in the western Pacific (**b**, **c**), spreading above the 1,000-km horizon, and in south America (**d**); in **c** and **e**, the fossil Farallon subduction extends through the lower mantle. Blue zones in the vicinity of Hawaii in the lower mantle may potentially be downwellings corresponding to other fossil slabs, although this warrants further study. In **e**, we note the particularly broad African plume, one lobe of which extends to the mantle transition zone, the other giving rise in the mid lower mantle to a thinner, weaker plume beneath St Helena.

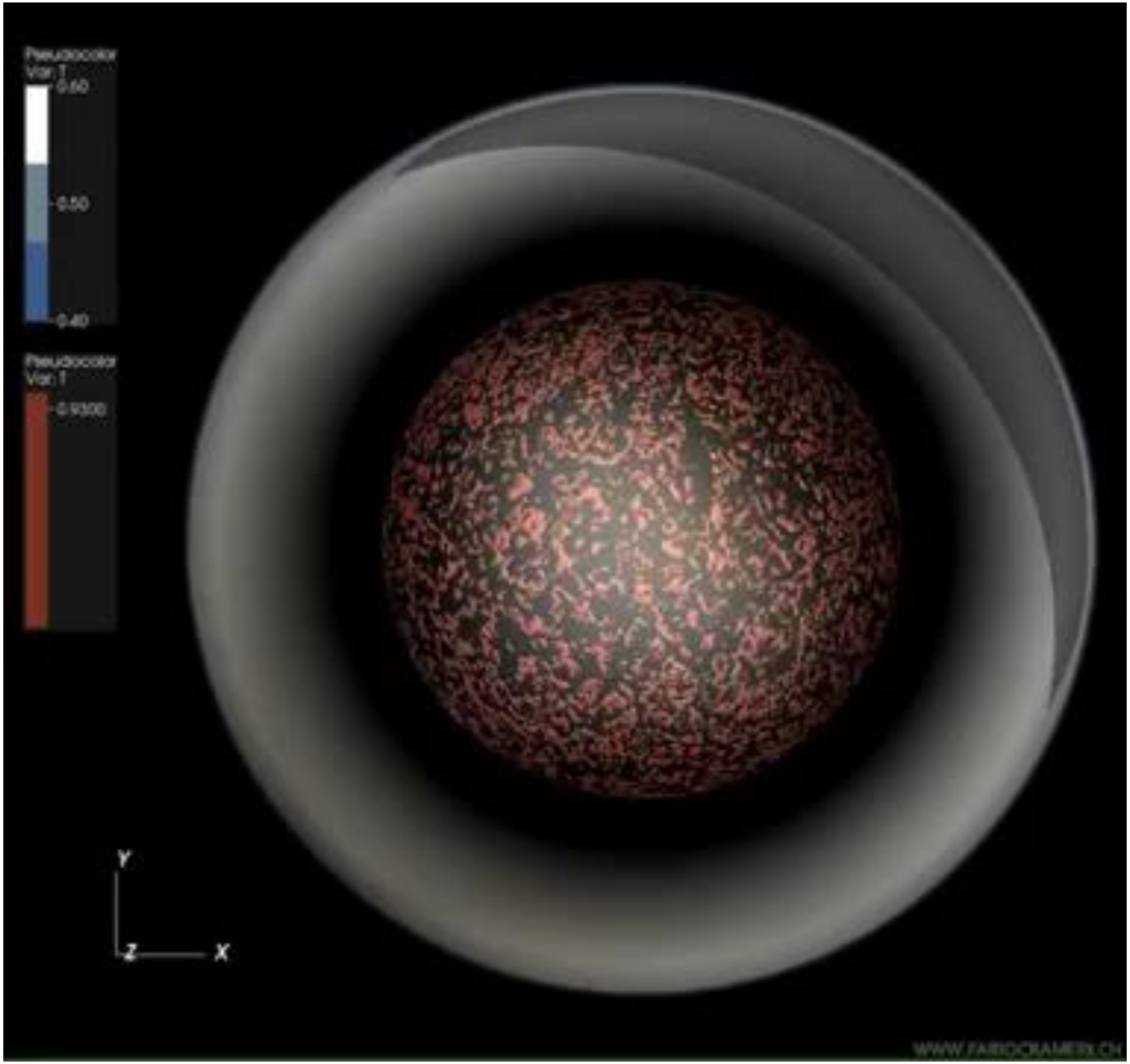

https://www.youtube.com/watch?v=iZPIk8-ABvM

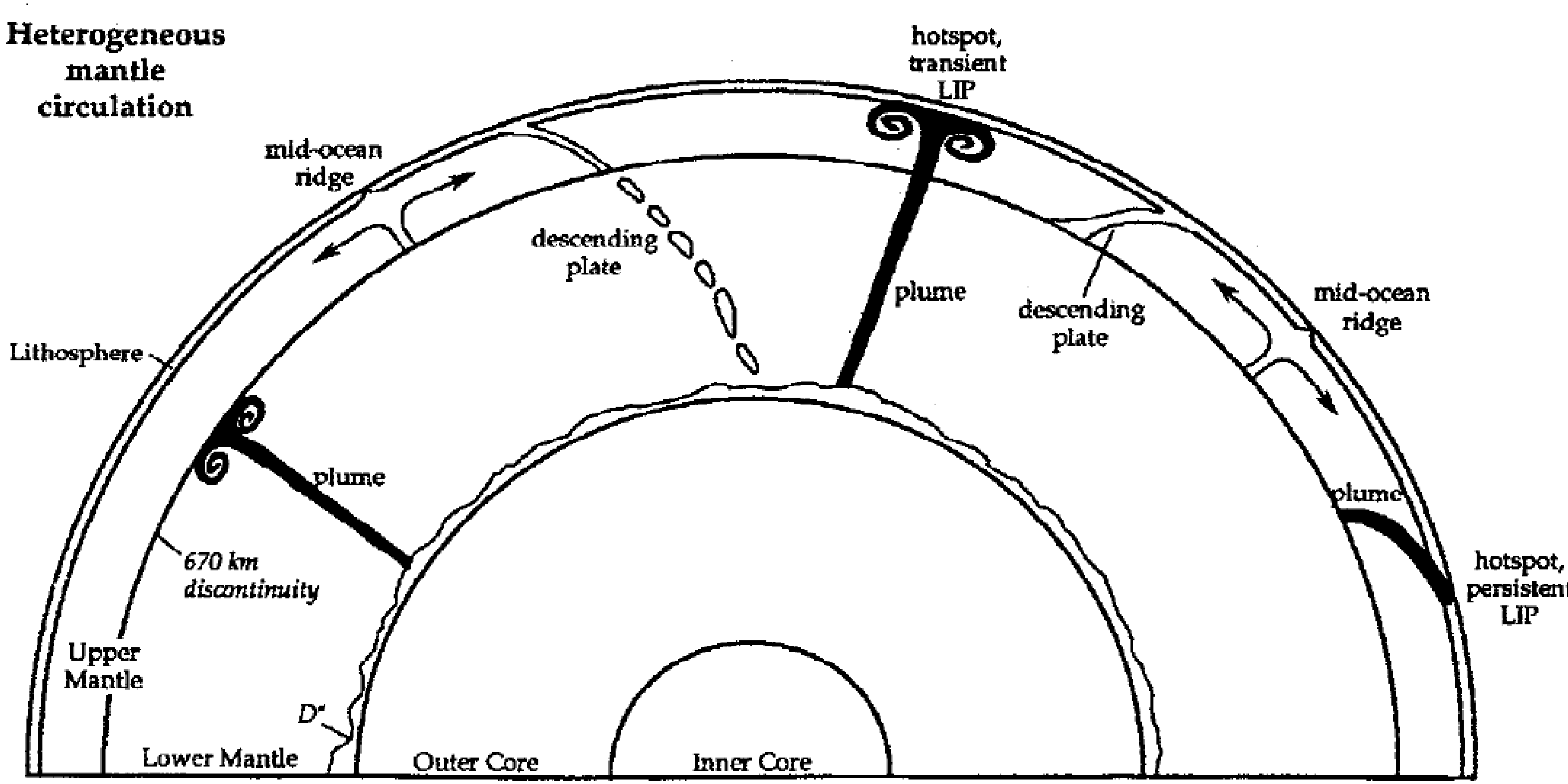

Débat sur l'ancrage des points chaud et des modèles de convection à une ou deux couches

Expression des points chaud multiples:

→ LIP → Principalement Basaltes (Q-ol) Tholeitique

→ OIB → Principalement Basaltes (Q-ol) Tholeitique + Alc

→ RIFT → Grande diversité Thol / Alc / Carb …

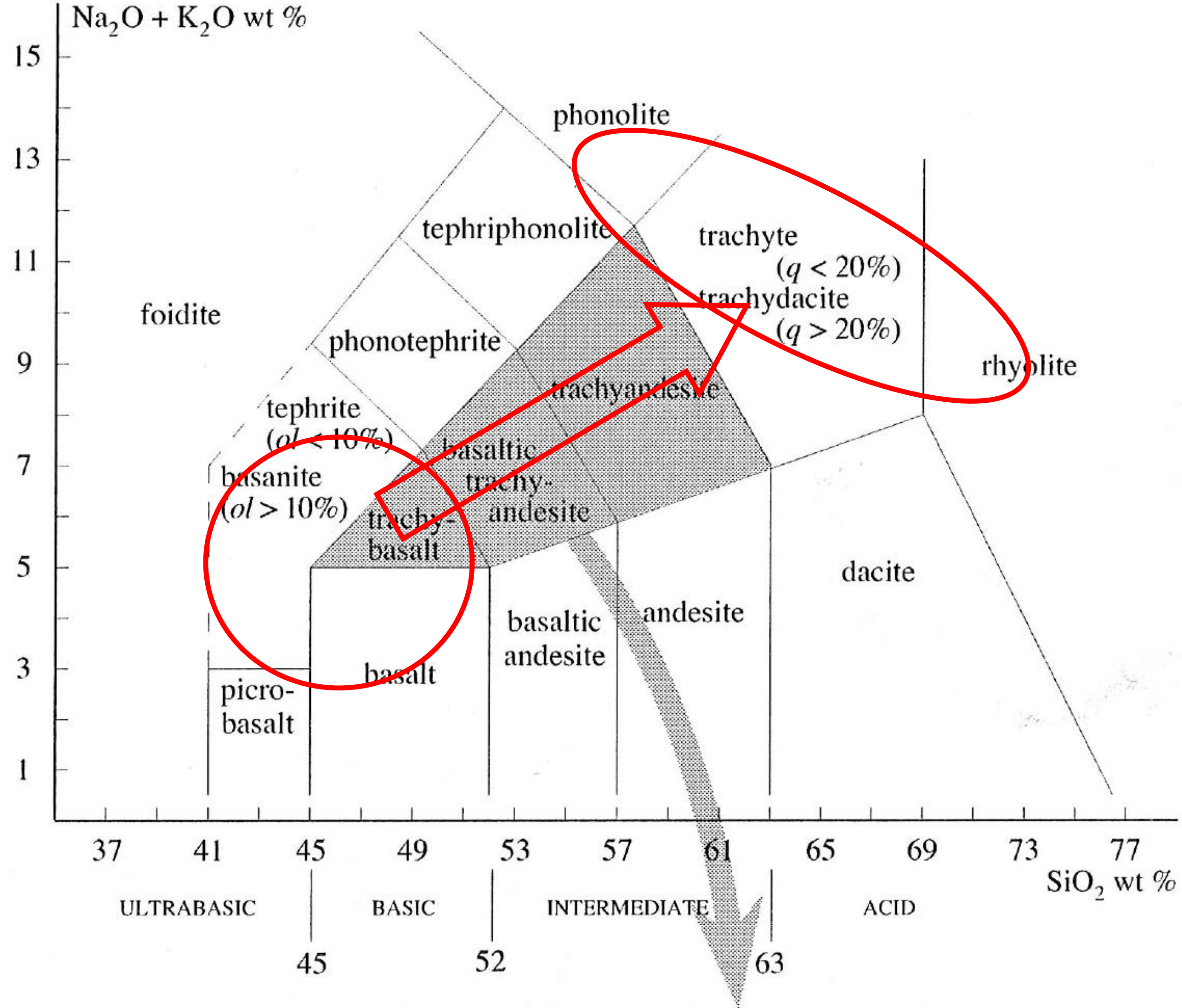

Further subdivisions of shaded fields	trachybasalt	basaltic trachyandesite	trachyandesite
$Na_2O - 2.0 \geq K_2O$	hawaiite	mugearite	benmoreite
$Na_2O - 2.0 < K_2O$	potassic trachybasalt	shoshonite	latite

A

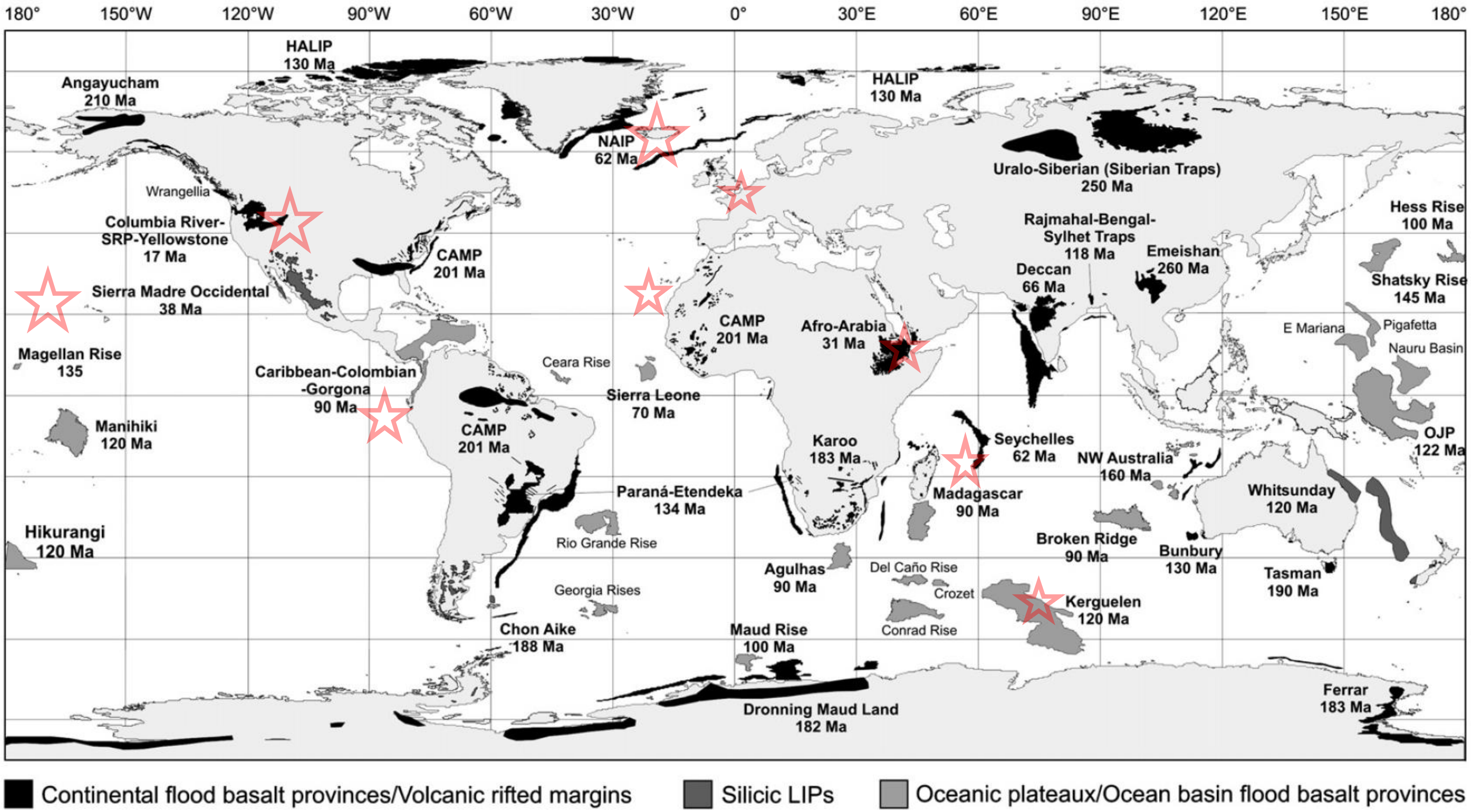

☆(Quelques) Point chaud (Hot-Spots) Actuels

Fig. 4. Revised global distribution of Large Igneous Provinces. A) LIP events from 0–275 Ma, updated and revised from the PLATES project database and map (Institute of Geophysics, University of Texas, Austin). Map excludes seamount groups, submarine ridges and anomalous seafloor-spreading crust that have previously been considered LIPs by Coffin and Eldholm (1992, 1994, 2001, 2005). Interpreted remnants of Mesozoic oceanic plateaus accreted around the Pacific margins (Sorachi, Japan; western Cordillera of Colombia and Ecuador; Cache Creek, Canada) are not shown because of the lack of detailed information on their original areal extent, volume and duration. Annotated ages denote the onset of the main phase or first pulse of magmatism to the LIP event; note that some LIPs have precursor magmatism at lower intensity up to 10 Myr prior. Some LIPs are shown in small typeface to aid in figure clarity. Abbreviations: CAMP, Central Atlantic Magmatic Province; HALIP, High Arctic Large Igneous Province; NAIP, North Atlantic Igneous Province; OJP, Ontong Java Plateau. B) LIP events from 275–550 Ma. The inferred extent of each LIP event is shown by a dashed line, and many remain poorly mapped and studied. The number of well-defined LIP events (in terms of area, volume, duration and setting) is much reduced (in comparison with the younger record) no examples of accreted oceanic LIPs have been recorded for this period, which generally corresponds to Gondwanaland assembly.

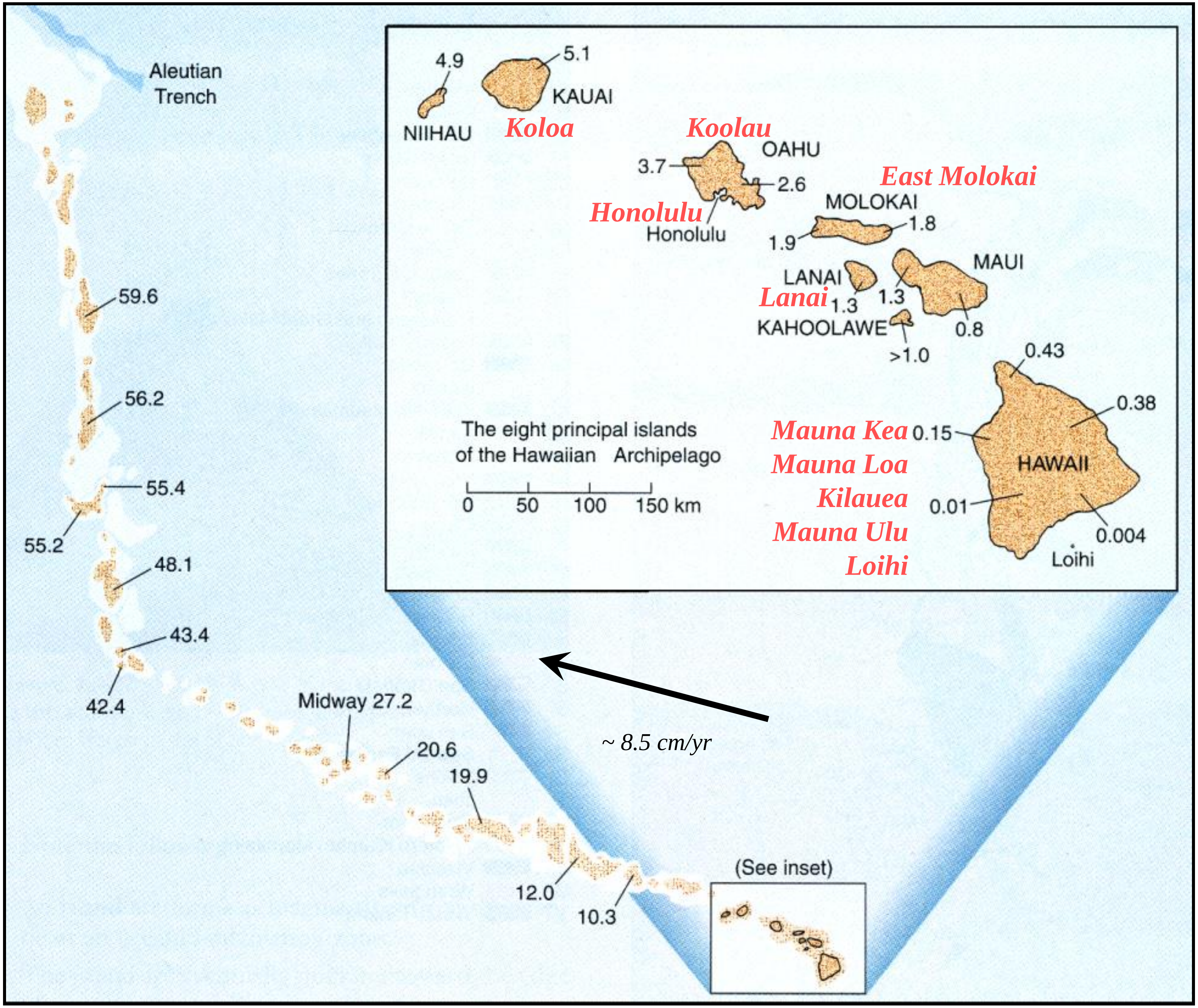
Aleutian Trench
59.6
56.2
55.4
55.2
48.1
43.4
42.4
Midway 27.2
20.6
19.9
12.0
10.3
(See inset)
~ 8.5 cm/yr
4.9
5.1
KAUAI
NIIHAU
Koloa
Koolau
OAHU
3.7
2.6
East Molokai
MOLOKAI
Honolulu
Honolulu
1.9
1.8
LANAI
MAUI
Lanai
1.3
1.3
KAHOOLAWE
0.8
>1.0
0.43
0.38
The eight principal islands of the Hawaiian Archipelago
0 50 100 150 km
Mauna Kea
0.15
Mauna Loa
HAWAII
Kilauea
0.01
Mauna Ulu
0.004
Loihi
Loihi

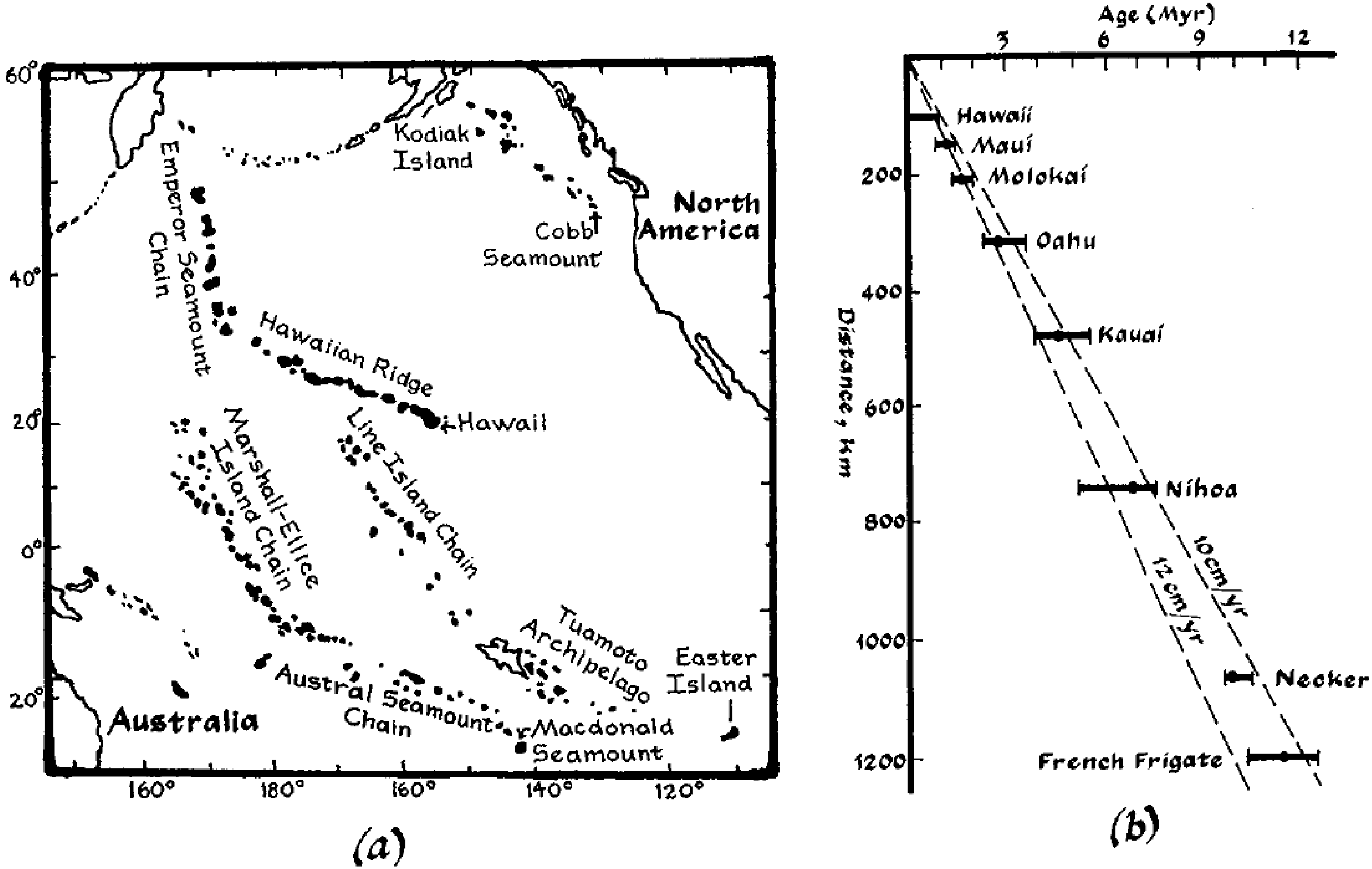

Figure 8-12 (a) Chains of volcanic islands and seamounts in the central Pacific. (b) Relationship between ages of the volcanoes of the Hawaiian Emperor Seamount Chain and distance from the hotspot near the island of Hawaii. (Adapted from G. B. Dalrymple, E. A. Silver, and E. D. Jackson, 1973, *Amer. Sci.* 61:294–308.)

OIB / Hawaiian Volcanism

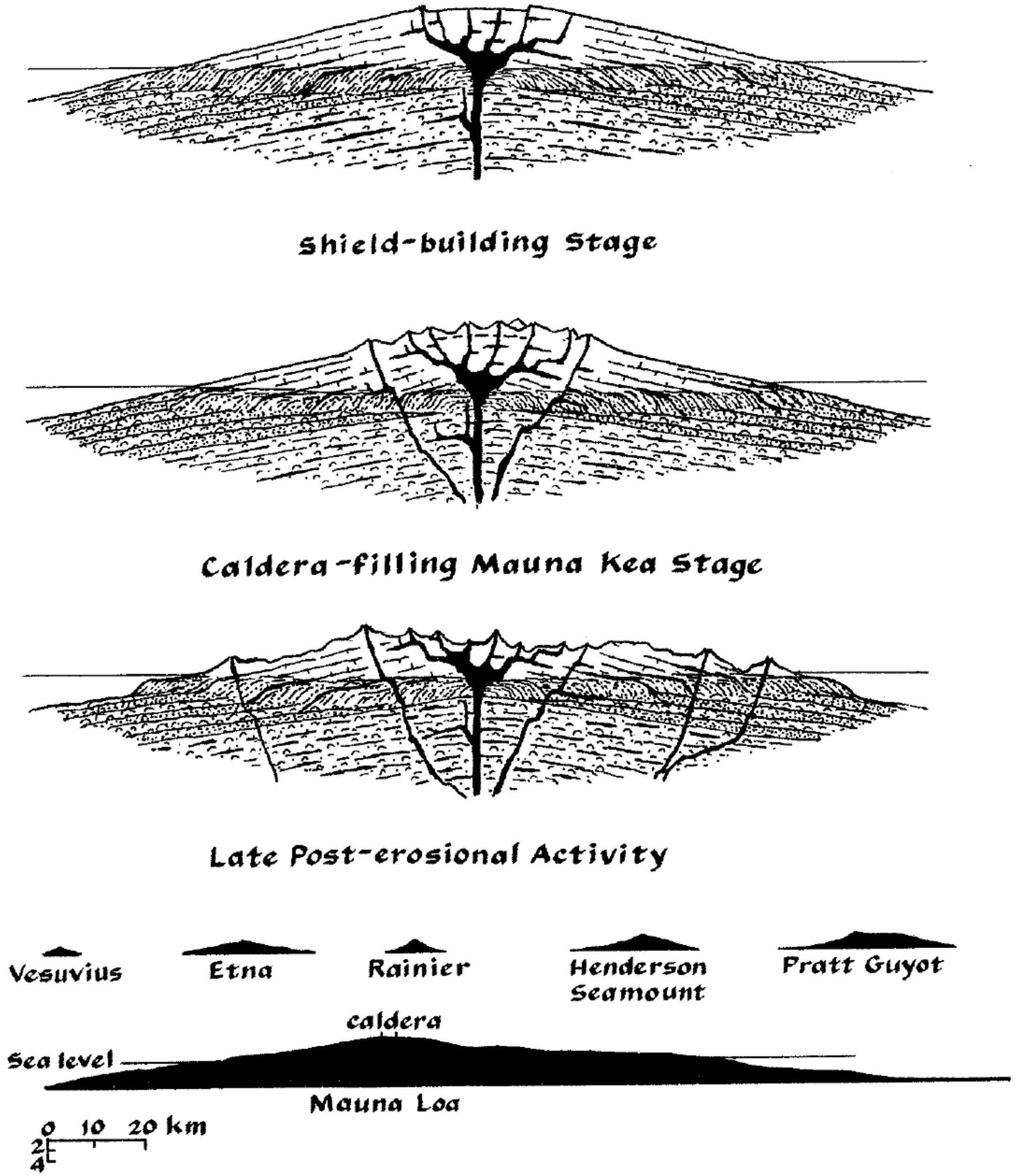

Figure 8-13 Stages of evolution of the Hawaiian volcanoes. The initial shield-building stage is followed by a period in which the caldera is filled and small vents break out in the summit region. Later, after an interval of erosion, a final stage is characterized by small eruptions of very alkaline magmas, mainly on the lower slopes. The enormous size of the volcanoes can be appreciated by comparing a profile through Mauna Loa with others, such as Etna, the largest continental volcano.

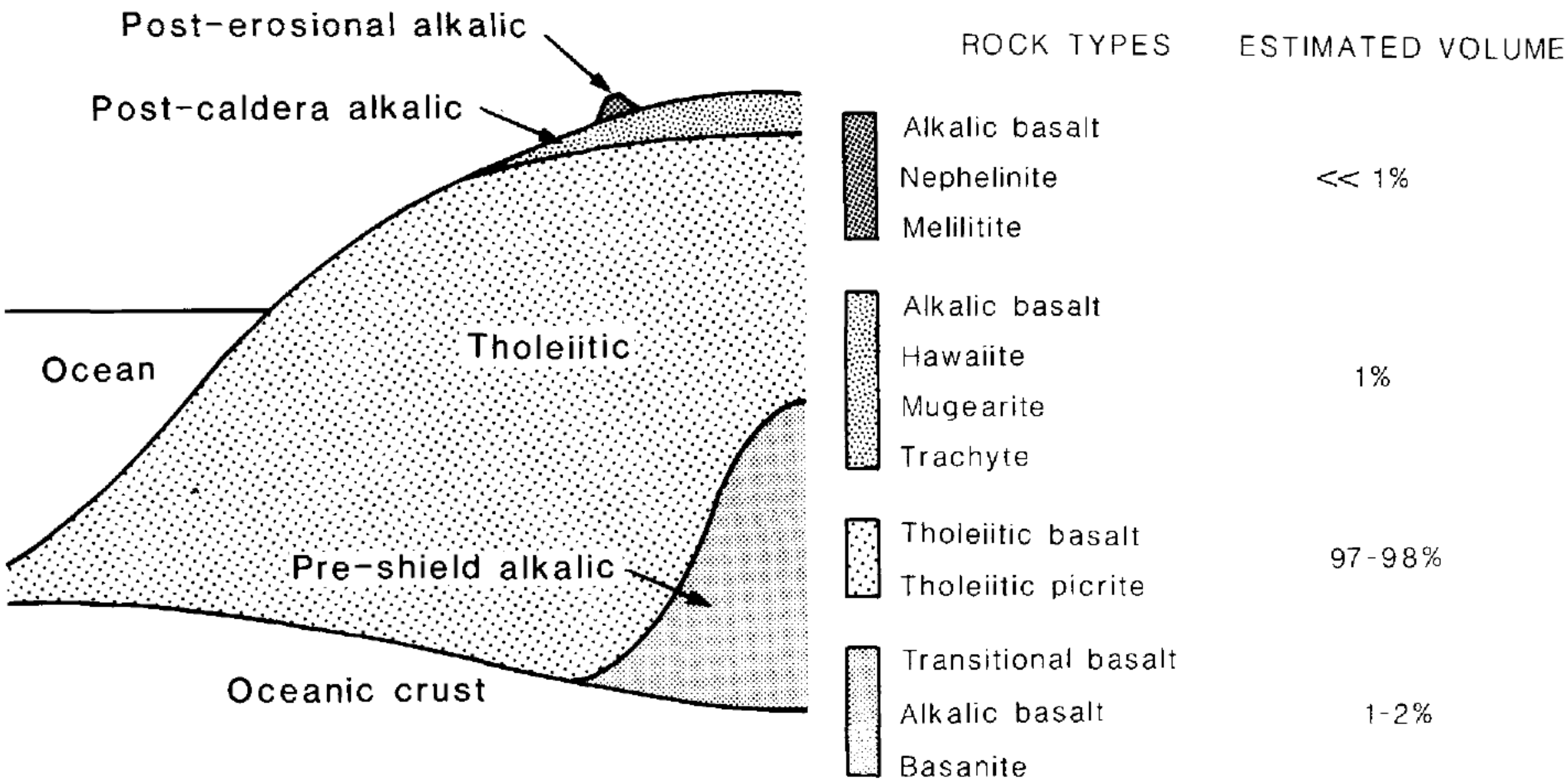

FIG. 3. Cross-section through a hypothetical Hawaiian volcano showing the age and volume relations of the four eruptive stages. The main rock types and their relative volumes are also shown.

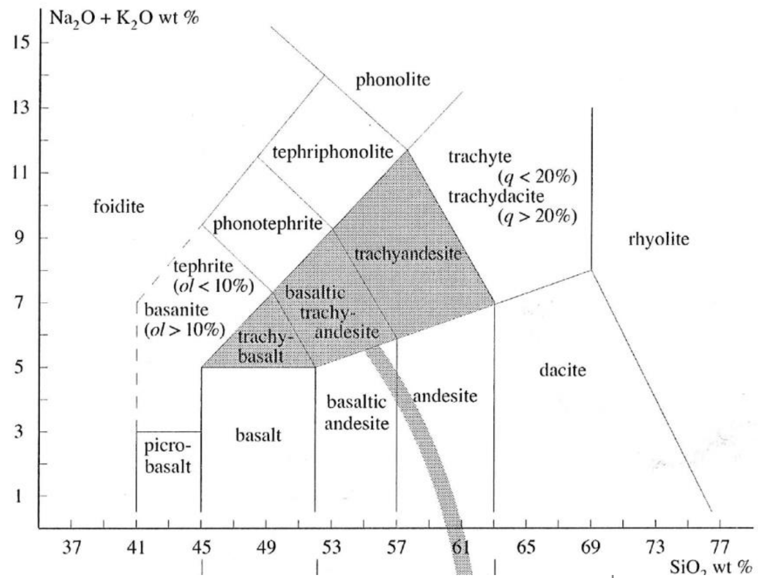

Further subdivisions of shaded fields	trachybasalt	basaltic trachyandesite	trachyandesite
$Na_2O - 2.0 \geq K_2O$	hawaiite	mugearite	benmoreite
$Na_2O - 2.0 < K_2O$	potassic trachybasalt	shoshonite	latite

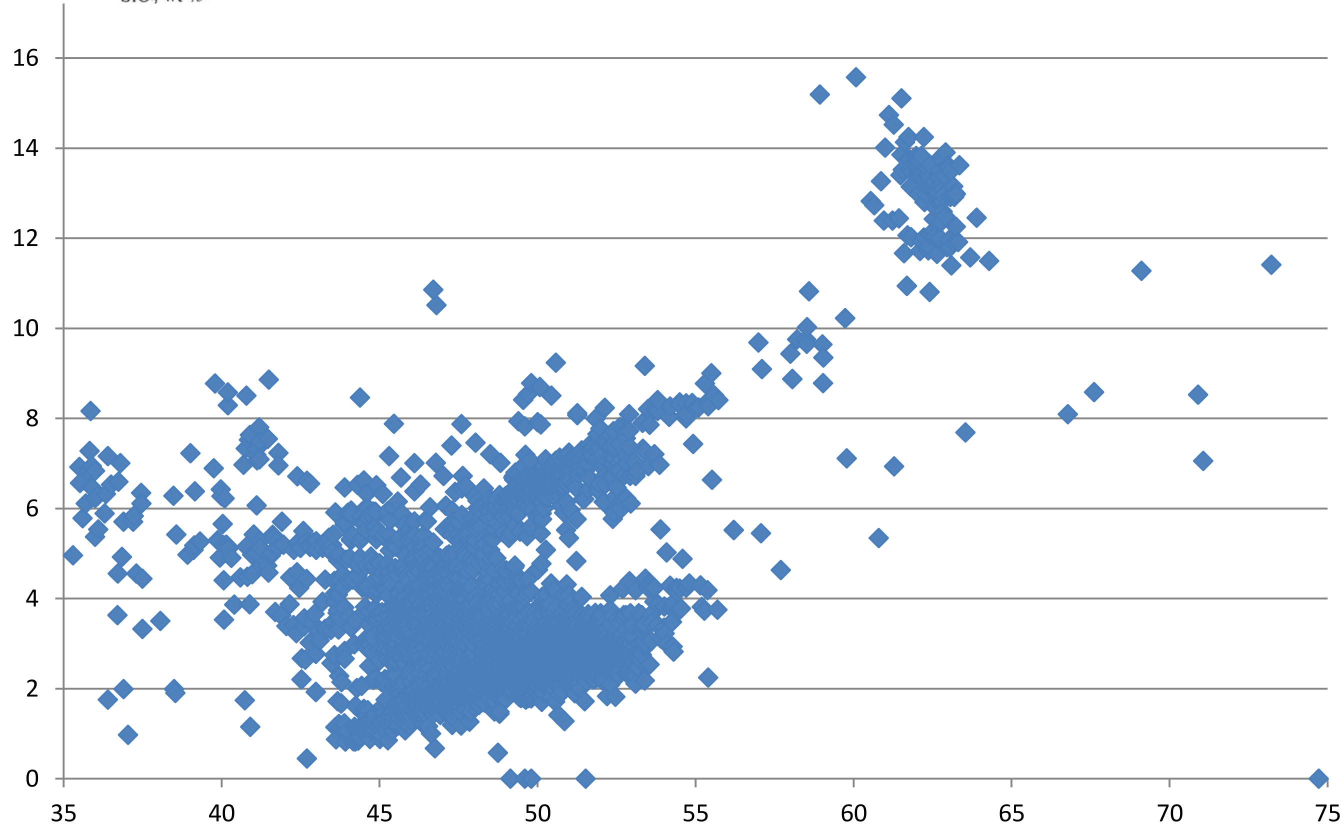

Suite Tholeitiique : *Kilauea, Mauna Ulu, Mauna Loa, Lanai, Koolau (Oahu)*

Oceanite (picrite) → **Ol-tholeiite** → **Qtz-tholeiite**

Suite Tholeiitique constitue ~98% des laves d'Hawaii

Olivine = phenocryst dominant → controle differentiation

Puis Cpx (Augite)

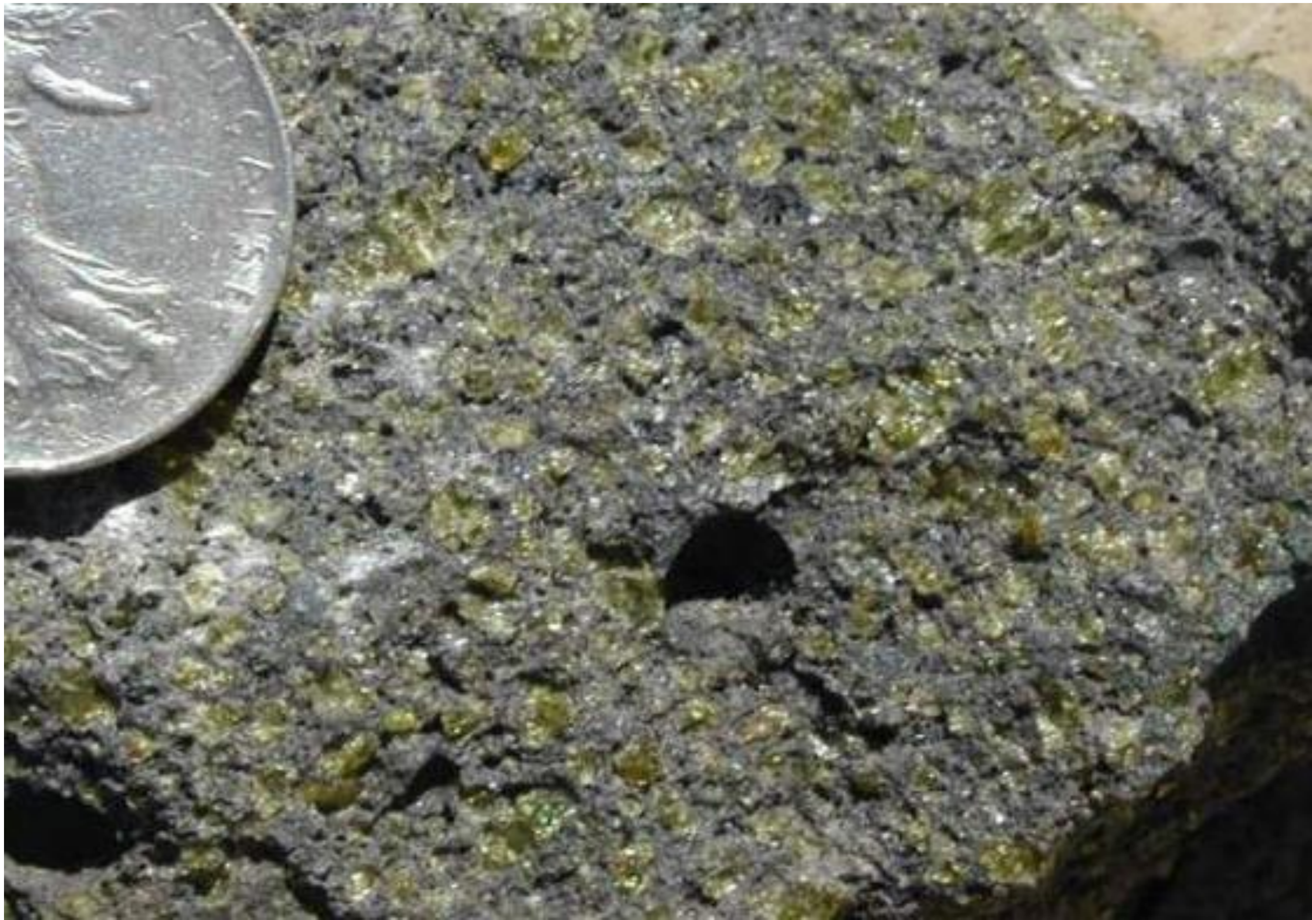

Suite Alcaline: *East-Molakai, Mauna Kea*

ankaramite → **AOB** (labradorite) → **hawaiite** (andesine) → **mugearite** (oligoclase) → **benmoreiite** → **trachyte**

Suite Alcaline → ~2 % of Hawaiian lavas.

Olivine / clinopyroxene (MgO > 10 wt.%): phenocrysts (Lave primitive: ankaramite)

Olivine / Augite / K-spar groundmass

Further subdivisions of shaded fields	trachybasalt	basaltic trachyandesite	trachyandesite
$Na_2O - 2.0 \geq K_2O$	hawaiite	mugearite	benmoreite
$Na_2O - 2.0 < K_2O$	potassic trachybasalt	shoshonite	latite

Post-Erosional Suite (0,1 %): *Honolulu Series, Oahu, and Koloa Series, Kauai*

A.O.B	**basanite**	**nephelinite**	**mellilitite**
(≤ 5% norm Ne)	(≥ 5% norm Ne)	(≥ 15% norm Ne)	(≥ 15% norm Me)
(modal feldspathoid)	(no modal plag)	(modal mellilite)	

Primitive with high Mg contents.

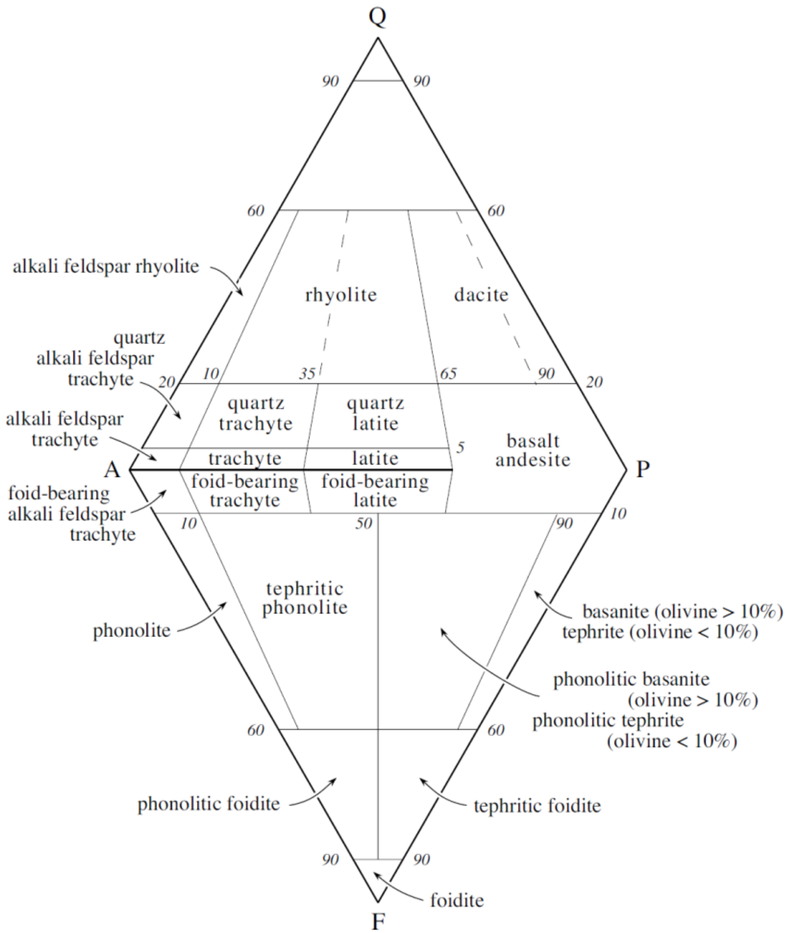

Fig. 2.11. QAPF modal classification of volcanic rocks (based on Streckeisen, 1978, Fig. 1). The corners of the double triangle are Q = quartz, A = alkali feldspar, P = plagioclase and F = feldspathoid. This diagram must not be used for rocks in which the mafic mineral content, M, is greater than 90%.

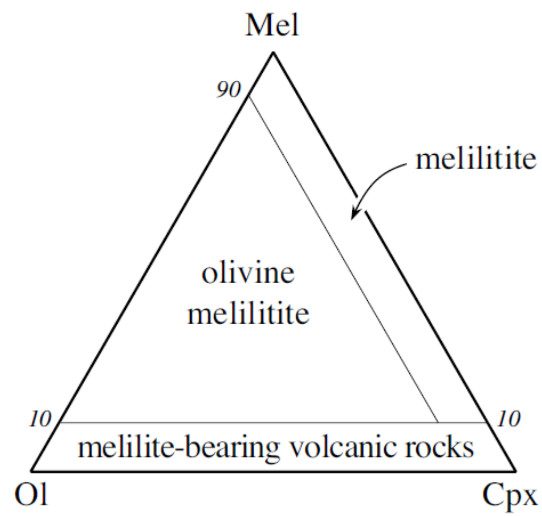

Fig. 2.3. Modal classification of volcanic rocks containing melilite (after Streckeisen, 1978, Fig. 5) based on the values of melilite (Mel), olivine (Ol) and clinopyroxene (Cpx).

Green 1967

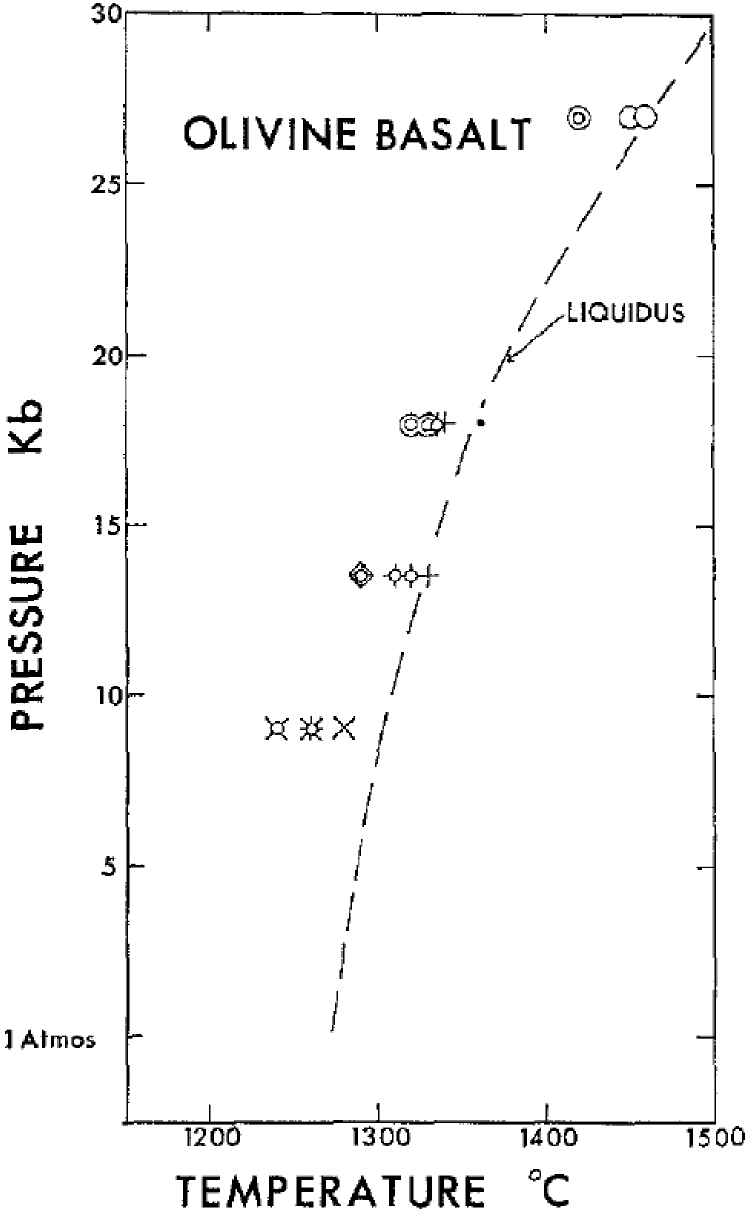

OLIVINE BASALT
LIQUIDUS
PRESSURE Kb
30
25
20
15
10
5
1 Atmos
1200
1300
1400
1500
TEMPERATURE °C

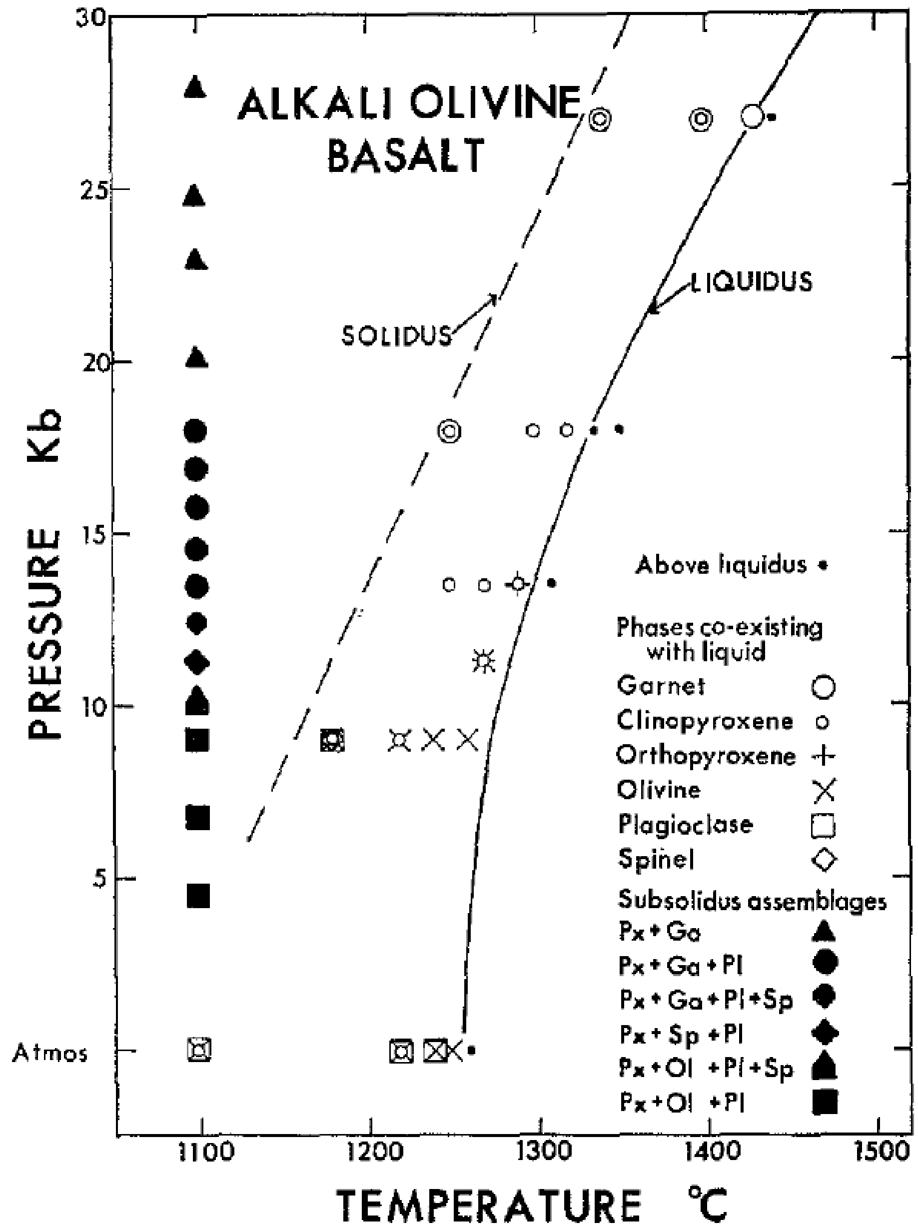

ALKALI OLIVINE BASALT
SOLIDUS
LIQUIDUS
PRESSURE Kb
30
25
20
15
10
5
Atmos
1100
1200
1300
1400
1500
TEMPERATURE °C
Above liquidus •
Phases co-existing with liquid
Garnet
Clinopyroxene
Orthopyroxene
Olivine
Plagioclase
Spinel
Subsolidus assemblages
Px + Ga
Px + Ga + Pl
Px + Ga + Pl + Sp
Px + Sp + Pl
Px + Ol + Pl + Sp
Px + Ol + Pl

Hawaiian tholeiites enrichies en incompatibles / MORB, + spectre convex typique

LILE !! → Phases hydratée residuelle (Anph / Phlogopite)

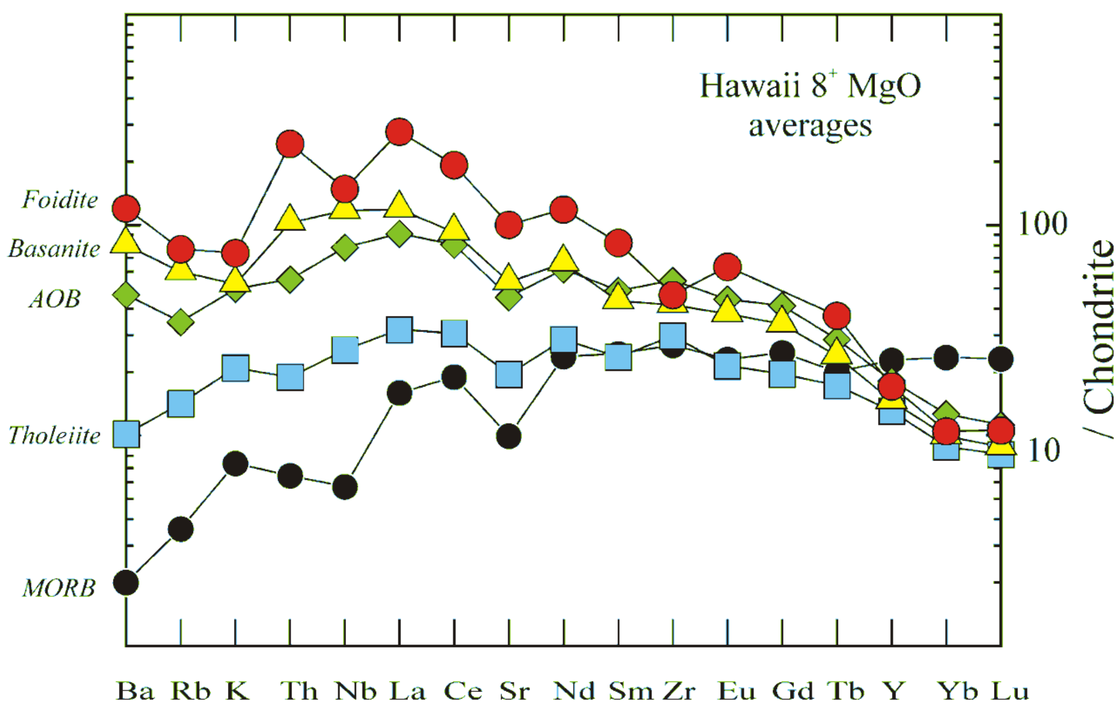

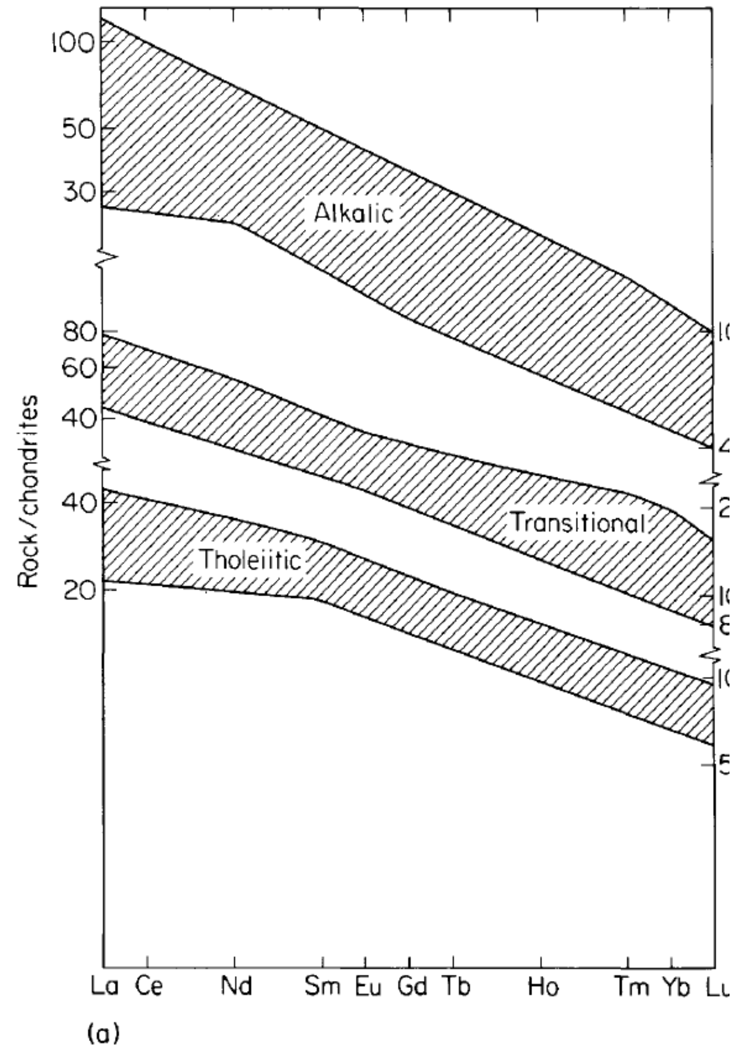

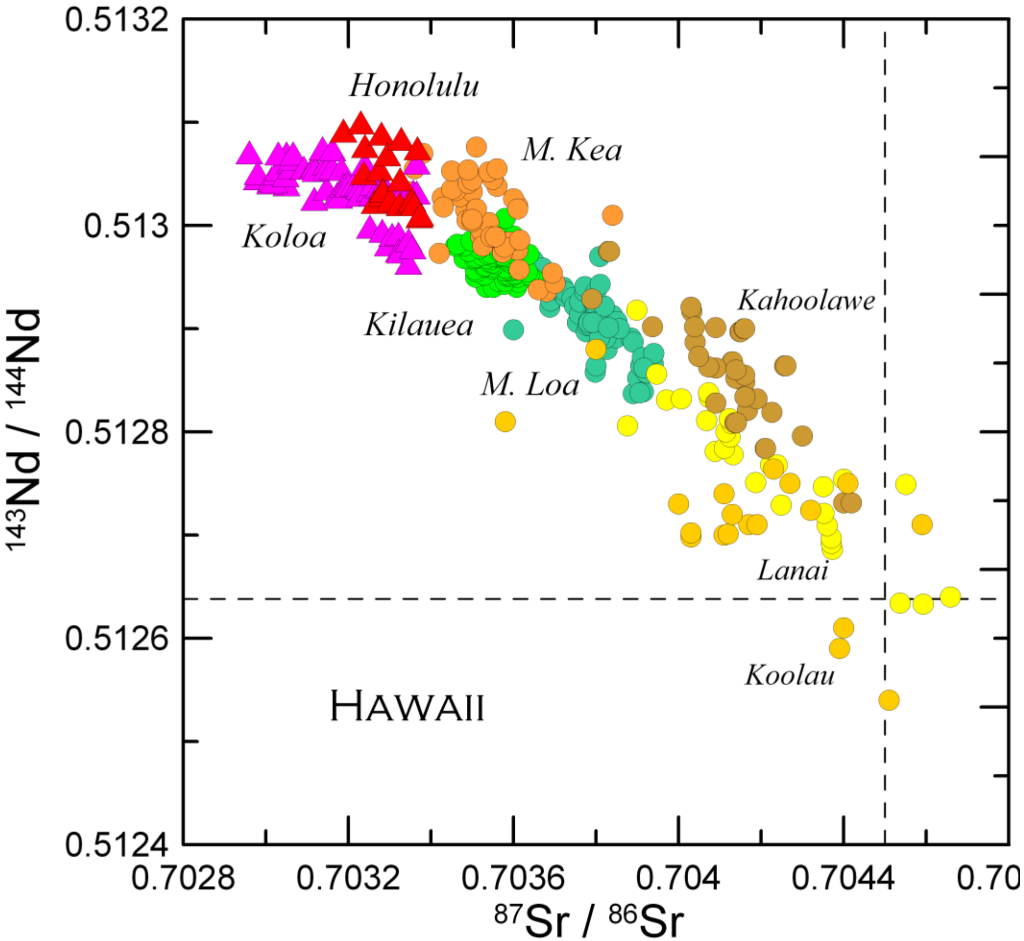

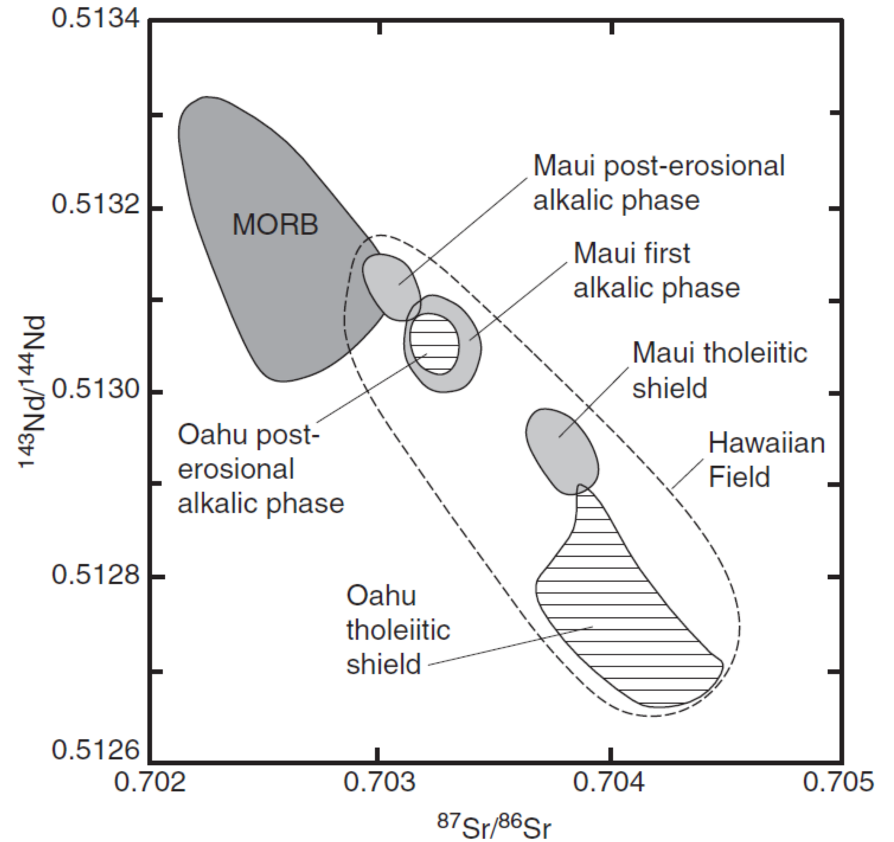

FIGURE 21 $^{143}Nd/^{144}Nd$ versus $^{87}Sr/^{86}Sr$ for Maui and Oahu Hawaiian early tholeiitic shield-building and, later, alkaline lavas. From Wilson (1989). Copyright © by permission Kluwer Academic Publishers.

Source des OIB:

Manteau contaminé

Chaque OIB est different

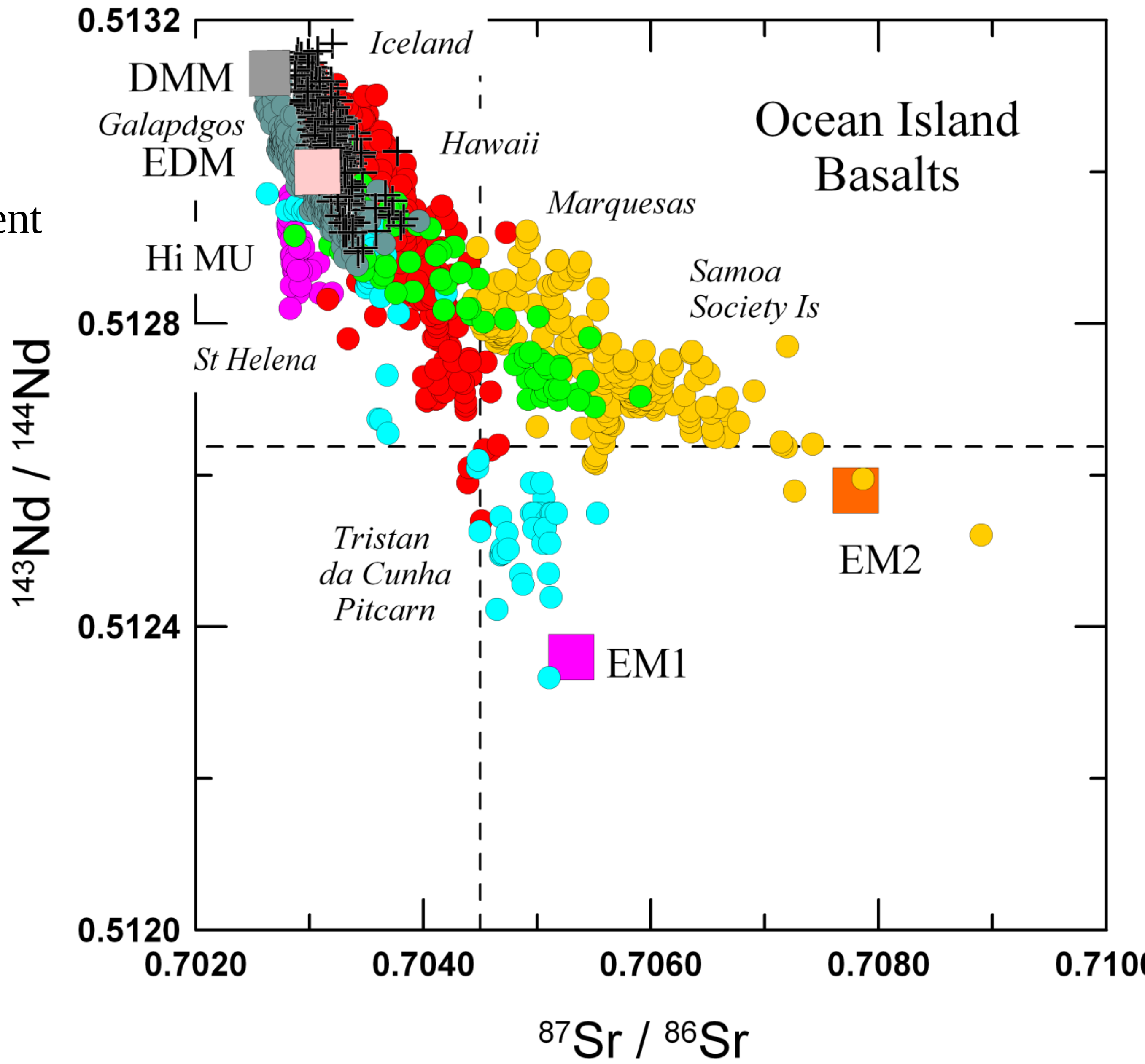

Les Olivines sont clairement plus enrichis en Ni que les Olivines des MORB: Sources !

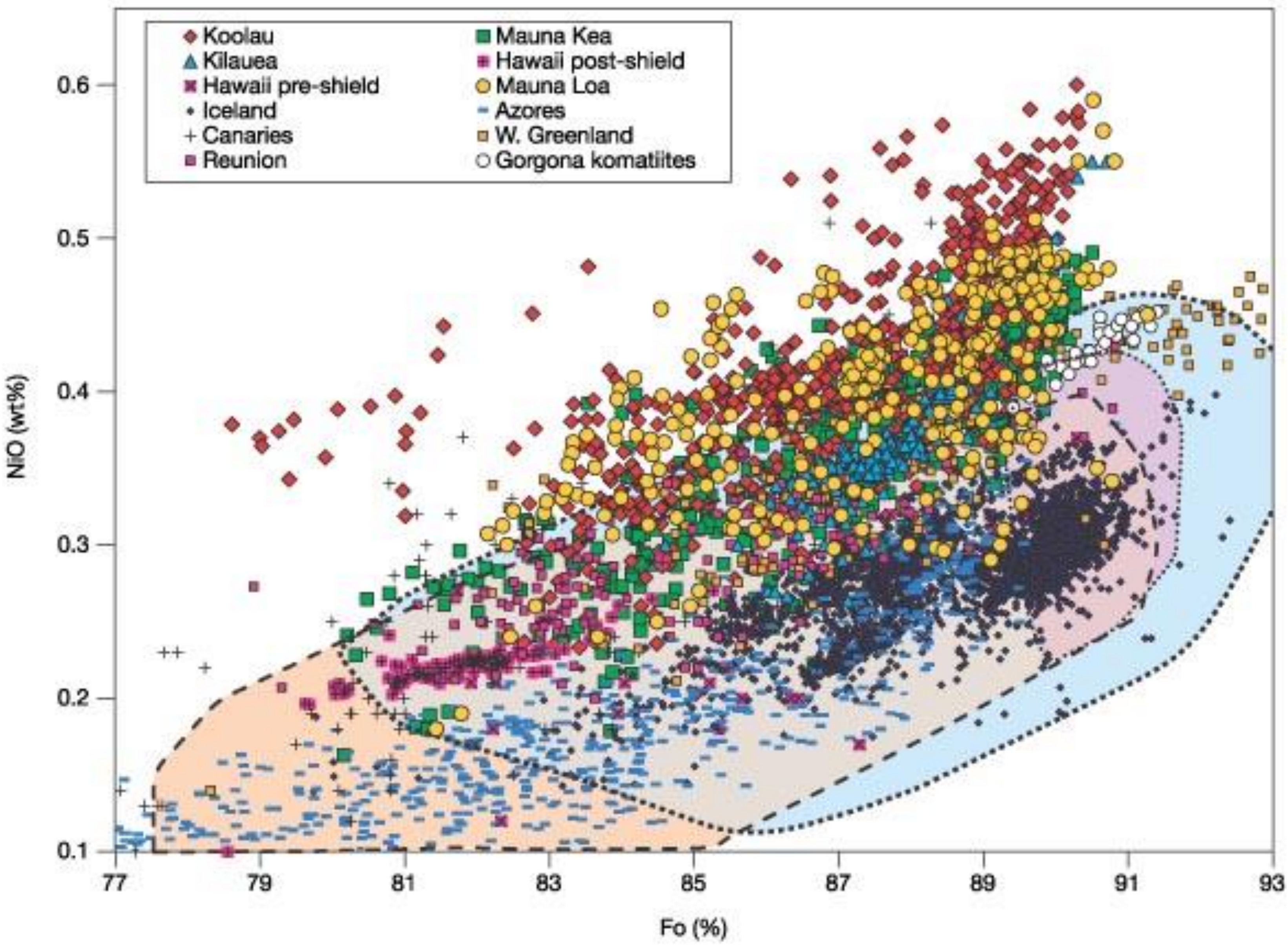

Almklovladen Norway

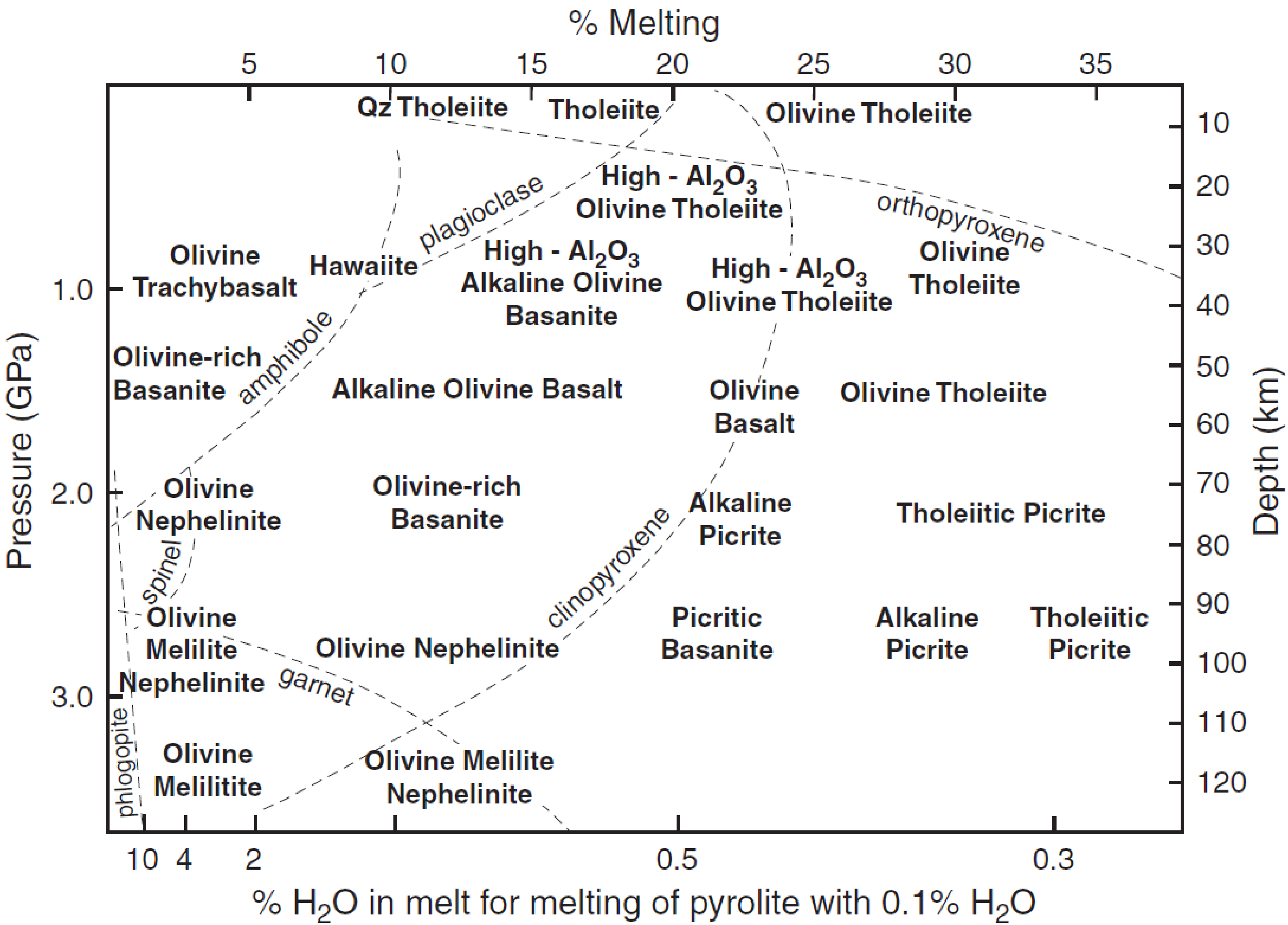
% Melting
5
10
15
20
25
30
35
Qz Tholeiite
Tholeiite
Olivine Tholeiite
High - Al_2O_3 Olivine Tholeiite
plagioclase
orthopyroxene
Olivine Trachybasalt
Hawaiite
High - Al_2O_3 Alkaline Olivine Basanite
High - Al_2O_3 Olivine Tholeiite
Olivine Tholeiite
Olivine-rich Basanite
amphibole
Alkaline Olivine Basalt
Olivine Basalt
Olivine Tholeiite
Olivine Nephelinite
Olivine-rich Basanite
Alkaline Picrite
Tholeiitic Picrite
spinel
clinopyroxene
Olivine Melilite Nephelinite
Olivine Nephelinite
Picritic Basanite
Alkaline Picrite
Tholeiitic Picrite
garnet
phlogopite
Olivine Melilitite
Olivine Melilite Nephelinite
Pressure (GPa)
1.0
2.0
3.0
Depth (km)
10
20
30
40
50
60
70
80
90
100
110
120
10
4
2
0.5
0.3
% H_2O in melt for melting of pyrolite with 0.1% H_2O

Green 1970

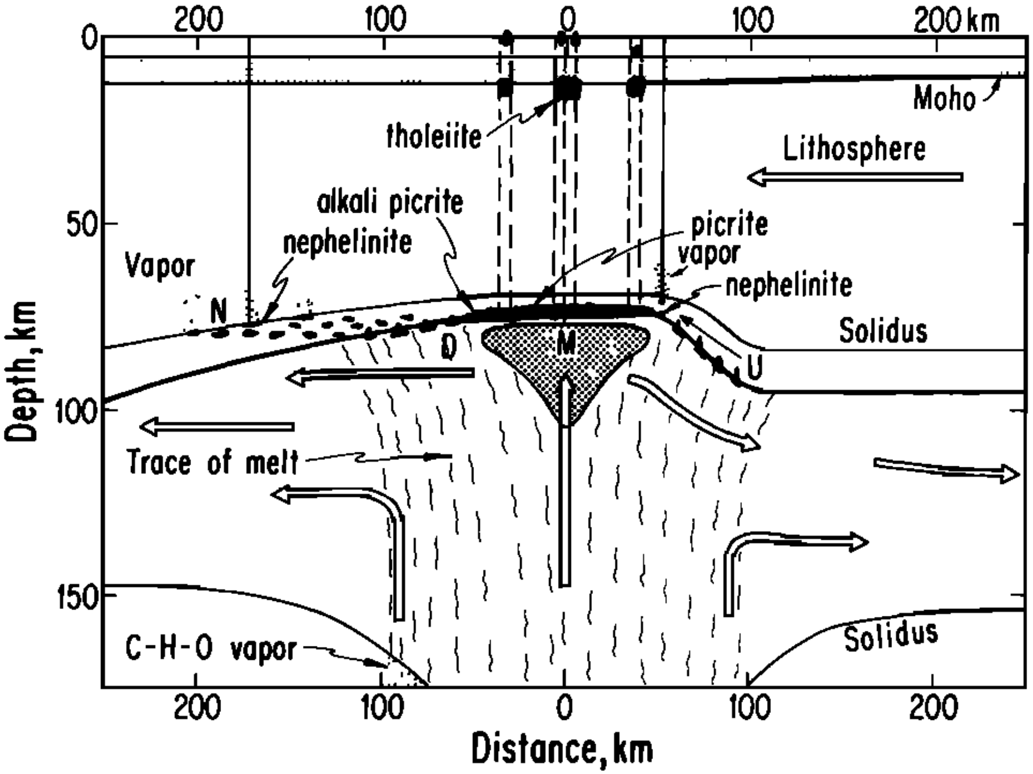

Fig. 7. Petrological structure of lithosphere and upper plume corresponding to Figure 6, with expanded vertical scale. Picritic magmas enter lithosphere from melting region M. Volatile-charged magmas enter the lithosphere on either side of M, with subsequent percolation retarded. As they approach the solidus, vapor is evolved (e.g., at N). enhancing the prospect of explosive eruption directly through the lithosphere. Paths followed by these magmas to the solidus differ according to their position on the upstream (U) or downstream (D) side of the plume, as depicted also on Figure 8.

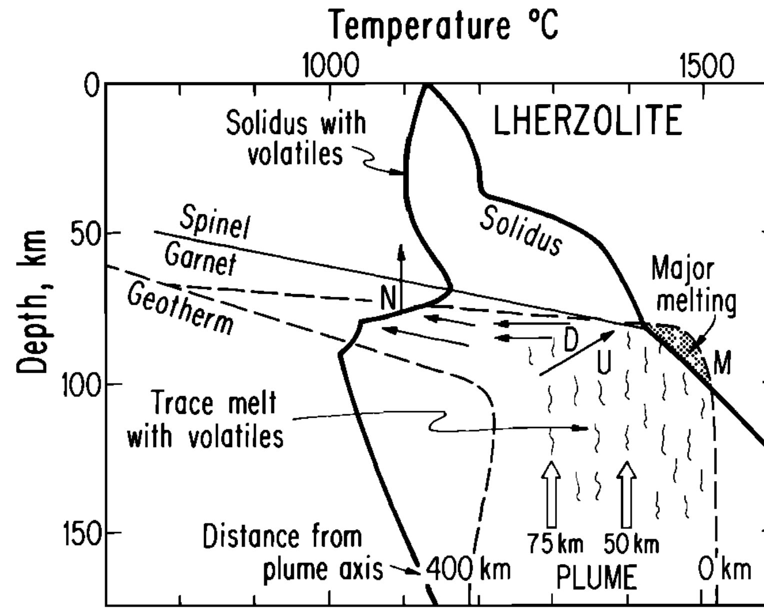

Fig. 8. Phase boundaries and plume geotherms from Figure 3 as depth-temperature framework for tracing paths of melt in Figure 7. The temperature of the volatile-charged interstitial melt rising in the plume varies as function of distance from the plume axis. Nephelinite magmas can be erupted if the magma reaches the solidus in the region of N. After the magma enters the lithosphere, magma on the upstream side of the axis (U) may rise up with decreasing temperature to the solidus at N, or it may be carried into the region of the high-temperature melt above M (Figure 7). On the downstream side of the plume axis (D), the magma is transported laterally with decreasing temperature to eruption sites well away from the axis (Figure 7).

Wyllie 1988

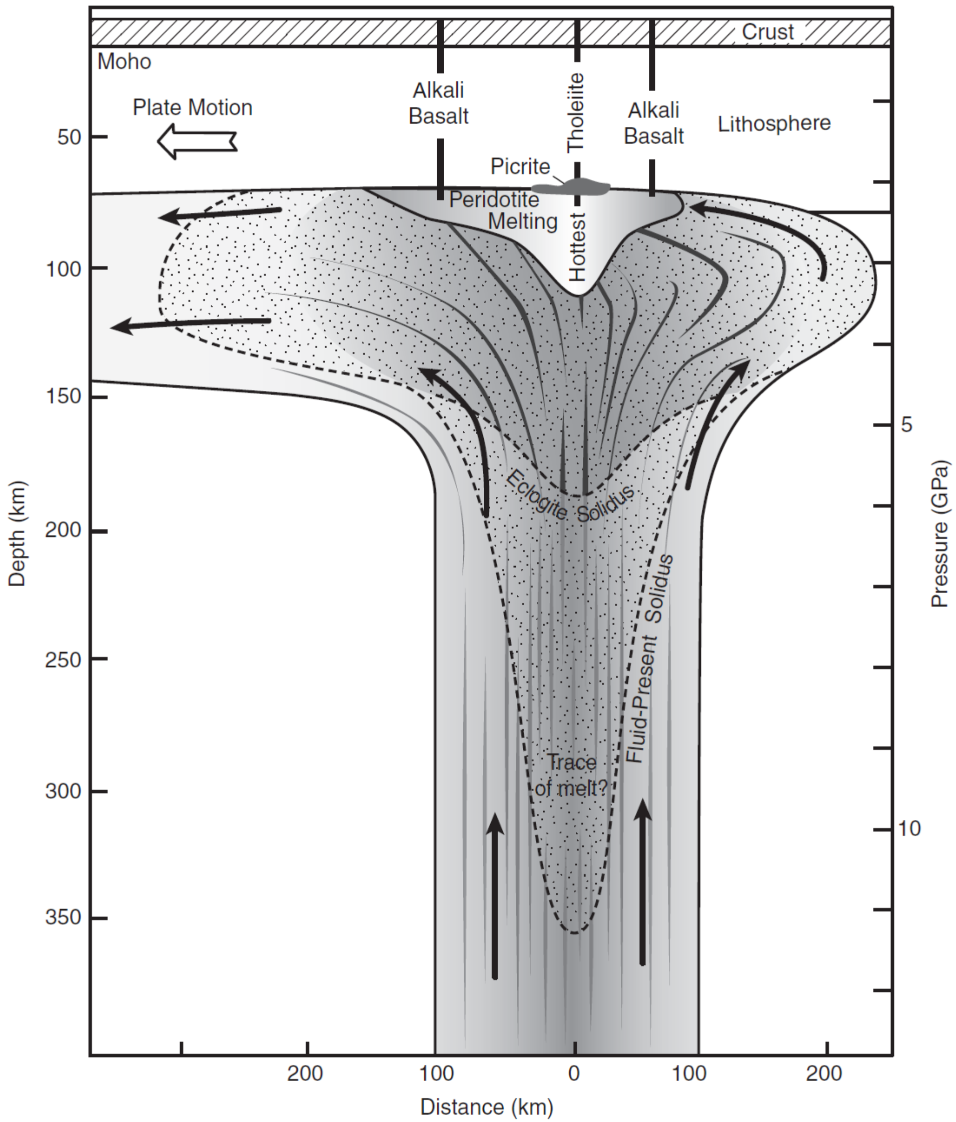

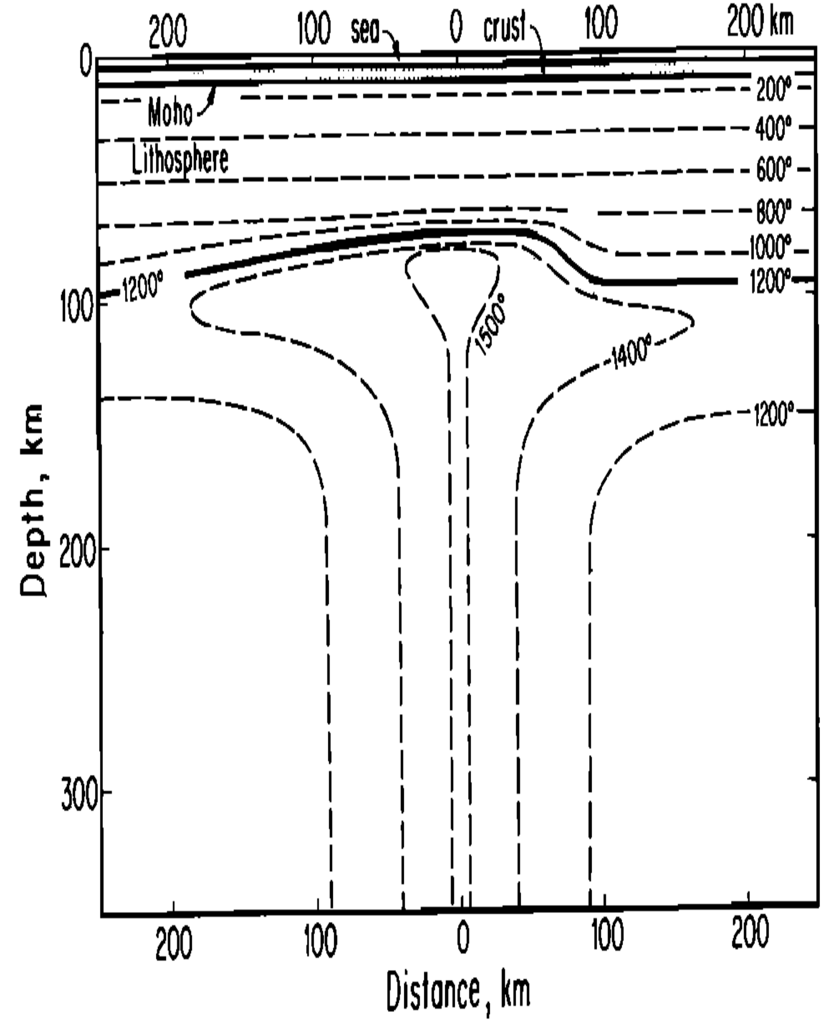

FIGURE 20 Diagrammatic plume-tail melting model. Rising plume material (heavy arrows are flow lines) is hotter toward the axis. Fluid-present melting of mantle lherzolite may begin at depths of about 350 km (stippled area), but the extent of such melts depends on the amount of fluid present and is probably minor. Melting of recycled crustal pods and stringers (dark streaks) may also begin near this depth, and such melting may be more extensive locally. Major lherzolite melting occurs at depths near 100 km. The melt fraction is greatest near the plume axis, producing picrites and tholeiites. The extent of plume asymmetry depends on plume flux and plate velocity. Plume-*head* melting is much more extensive. Based on Wyllie (1988b).

Model de fusion complex

Fusion d'eclogite → Si-rich Melt

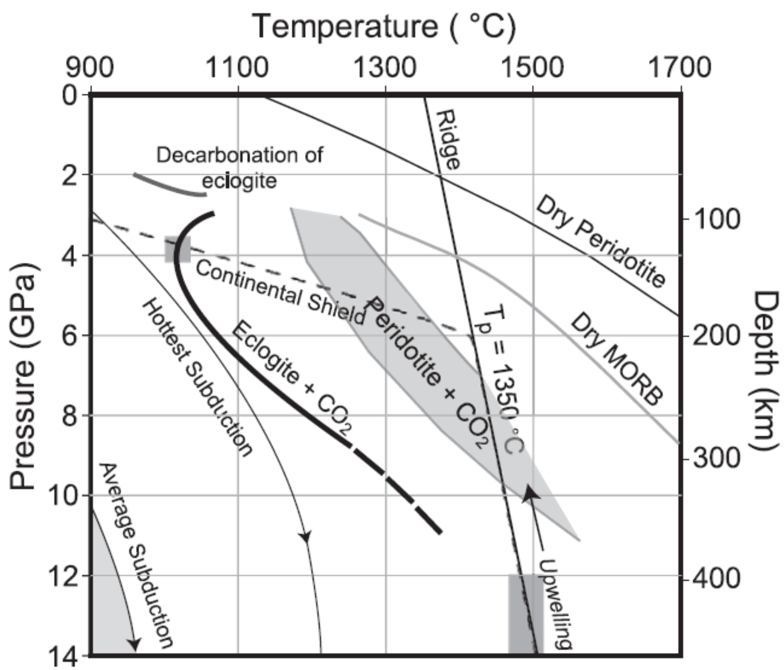

Reaction avec peridotite → pyroxenite

Pyroxenite + peridotite melts…

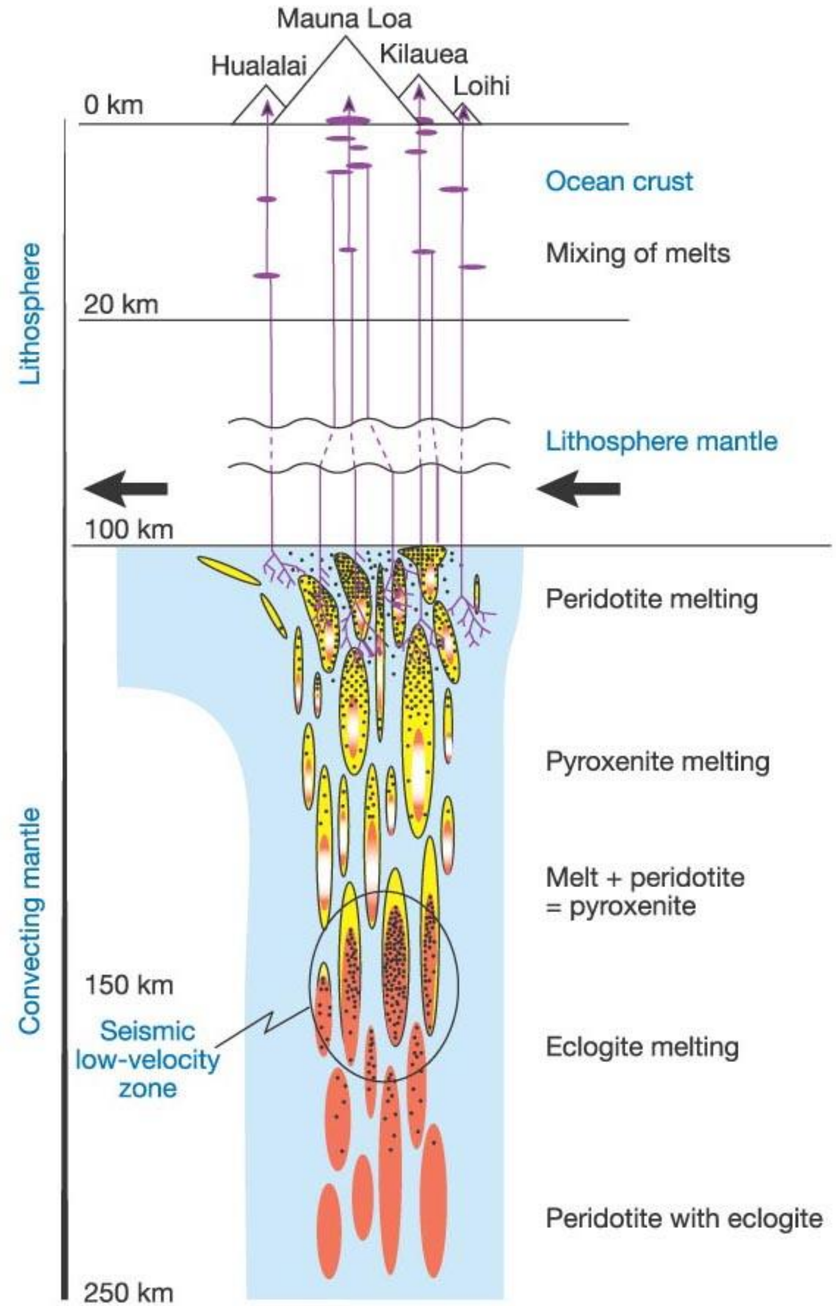

La variabilité de la composition chimique des MORB influencé par la proximité des hot spots

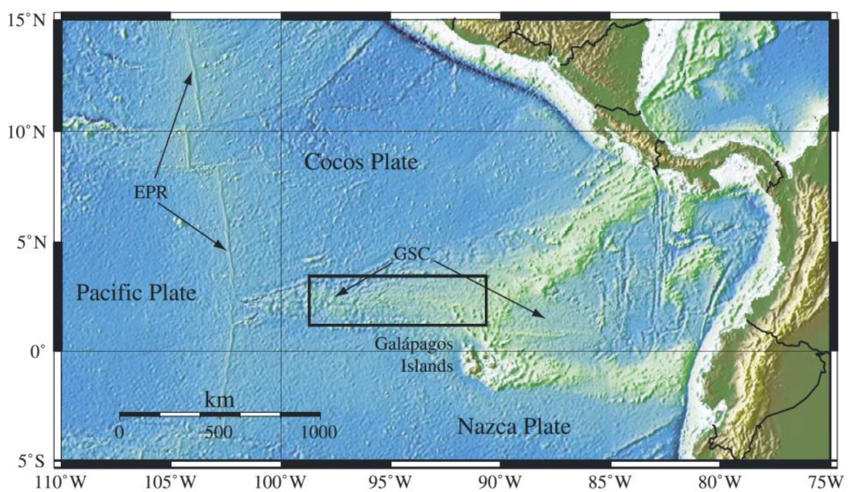

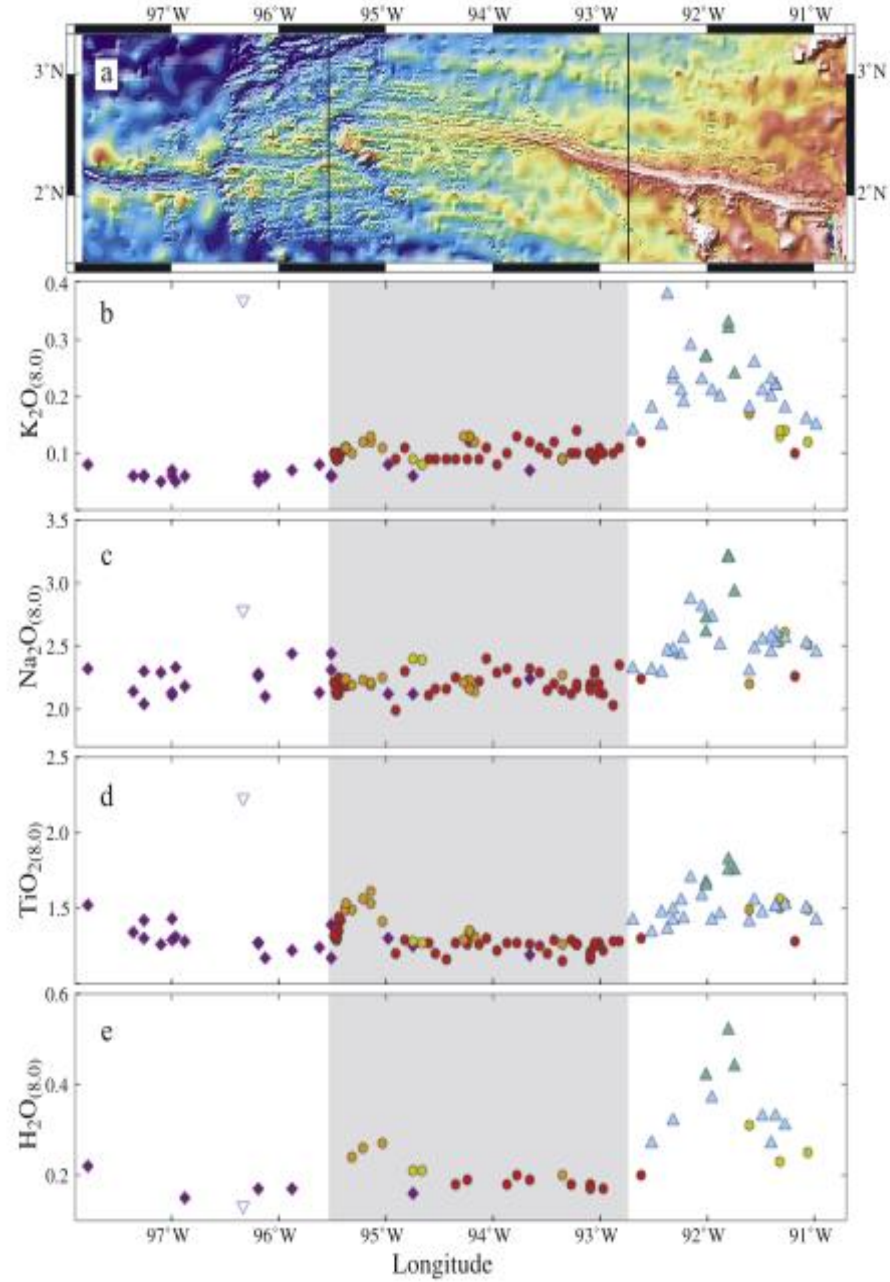

Cushman et al. (2004)

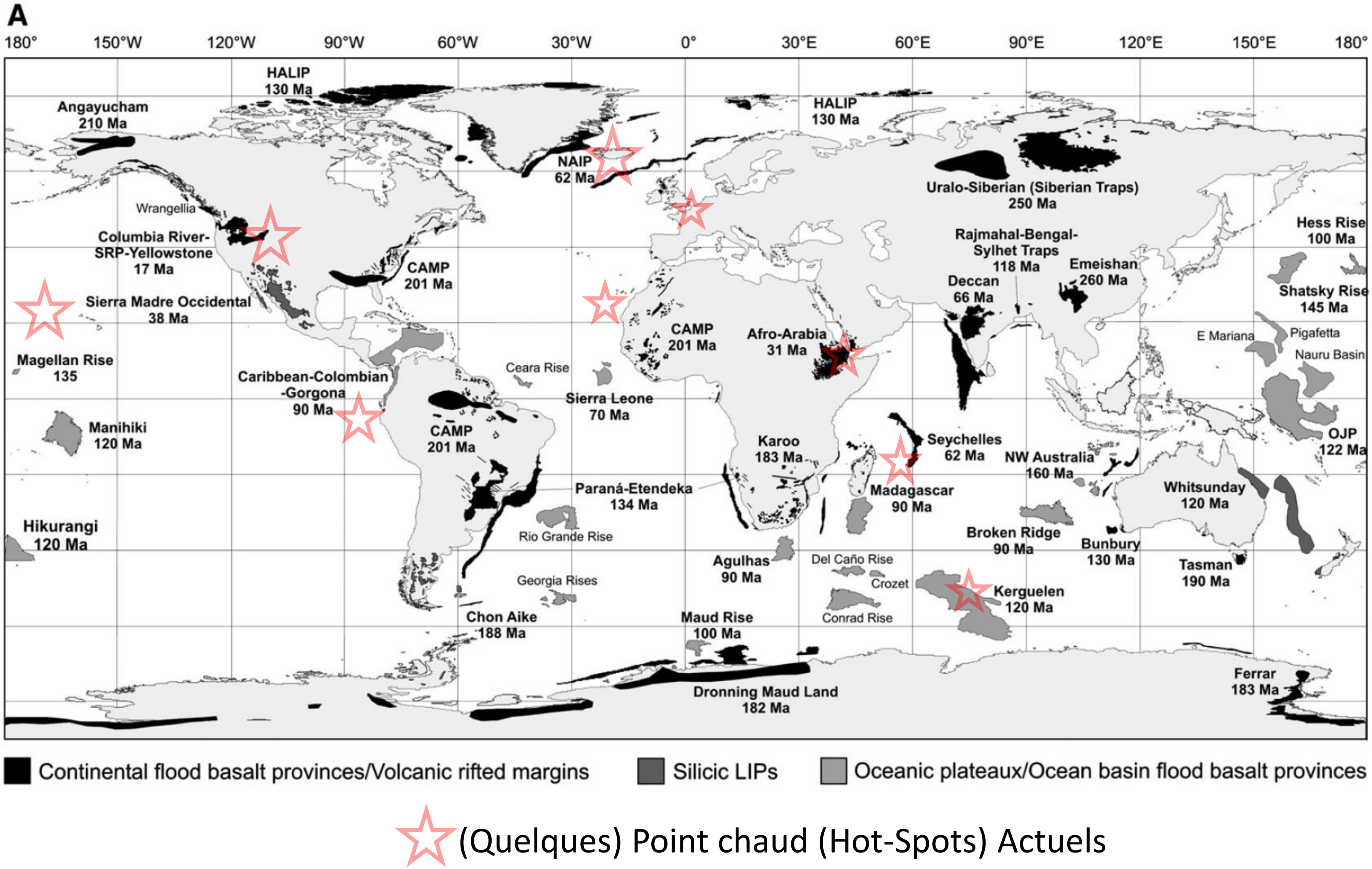

Fig. 4. Revised global distribution of Large Igneous Provinces. A) LIP events from 0–275 Ma, updated and revised from the PLATES project database and map (Institute of Geophysics, University of Texas, Austin). Map excludes seamount groups, submarine ridges and anomalous seafloor-spreading crust that have previously been considered LIPs by Coffin and Eldholm (1992, 1994, 2001, 2005). Interpreted remnants of Mesozoic oceanic plateaus accreted around the Pacific margins (Sorachi, Japan; western Cordillera of Colombia and Ecuador; Cache Creek, Canada) are not shown because of the lack of detailed information on their original areal extent, volume and duration. Annotated ages denote the onset of the main phase or first pulse of magmatism to the LIP event; note that some LIPs have precursor magmatism at lower intensity up to 10 Myr prior. Some LIPs are shown in small typeface to aid in figure clarity. Abbreviations: CAMP, Central Atlantic Magmatic Province; HALIP, High Arctic Large Igneous Province; NAIP, North Atlantic Igneous Province; OJP, Ontong Java Plateau. B) LIP events from 275–550 Ma. The inferred extent of each LIP event is shown by a dashed line, and many remain poorly mapped and studied. The number of well-defined LIP events (in terms of area, volume, duration and setting) is much reduced (in comparison with the younger record) no examples of accreted oceanic LIPs have been recorded for this period, which generally corresponds to Gondwanaland assembly.

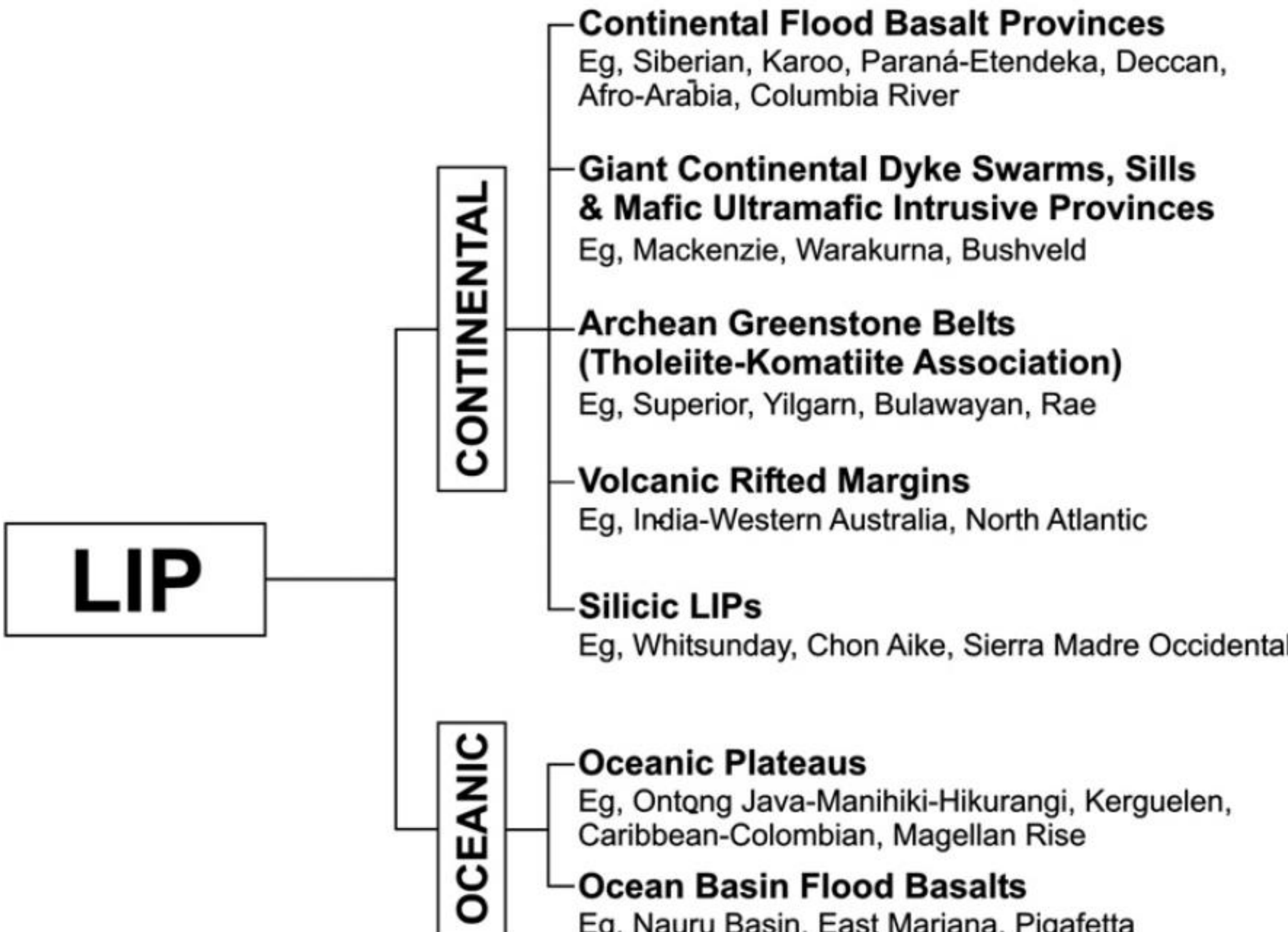
LIP
CONTINENTAL
Continental Flood Basalt Provinces
Eg, Siberian, Karoo, Paraná-Etendeka, Deccan, Afro-Arabia, Columbia River
Giant Continental Dyke Swarms, Sills & Mafic Ultramafic Intrusive Provinces
Eg, Mackenzie, Warakurna, Bushveld
Archean Greenstone Belts (Tholeiite-Komatiite Association)
Eg, Superior, Yilgarn, Bulawayan, Rae
Volcanic Rifted Margins
Eg, India-Western Australia, North Atlantic
Silicic LIPs
Eg, Whitsunday, Chon Aike, Sierra Madre Occidental
OCEANIC
Oceanic Plateaus
Eg, Ontong Java-Manihiki-Hikurangi, Kerguelen, Caribbean-Colombian, Magellan Rise
Ocean Basin Flood Basalts
Eg, Nauru Basin, East Mariana, Pigafetta

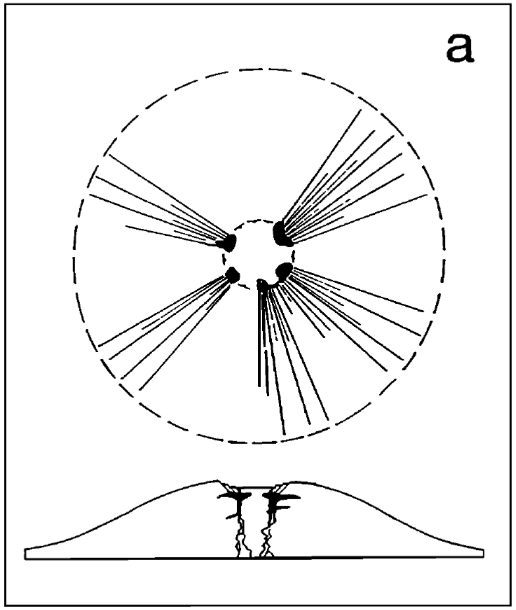

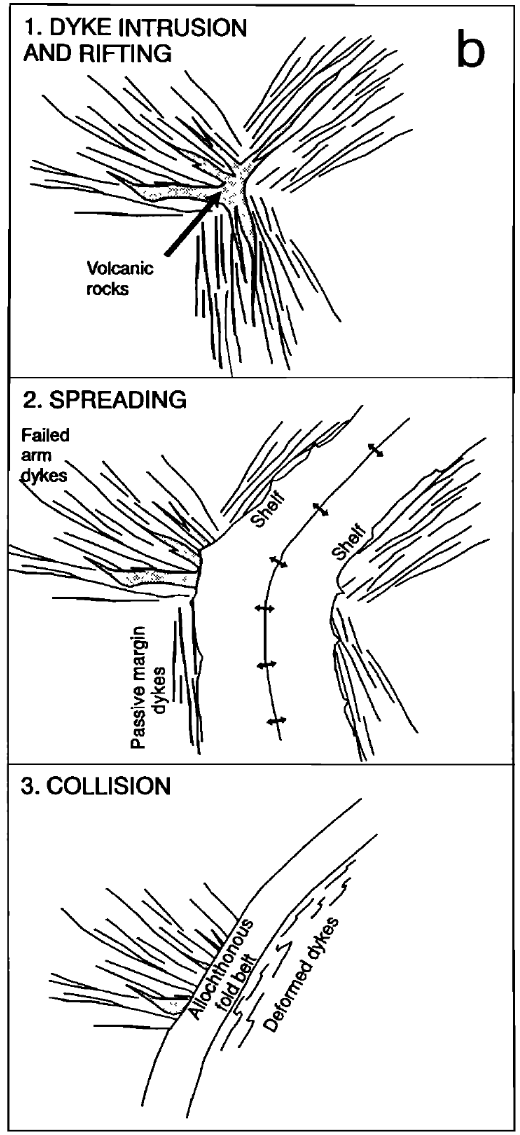

Figure 11. (a) Model of *Baragar et al.* [1996] for magmatism related to plume-induced uplift as described in the text. Reprinted with permission of Oxford University Press. (b) Model of *Fahrig* [1987] for three-stage plate tectonic cycle in the evolution of mafic continental dyke swarms. Reproduced with the permission of the Geological Association of Canada.

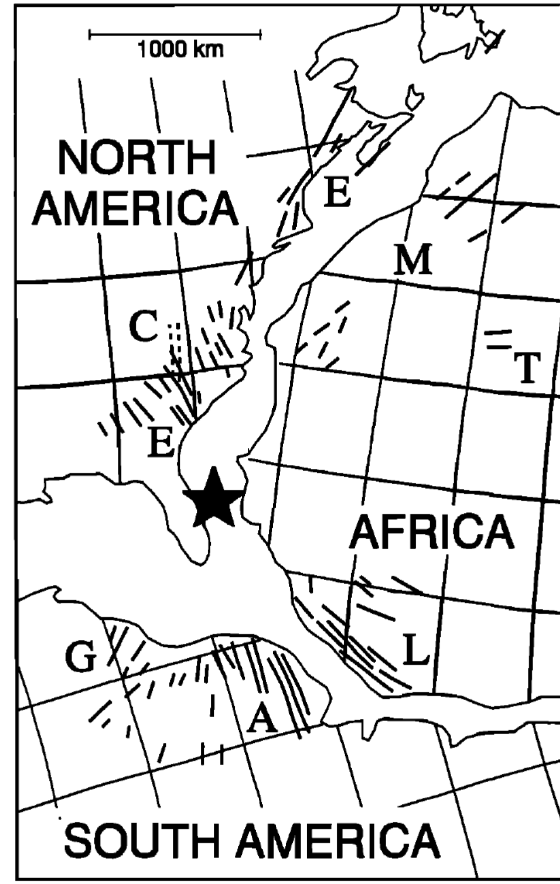

Figure 12. Dyke swarms of the 200 Ma Central Atlantic magmatic event of North America, South America, and Africa [after *May*, 1971; *McHone et al.*, 1987; *Oliveira et al.*, 1990; *Sebai et al.*, 1991b] in a reconstruction of Rowley [in *Keppie and Dallmeyer*, 1989]. In North America these consist of the Eastern North America (E) subswarm which is locally crosscut (dashed lines) by the slightly younger Charleston (C) subswarm [*Ragland et al.*, 1983; *Smith*, 1987; *de Boer et al.*, 1988]. In Africa, the dykes [e.g., *Sebai et al.*, 1991b] are divided on the basis of distribution into the Morocco[pm] (M), Liberia[pm] (L), and Taoudenni[pm] (T) subswarms. In South America numerous subswarms [*Sial et al.*, 1987; *Gibbs*, 1987; *Choudhuri et al.*, 1991] are grouped into the north-northwest trending Amapá (A) and related subswarms (Cassiporé, Jari, Cayenne, Apatoe), and in Guyana[pm] (G), the northeast-trending Cerro Bolivar, Supenaam and Tukutu River and possibly the Rio Trombetas subswarms [*Choudhuri et al.*, 1991; *Ernst et al.*, 1995b, 1996; *Sial et al.*, 1987; *Gibbs*, 1987]. The star marks the focal point of the swarms.

Columbia River Flood Basalts

~15 ± 1 Ma

Deccan Traps

~67 ± 1 Ma

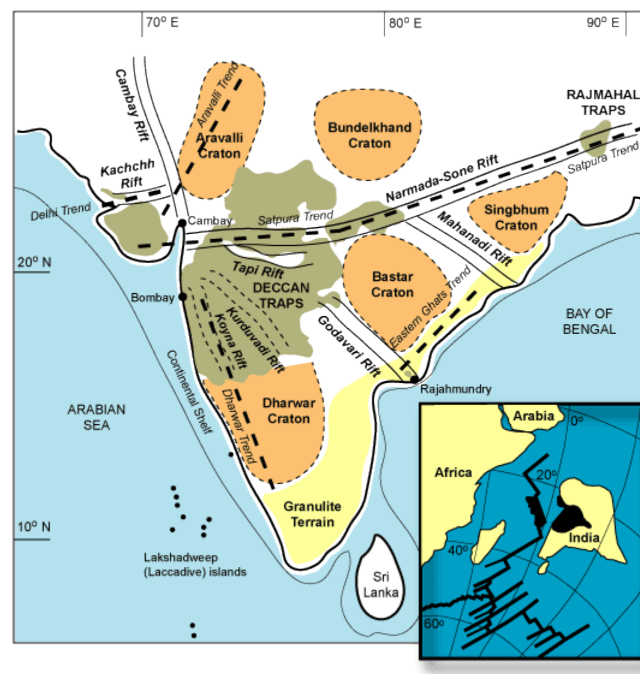

Province	Age	Volume $\times 10^3$ km^3	Types of Basalt Qtz Thol.	Oliv. Thol.	Alk. Bas.
Lake Superior	Precambrian	1,300	42	51	7
Siberia	Permo-Triassic	> 2,000	28	69	3
Karoo, S. Africa	Jurassic	2,000	57	37	6
Paraná, Brazil	Cretaceous	> 1,500	72	28	0
Ontong-Java	Cretaceous	40,000	20	80	0
Brito-Arctic	Eocene	1,800	5	50	45
Deccan, India	Eocene	1000–2500	55	35	10
Columbia River	Mid-Miocene	174	30	70	0

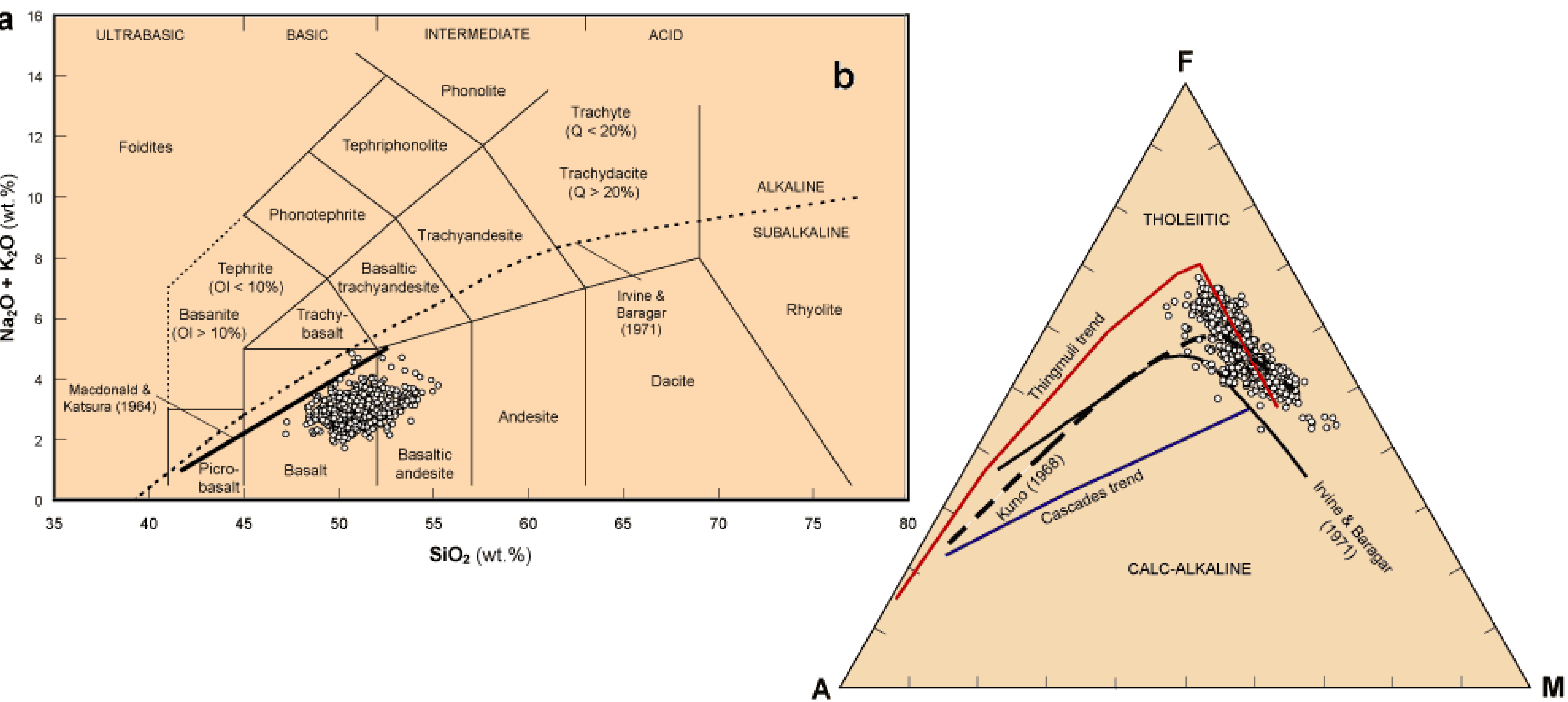

		Volume	Types of Basalt		
Province	Age	× 10^3 km^3	Qtz Thol.	Oliv. Thol.	Alk. Bas.
Lake Superior	Precambrian	1,300	42	51	7
Siberia	Permo-Triassic	> 2,000	28	69	3
Karoo, S. Africa	Jurassic	2,000	57	37	6
Paraná, Brazil	Cretaceous	> 1,500	72	28	0
Ontong-Java	Cretaceous	40,000	20	80	0
Brito-Arctic	Eocene	1,800	5	50	45
Deccan, India	Eocene	1000–2500	55	35	10
Columbia River	Mid-Miocene	174	30	70	0

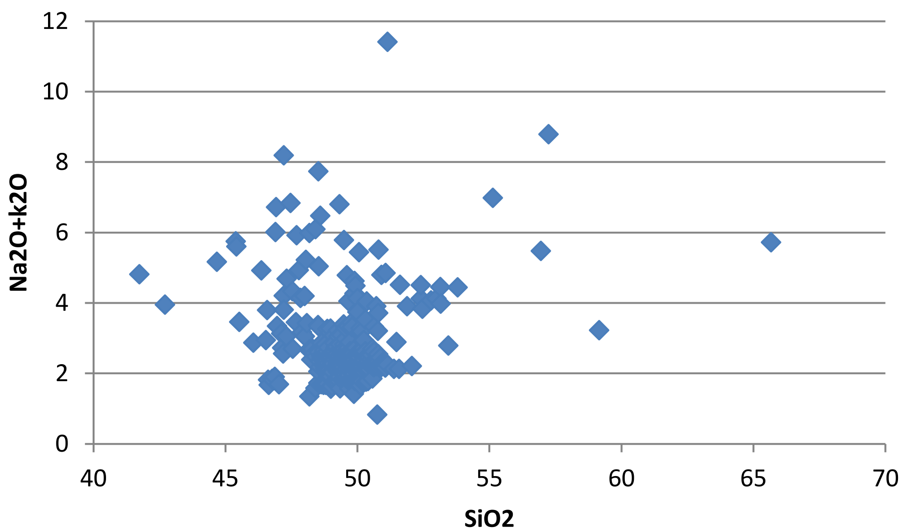

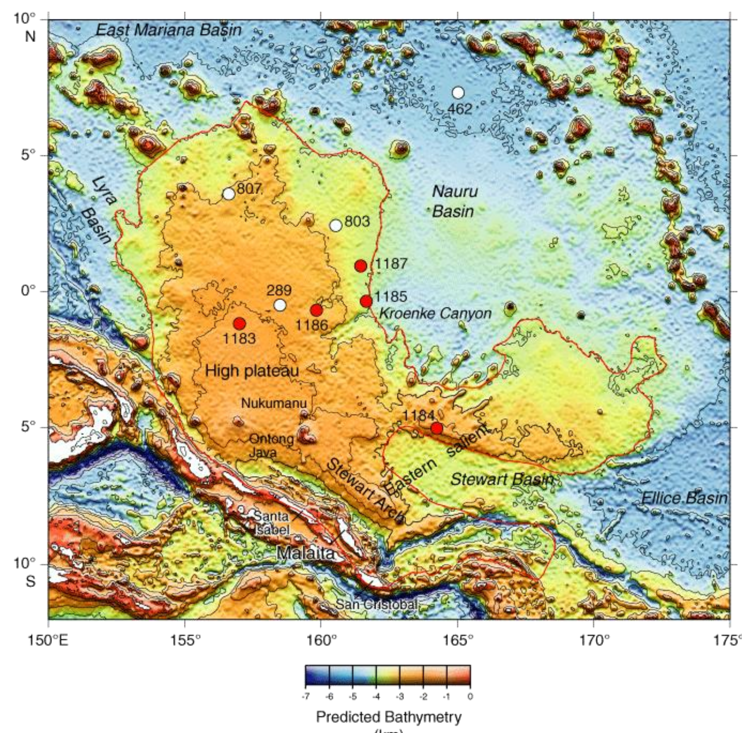

Mid-Cretaceous

122 & 90 mys

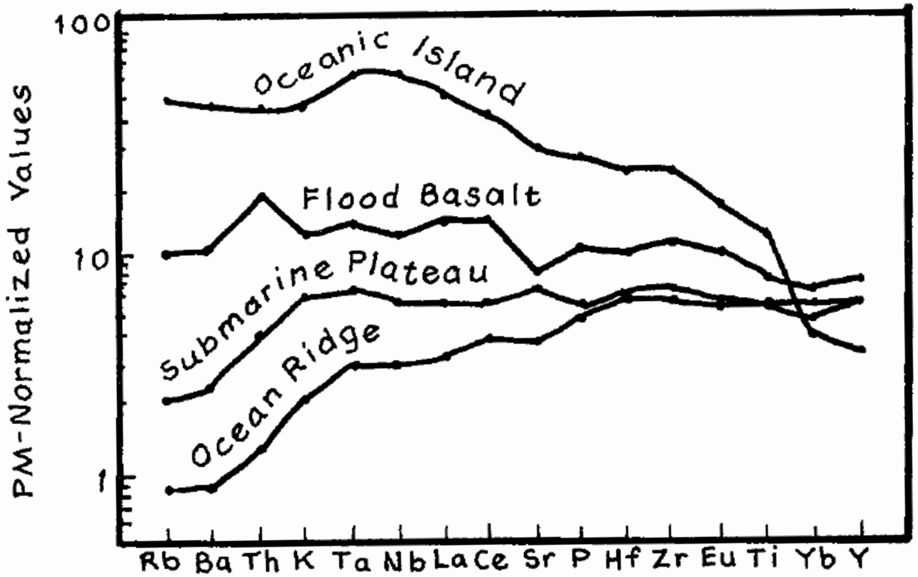
PM-Normalized Values
100
10
1
Oceanic Island
Flood Basalt
Submarine Plateau
Ocean Ridge
Rb Ba Th K Ta Nb La Ce Sr P Hf Zr Eu Ti Yb Y

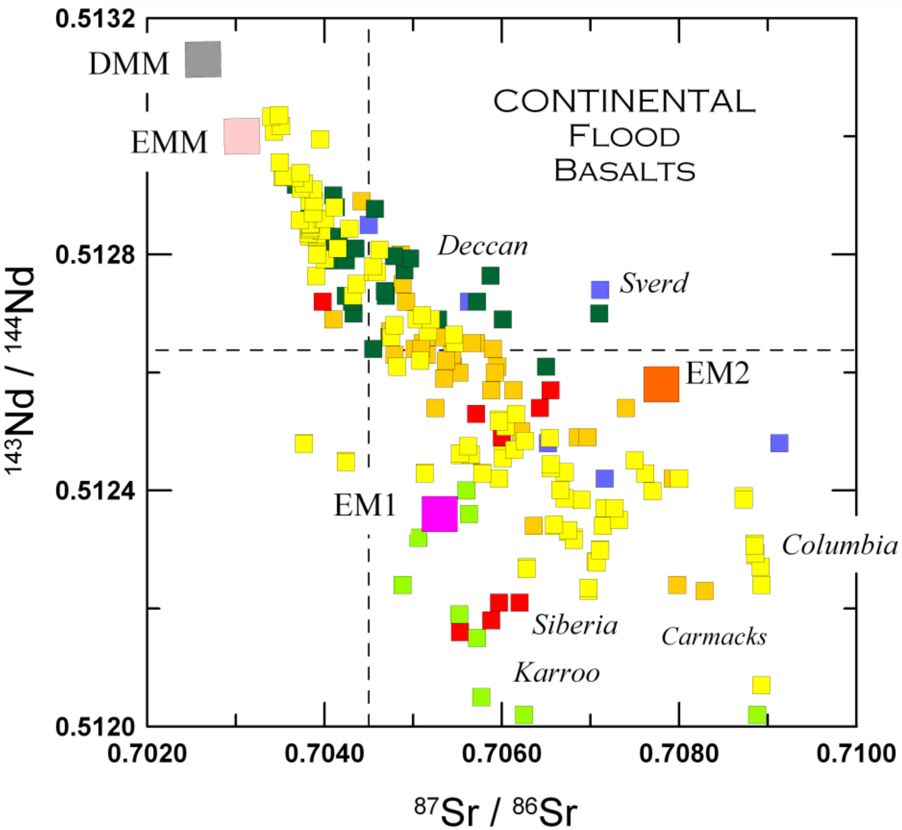
CONTINENTAL
FLOOD
BASALTS
DMM
EMM
EM1
EM2
Deccan
Sverd
Columbia
Siberia
Carmacks
Karroo
0.5132
0.5128
0.5124
0.5120
0.7020
0.7040
0.7060
0.7080
0.7100
^{143}Nd / ^{144}Nd
^{87}Sr / ^{86}Sr

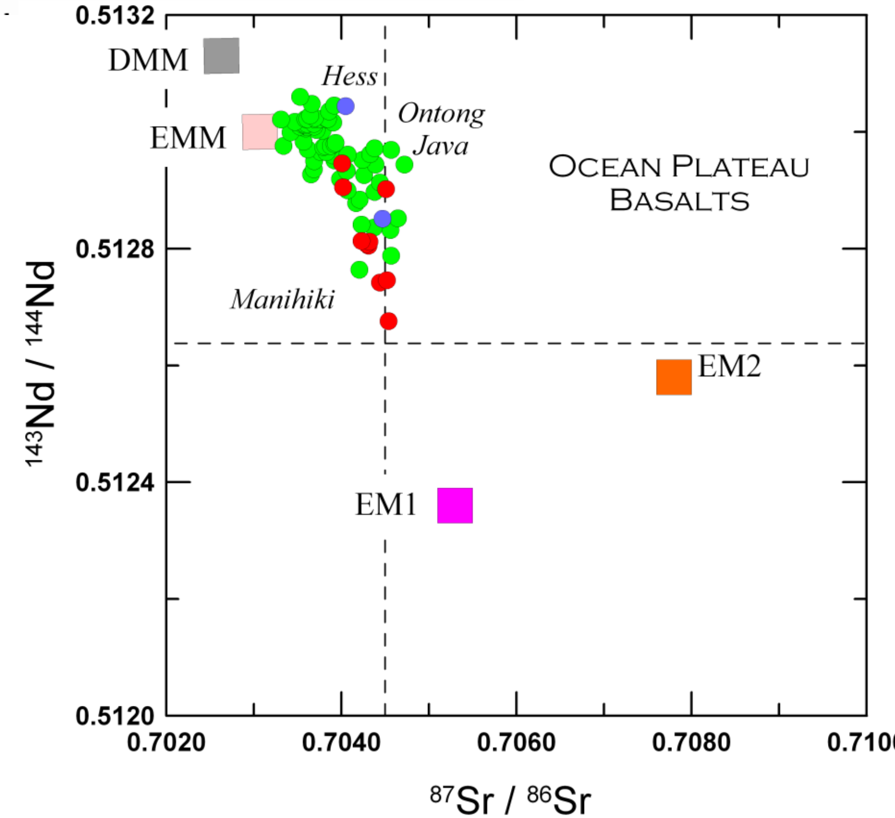
OCEAN PLATEAU
BASALTS
DMM
EMM
EM1
EM2
Hess
Ontong
Java
Manihiki
0.5132
0.5128
0.5124
0.5120
0.7020
0.7040
0.7060
0.7080
0.7100
^{143}Nd / ^{144}Nd
^{87}Sr / ^{86}Sr

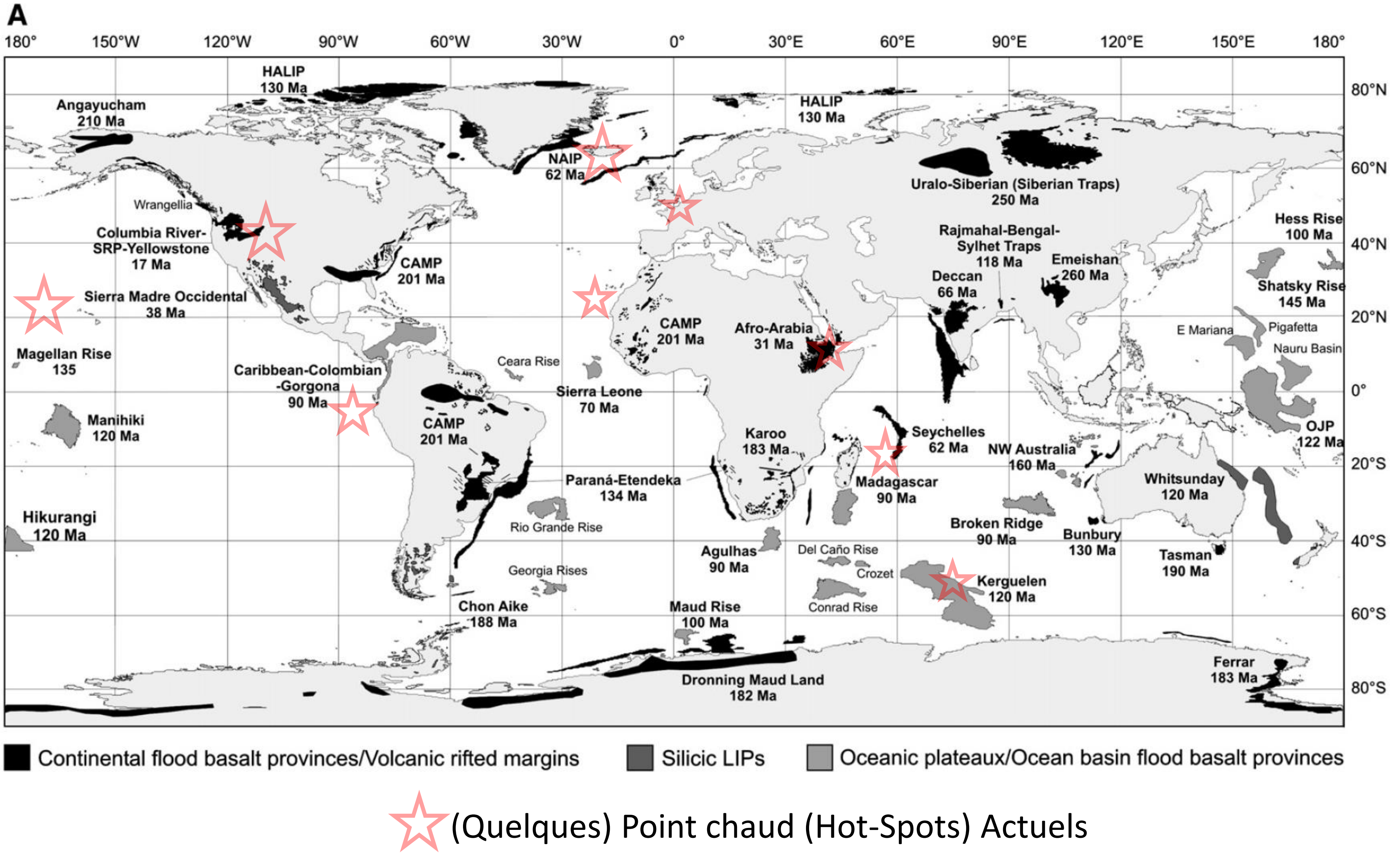

Fig. 4. Revised global distribution of Large Igneous Provinces. A) LIP events from 0–275 Ma, updated and revised from the PLATES project database and map (Institute of Geophysics, University of Texas, Austin). Map excludes seamount groups, submarine ridges and anomalous seafloor-spreading crust that have previously been considered LIPs by Coffin and Eldholm (1992, 1994, 2001, 2005). Interpreted remnants of Mesozoic oceanic plateaus accreted around the Pacific margins (Sorachi, Japan; western Cordillera of Colombia and Ecuador; Cache Creek, Canada) are not shown because of the lack of detailed information on their original areal extent, volume and duration. Annotated ages denote the onset of the main phase or first pulse of magmatism to the LIP event; note that some LIPs have precursor magmatism at lower intensity up to 10 Myr prior. Some LIPs are shown in small typeface to aid in figure clarity. Abbreviations: CAMP, Central Atlantic Magmatic Province; HALIP, High Arctic Large Igneous Province; NAIP, North Atlantic Igneous Province; OJP, Ontong Java Plateau. B) LIP events from 275–550 Ma. The inferred extent of each LIP event is shown by a dashed line, and many remain poorly mapped and studied. The number of well-defined LIP events (in terms of area, volume, duration and setting) is much reduced (in comparison with the younger record) no examples of accreted oceanic LIPs have been recorded for this period, which generally corresponds to Gondwanaland assembly.

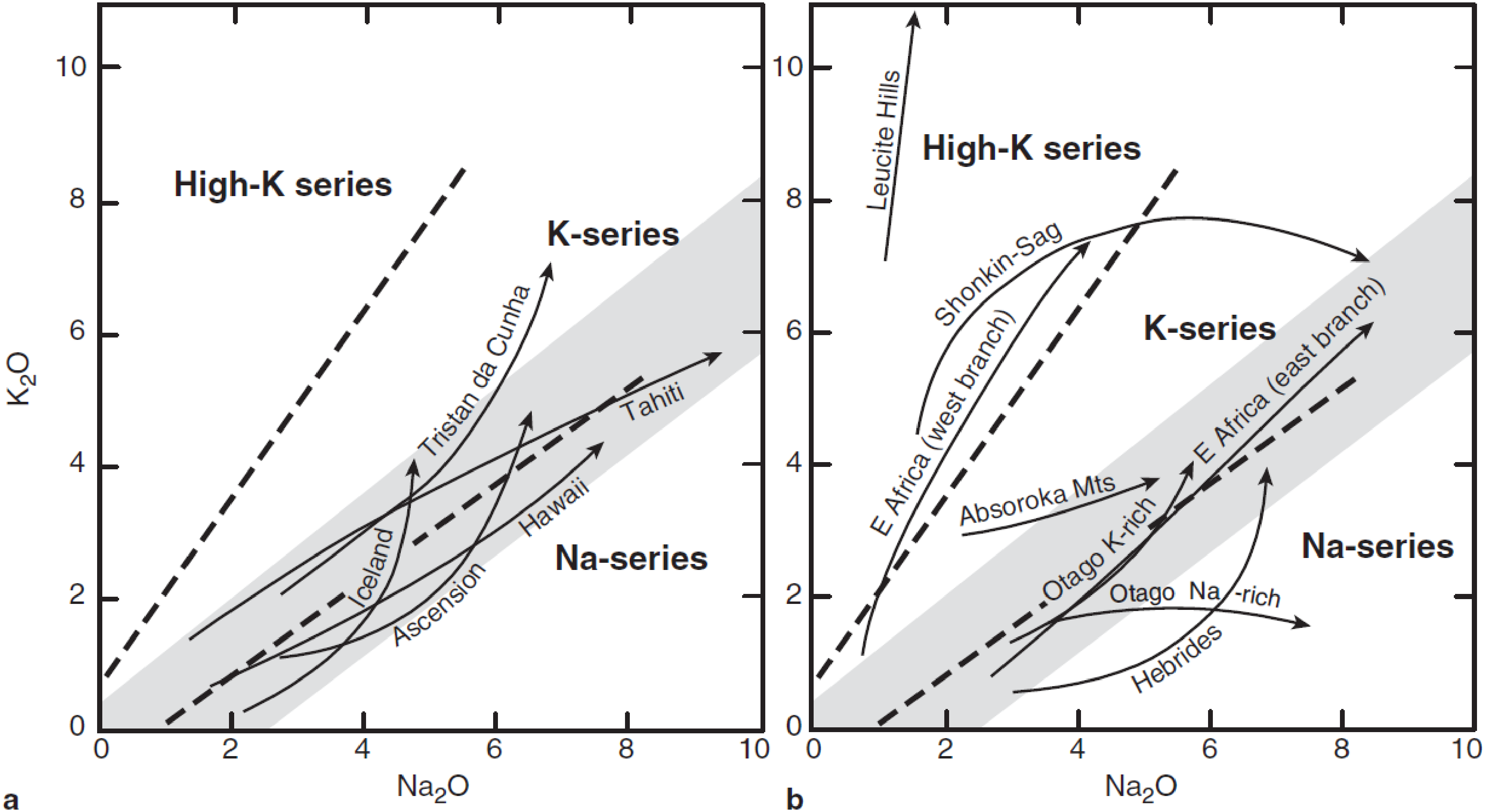

FIGURE 1 Variations in alkali ratios for **(a)** oceanic and **(b)** continental alkaline series. The heavy dashed lines distinguish the alkaline magma subdivisions from Figure 8.14, and the shaded area represents the range for the more common oceanic intraplate series. After McBirney (1993). Jones and Bartlett Publishers, Sudbury, MA. Reprinted with permission.

Rifting:
Des cratons aux océans…

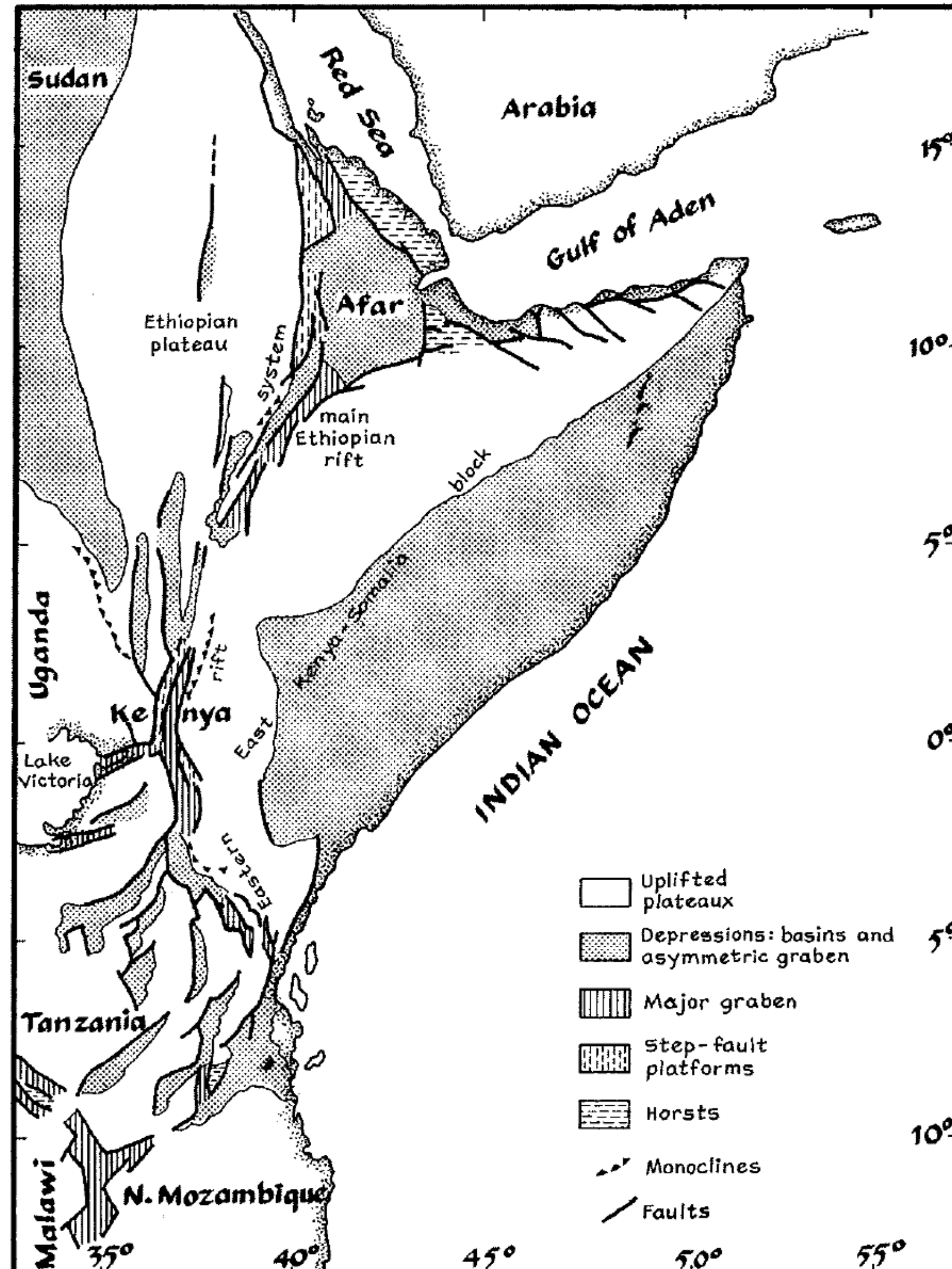

11-4 General map of the East African Rift zone.

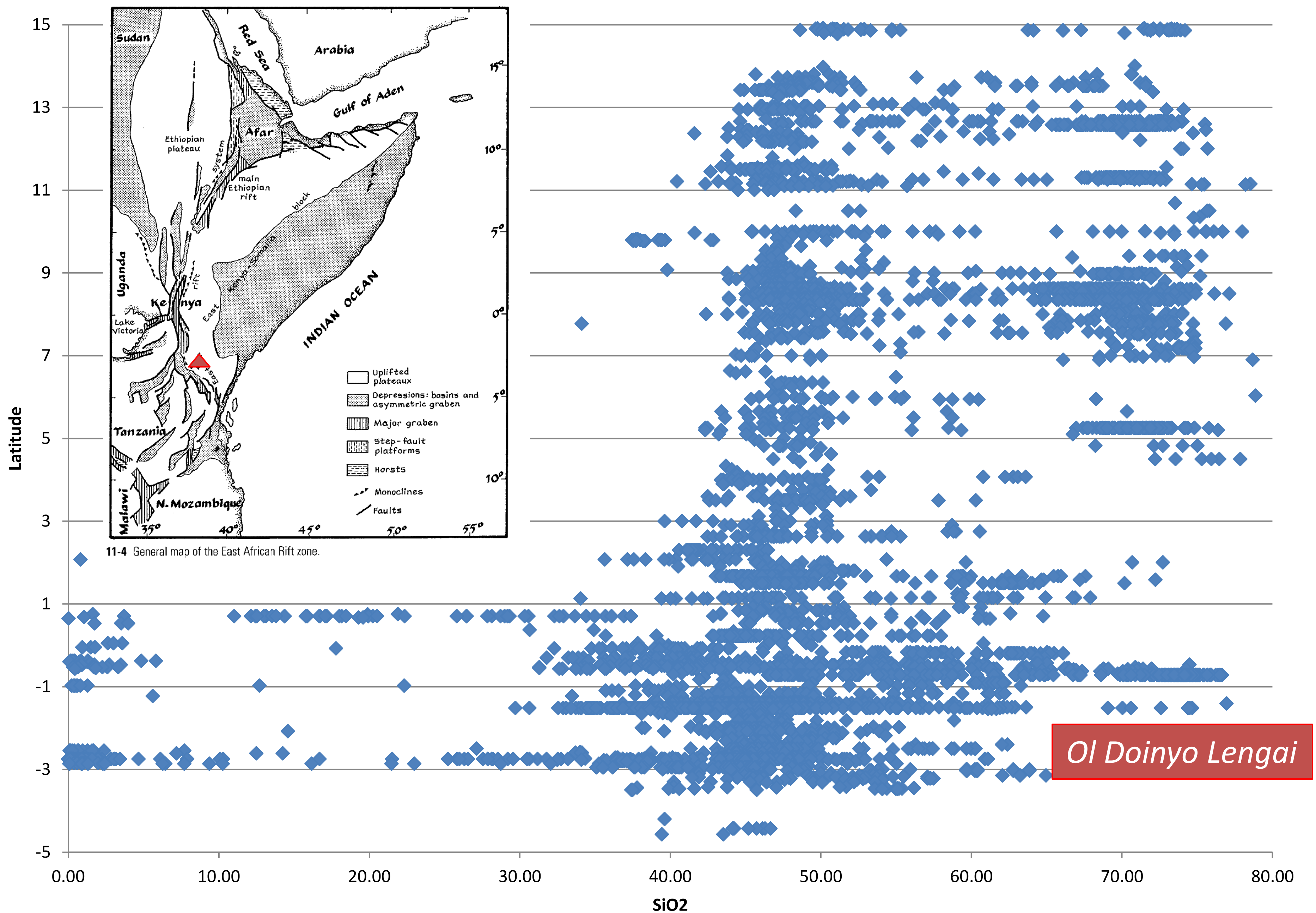

11-4 General map of the East African Rift zone.

2007

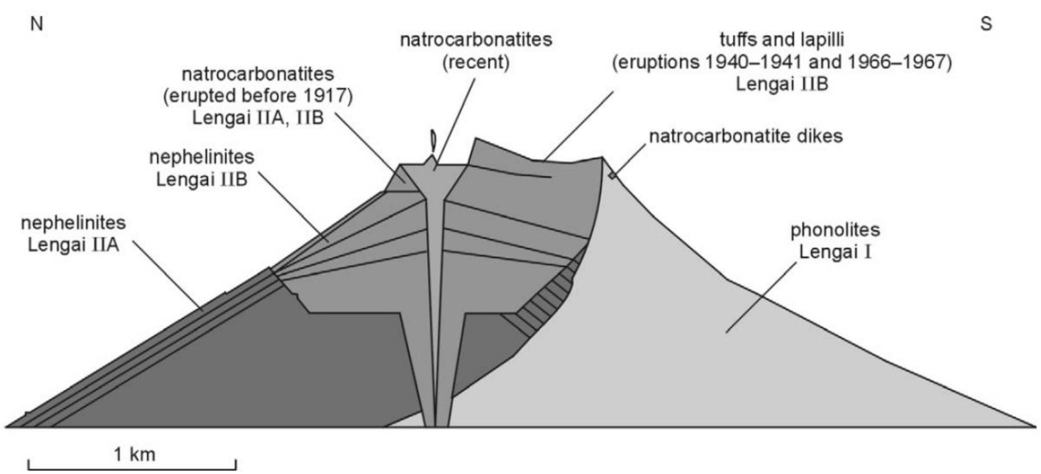

Fig. 1. Schematic cross section of the upper part of Oldoinyo Lengai Volcano (Klaudius and Keller, 2006; Zaitsev, 2010b).

https://www.youtube.com/watch?v=qputaVyn7TE

TABLE 5 Representative Carbonatite Compositions

%	Calcite–Carbonatite	Dolomite–Carbonatite	Ferro–Carbonatite	Natro–Carbonatite
SiO_2	2.72	3.63	4.7	0.16
TiO_2	0.15	0.33	0.42	0.02
Al_2O_3	1.06	0.99	1.46	0.01
Fe_2O_3	2.25	2.41	7.44	0.05
FeO	1.01	3.93	5.28	0.23
MnO	0.52	0.96	1.65	0.38
MgO	1.80	15.06	6.05	0.38
CaO	49.1	30.1	32.8	14.0
Na_2O	0.29	0.29	0.39	32.2
K_2O	0.26	0.28	0.39	8.38
P_2O_5	2.10	1.90	1.97	0.85
H_2O+	0.76	1.20	1.25	0.56
CO_2	36.6	36.8	30.7	31.6
BaO	0.34	0.64	3.25	1.66
SrO	0.86	0.69	0.88	1.42
F	0.29	0.31	0.45	2.50
Cl	0.08	0.07	0.02	3.40
S	0.41	0.35	0.96	–
SO_3	0.88	1.08	4.14	3.72

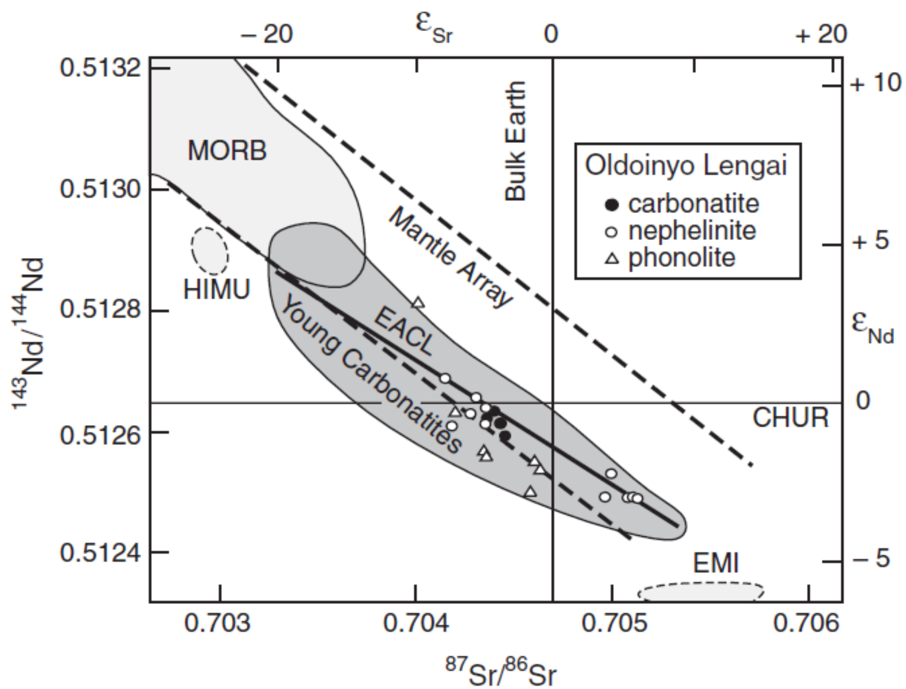

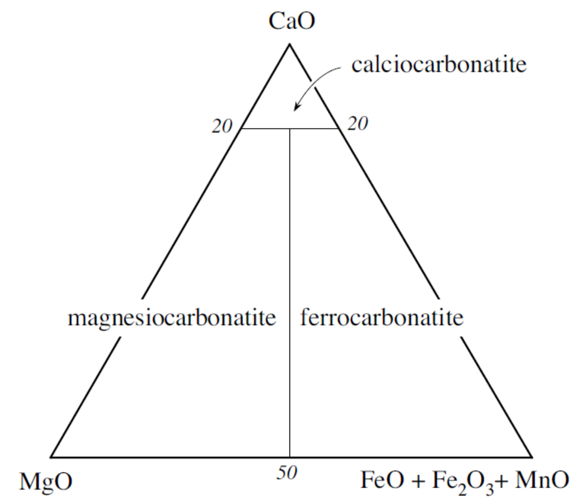

Fig. 2.2. Chemical classification of carbonatites with SiO_2 < 20% using wt % oxides (Woolley & Kempe, 1989). Carbonatites in which SiO_2 > 20% are silicocarbonatites.

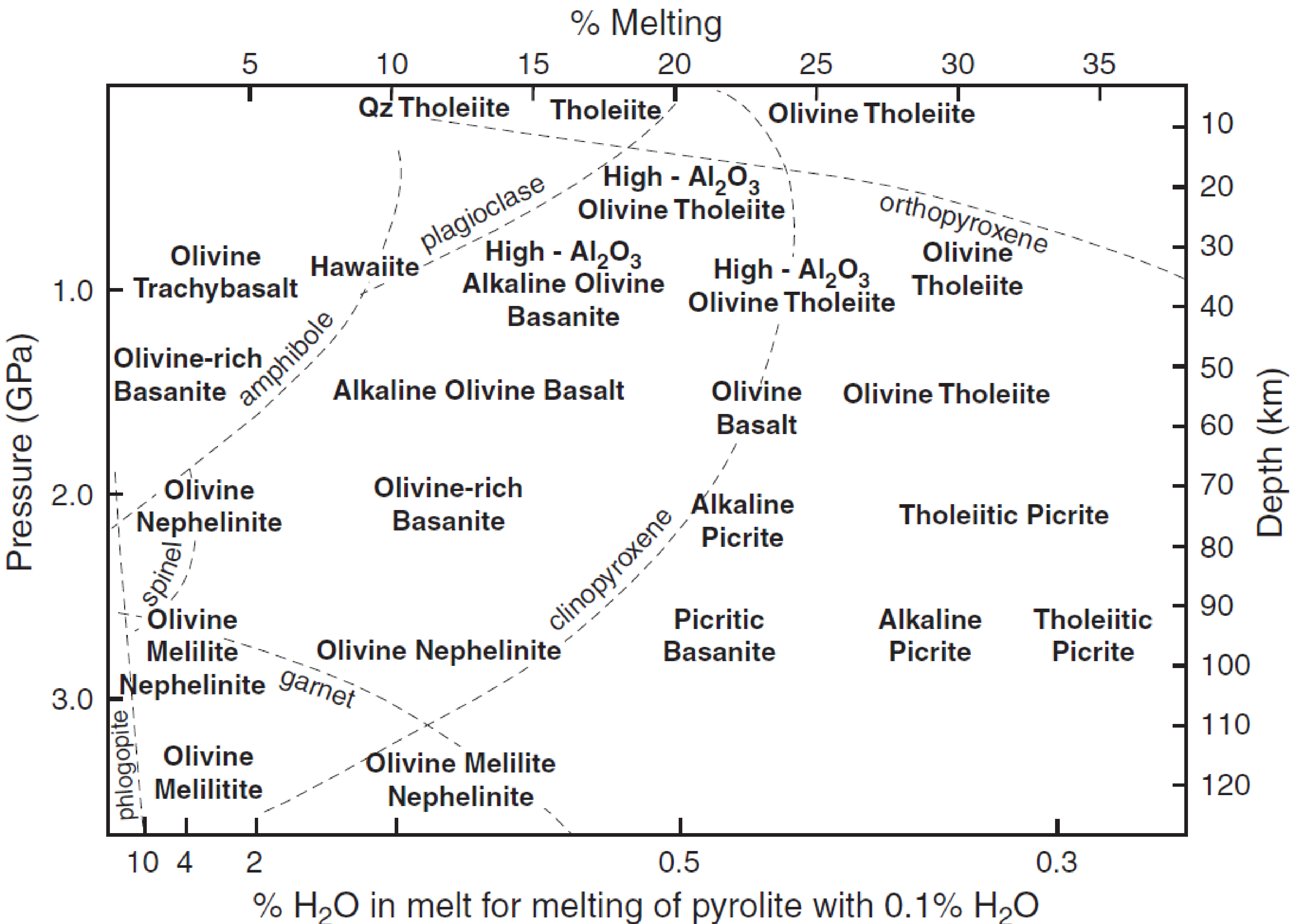

+ CO_2 ??

Green 1970

Dasgupta Jpet 2007

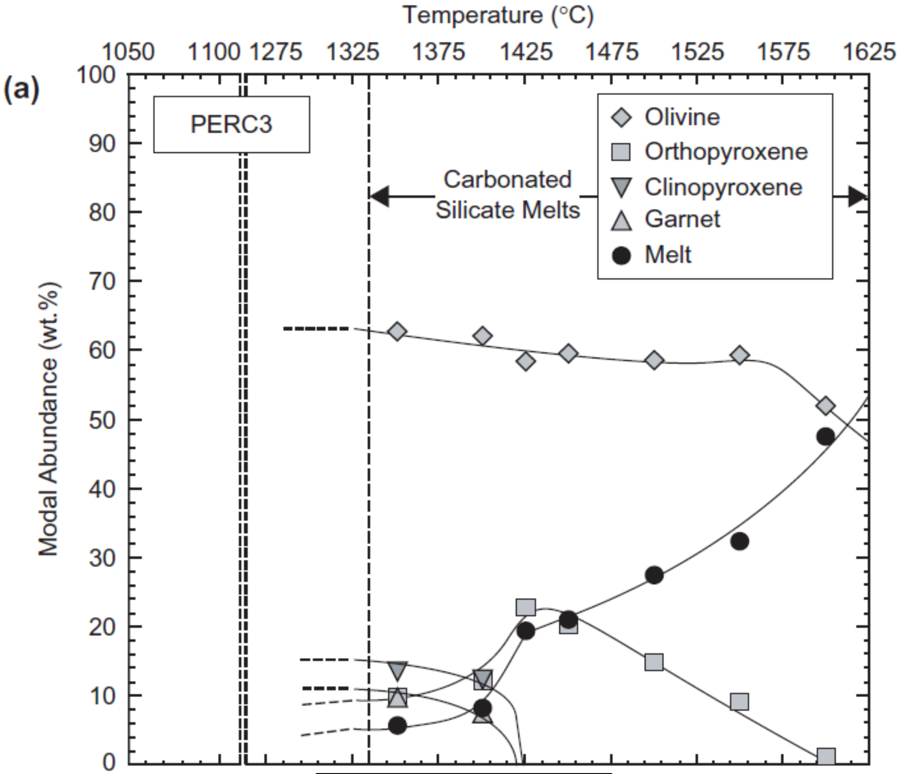

1 Wt % CO2

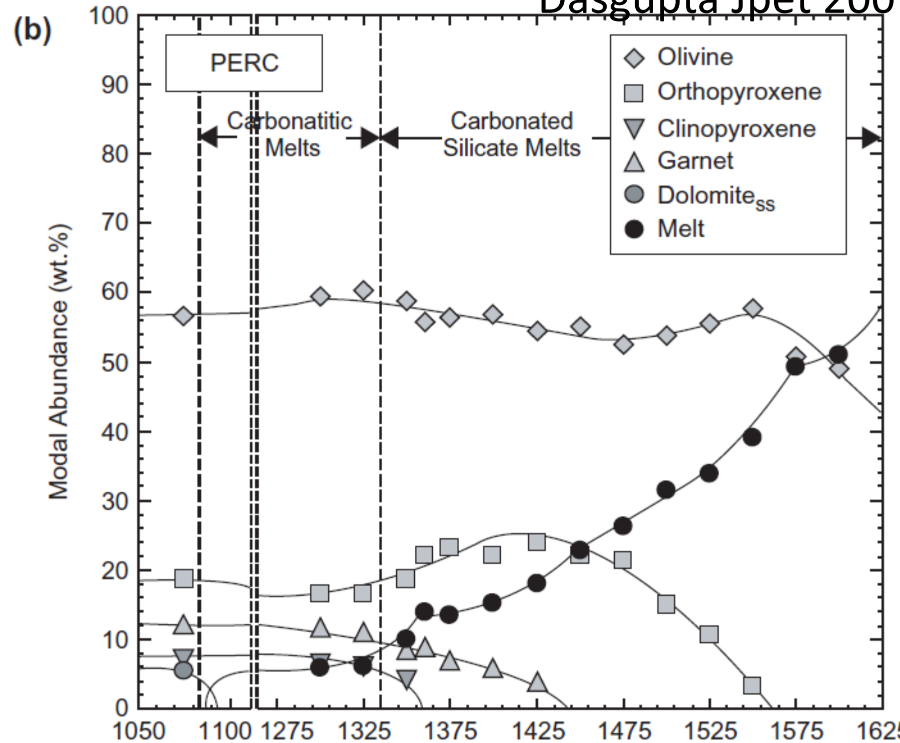

2.5 Wt % CO2

Bulk composition	Melting interval	Melting reactions
PERC	cbL-out to cpx-out: 10–13%	1·0 ol + 1·4 cpx = 1·1 opx + 0·3 gt + 1·0 sL
	cpx-out to gt-out: 13–23%	1·0 gt = 1·0 sL
	gt-out to opx-out: 23–50%	1·1 opx = 0·1 ol + 1·0 sL
PERC3	cbL-out to cpx and gt-out: 6–19%	1·0 cpx + 0·6 gt + 0·3 ol = 0·9 opx + 1·0 sL
	cpx and gt-out to opx-out: 19–47%	0·2 ol + 0·8 opx = 1·0 sL

sL = Carb-Silic melt
cbL = carb-rich melt

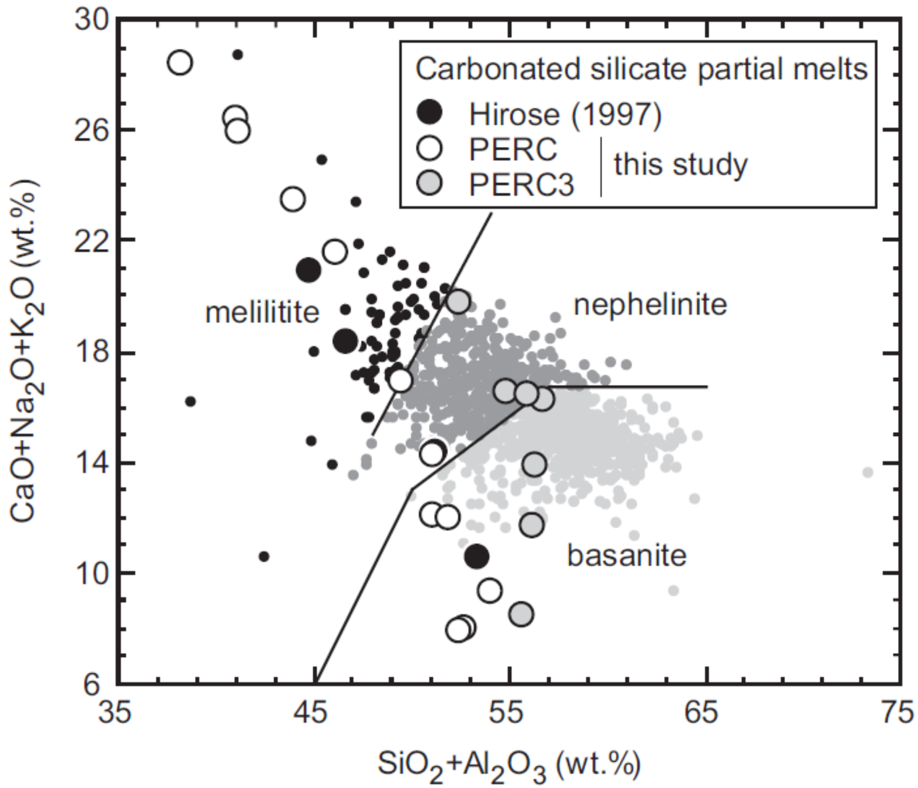

Fig. 11. Classification of alkalic to strongly alkalic ocean island lavas (GEOROC database: http://georoc.mpch-mainz.gwdg.de/georoc/) as melilitites, nephelinites, and basanites, following the scheme of LeBas (1989). Also plotted are carbonated silicate partial melts of peridotite derived from this study and from Hirose (1997).

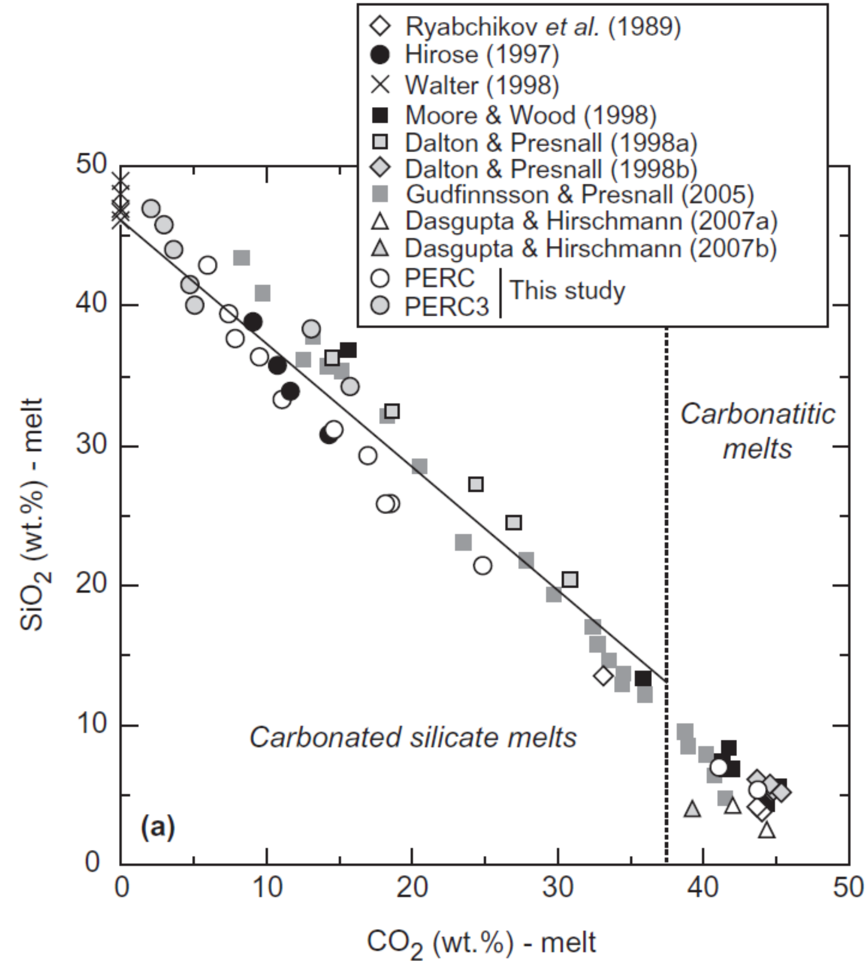

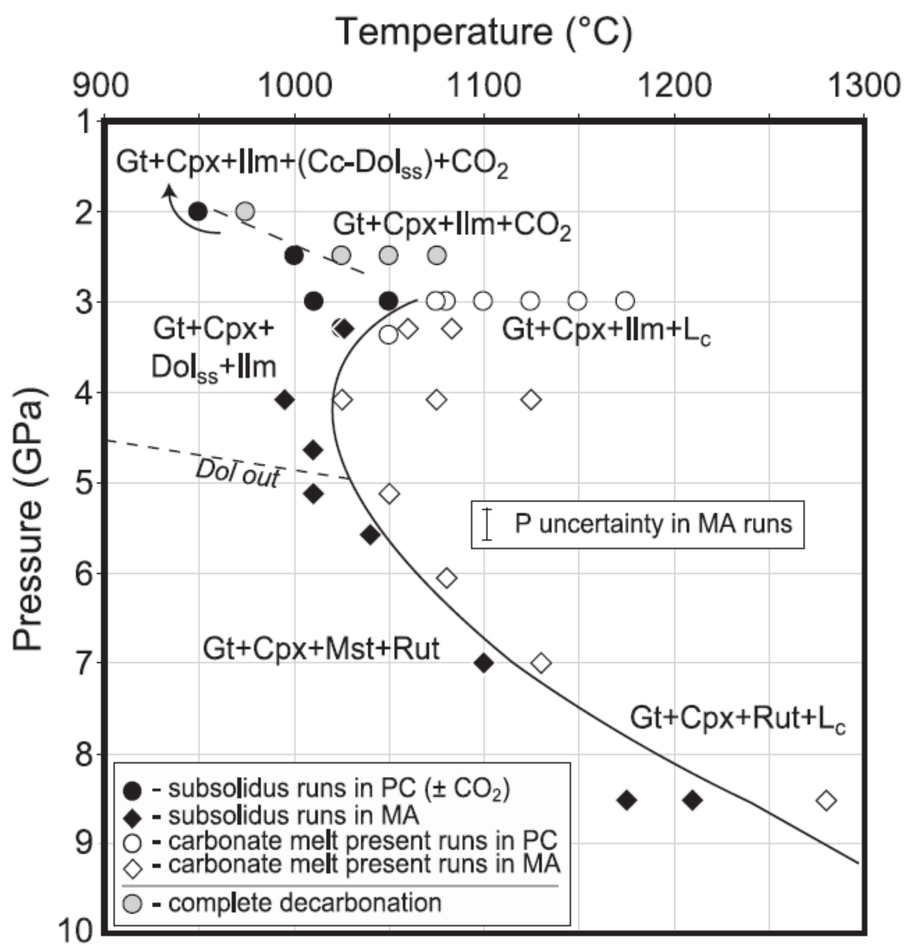

Fig. 3. Experimental constraints on the solidus of carbonated eclogite (SLEC1). Phase abbreviations as in Table 2. Phases within parentheses are present in trace amount. Pressure–temperature uncertainties for piston cylinder (PC) runs (±0.1 GPa, ±12 °C) and temperature uncertainty for multi-anvil (MA) runs (±10 °C) are within size of the symbols.

ECLOGITE + CO2

R. Dasgupta et al. / Earth and Planetary Science Letters 227 (2004) 73–85

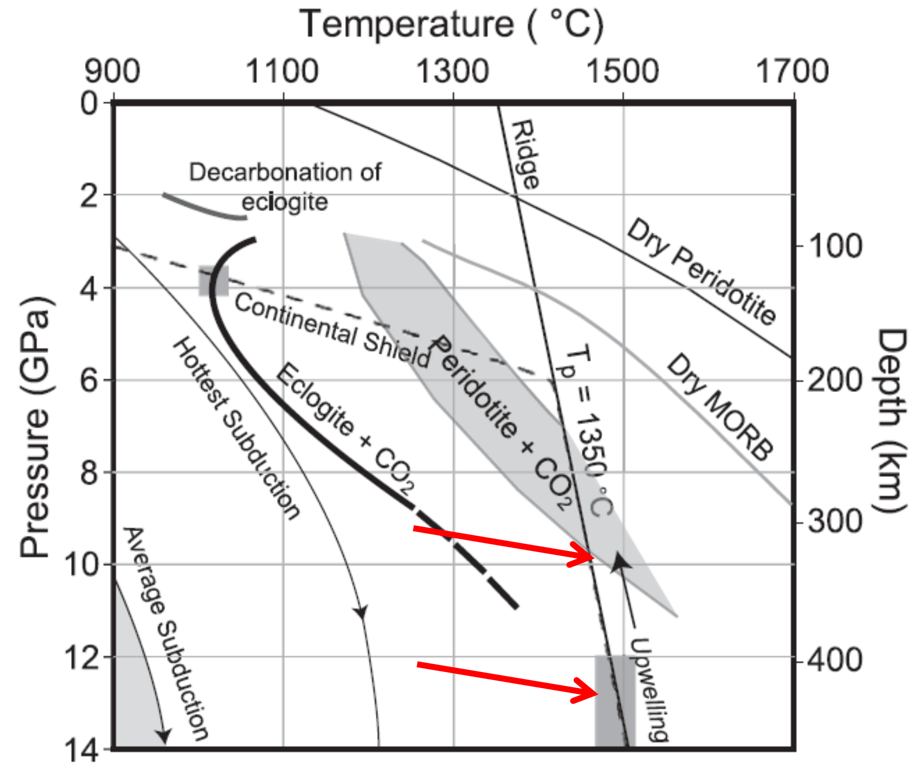

Fig. 6. Location of carbonated eclogite (SLEC1) solidus (Eclogite+CO_2) in relation to oceanic ridge geotherm (mantle potential temperature, T_p=1350 °C; [30]), calculated P–T conditions for subducting crust [25,26], and continental shield geotherm (40 mW/m^2) [31]. Also shown for reference are solidus of dry peridotite [22] and dry MORB [32]. Field of 'peridotite+CO_2' is bound by two different estimates of carbonated peridotite solidus [33,34] in the model CMAS–CO_2 system. Shaded region in the bottom left corner of the figure represents best estimate of subduction zone P–T conditions [25] along with the maximum estimate of expected temperature at depth ('Hottest Subduction', [26]). Gray-shaded boxes show likely conditions of generation of carbonate melt within eclogite in Earth's upper mantle for continental shield and convecting mantle settings.

Carbonatite

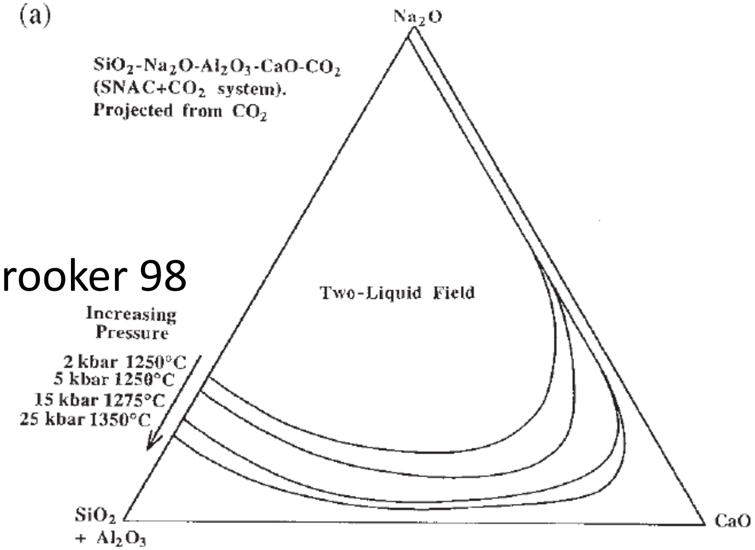

Brooker 98

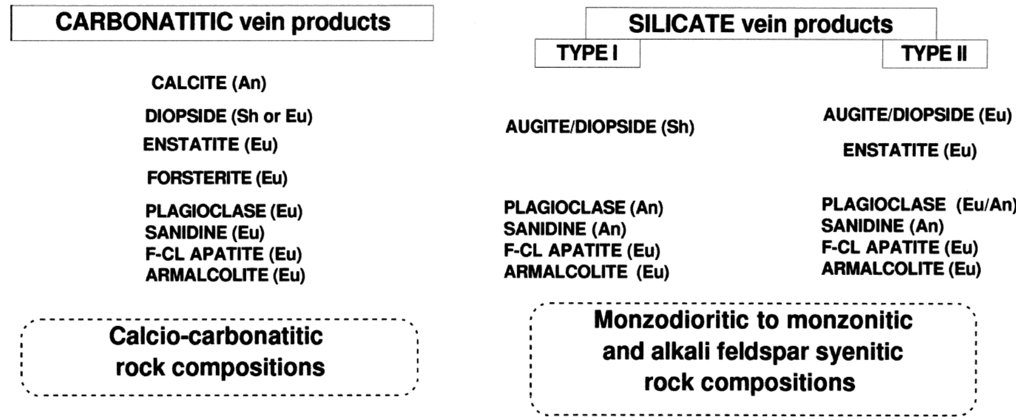

Fig. 10. Mineralogy of carbonatitic and silicate vein products, with the crystallization habit of each type of mineral (Sh: subhedral; Eu: al), and assumed rock compositions (see text for explanation).

Chalot-Prat 99

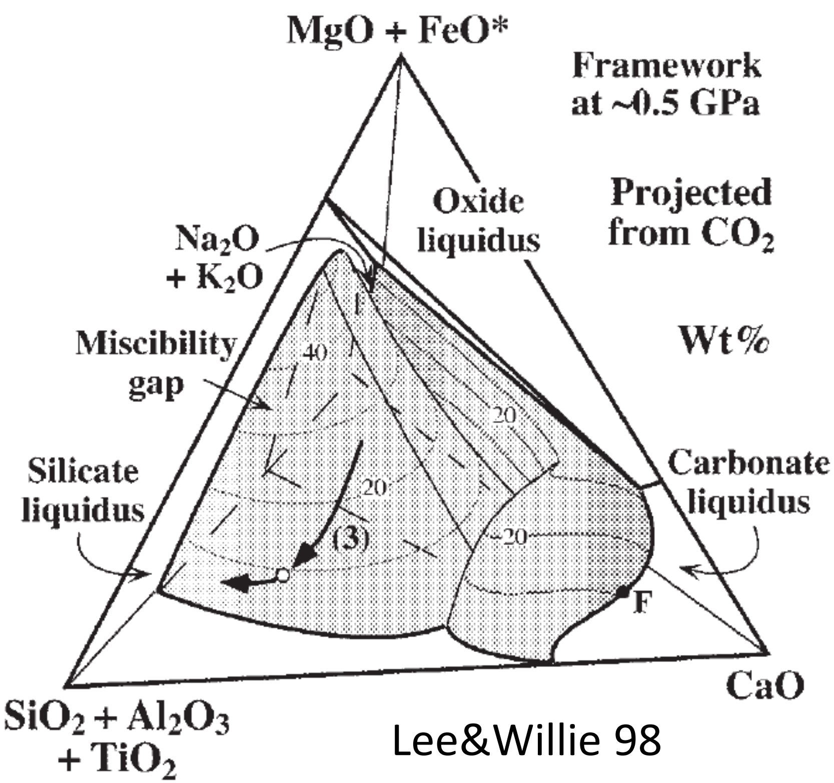

Lee&Willie 98

Fig. 4. Generalized pseudoquaternary phase diagram at 0·5 GPa (projected from CO_2), showing dark- and light-shaded liquidus surfaces for the silicate–carbonate field boundary and liquid miscibility gap, with contours for wt % (MgO + FeO*). The large oxide liquidus volume near the (MgO + FeO*) apex is related to the periclase field (Fig. 1b). (See Fig. 1b for liquid F.) Arrow (3) corresponds to path (3) in Fig. 3.

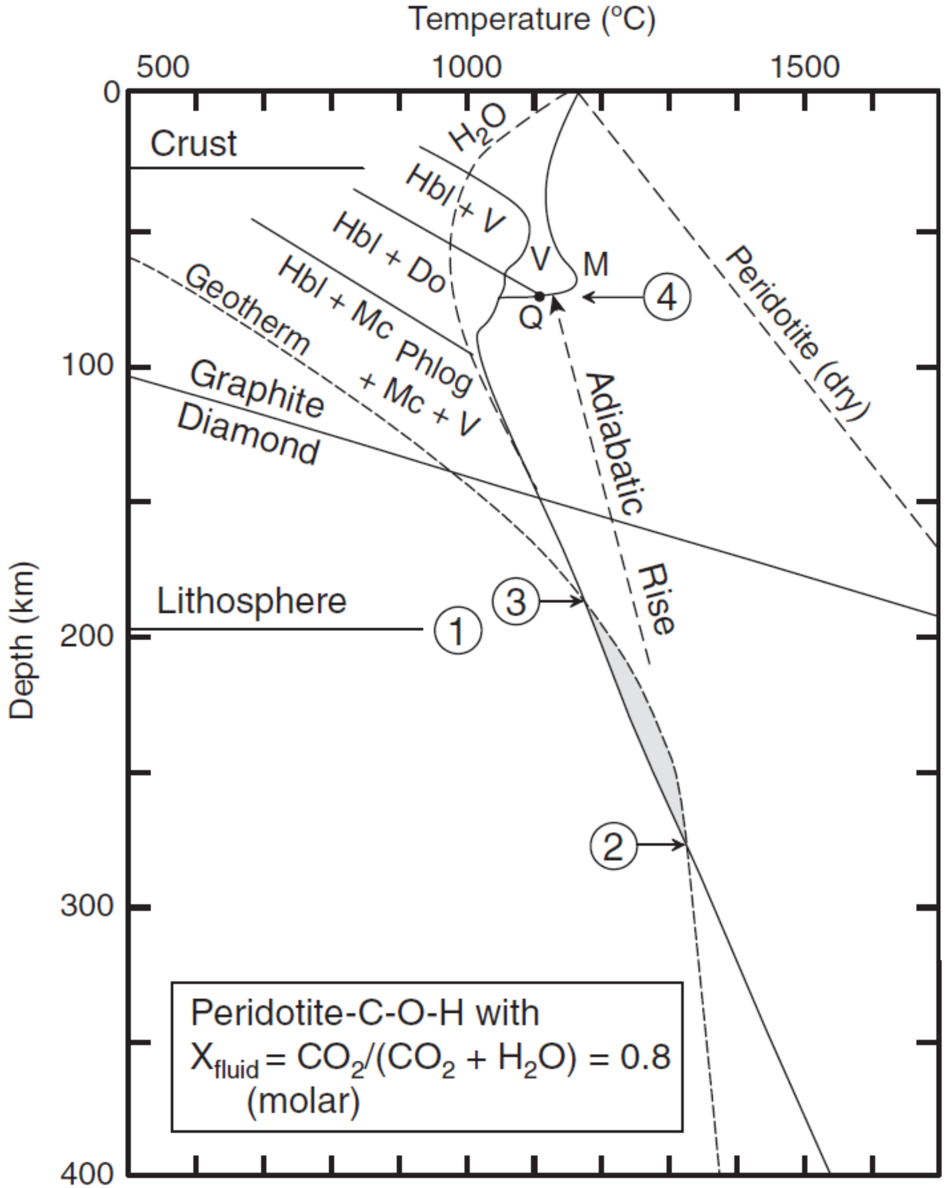

FIGURE 13 Solidus curve (heavy solid curve) for lherzolite-CO_2-H_2O with a defined ratio of $CO_2:H_2O = 0.8$. Dashed curves = H_2O-saturated and volatile-free peridotite solidi and the approximate shield geotherm. After Wyllie (1989).

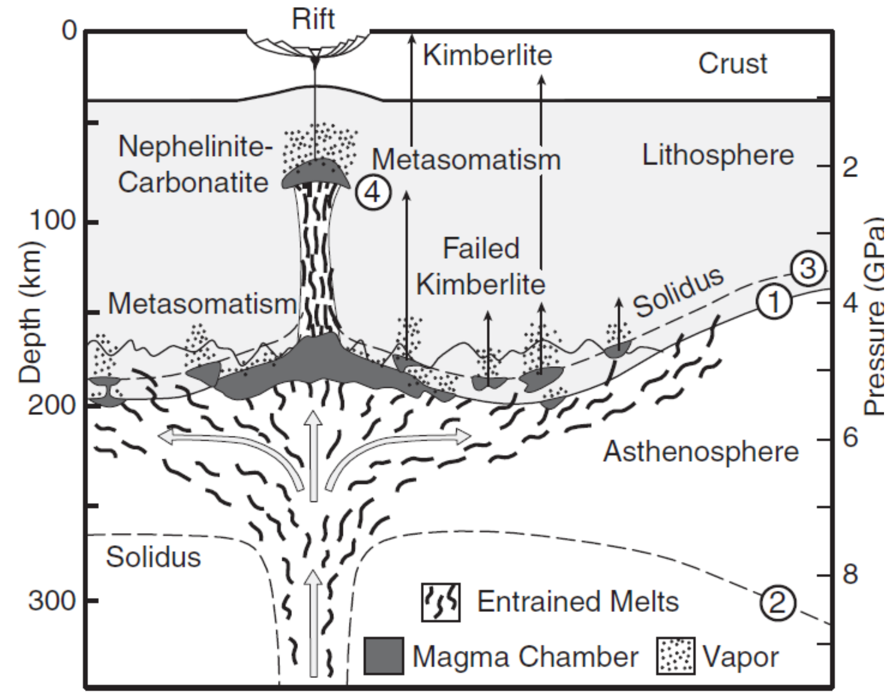

FIGURE 16 Schematic cross section of an asthenospheric mantle plume beneath a continental rift environment, and the genesis of nephelinite-carbonatites and kimberlite–carbonatites. Numbers correspond to Figure 13. After Wyllie (1989) and Wyllie et al. (1990).

Carbonatite =
Fusion + immiscibilité…

??

TABLE 1 Nomenclature of Selected Alkaline Igneous Rocks (Mostly Volcanic/Hypabyssal)

The mildly alkaline series (e.g., Hawaii): **Ankaramite** (alkali picrite)**, Alkali Basalt, Hawaiite, Mugearite**, **Benmoreite, Trachyte** is not discussed here.

Basanite Feldspathoid-bearing basalt. Usually contains nepheline, but may have leucite + olivine

Tephrite Olivine-free basanite.

Leucitite Volcanic rock that contains leucite + clinopyroxene ± olivine. It typically lacks feldspar.

Nephelinite Volcanic rock that contains nepheline + clinopyroxene ± olivine. It typically lacks feldspar.

Urtite Plutonic nepheline–pyroxene (aegirine–augite) rock with over 70% nepheline and no feldspar

Ijolite Plutonic nepheline–pyroxene rock with 30 to 70% nepheline.

Melilitite A predominantly melilite–clinopyroxene volcanic (if >10% olivine, called olivine melilitite).

Shoshonite K-rich basalt with K-feldspar ± leucite.

Phonolite Felsic alkaline volcanic with alkali feldspar + nepheline. (plutonic = **nepheline syenite)**.

Comendite Peralkaline rhyolite with molar $(Na_2O \pm K_2O)/Al_2O_3$ slightly>1. May contain Na-pyroxene or amphibole.

Pantellerite Peralkaline rhyolite with molar $(Na_2O + K_2O)/Al_2O_3 = 1.6 – 1.8$. Contains Na-pyroxene or amphibole.

Lamproite A group of peralkaline, volatile-rich, ultrapotassic, volcanic to hypabyssal rocks. The mineralogy is variable, but most contain phenocrysts of olivine + phlogopite ± leucite ± K-richterite ± clinopyroxene ± sanidine. Table 6.

Lamprophyre A diverse group of dark, porphyritic, mafic to ultramafic hypabyssal (or occasionally volcanic), commonly highly potassic (K > Al) rocks. They are normally rich in alkalis, volatiles, Sr, Ba, and Ti, with biotite-phlogopite and/or amphibole phenocrysts. They typically occur as shallow dikes, sills, plugs, or stocks. Table 7.

Kimberlite A complex group of hybrid volatile-rich (dominantly CO_2), potassic, ultramafic rocks with a fine-grained matrix and macrocrysts of olivine and several of the following: ilmenite, garnet, diopside, phlogopite, enstatite, chromite. Xenocrysts and xenoliths are also common.

Group I kimberlite Typically CO_2 rich and less potassic than group 2 kimberlite.

Group II kimberlite (orangeite) Typically H_2O rich and has a mica-rich matrix (also with calcite, diopside, and apatite).

Carbonatite An igneous rock composed principally of carbonate (typically calcite, ankerite, and/or dolomite), and commonly with clinopyroxene, alkalic amphibole, biotite, apatite, and/or magnetite. The Ca-Mg-rich carbonatites are technically not alkaline, but are commonly associated with, and thus included with, the alkaline rocks. Table 3.

For more details, see Sørensen (1974), Streckeisen (1978), Woolley et al. (1996), and Le Maitre et al. (2002).

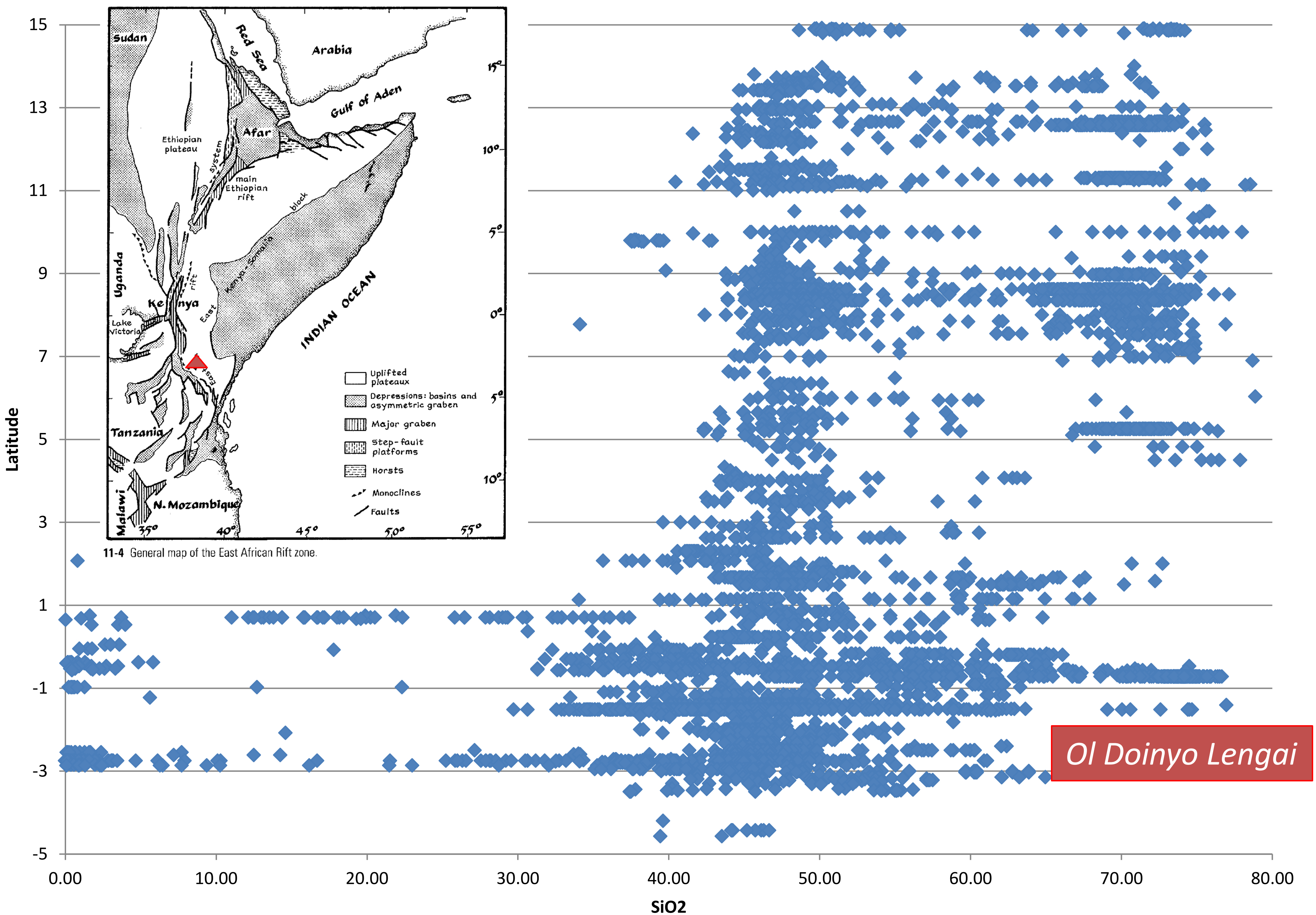

11-4 General map of the East African Rift zone.

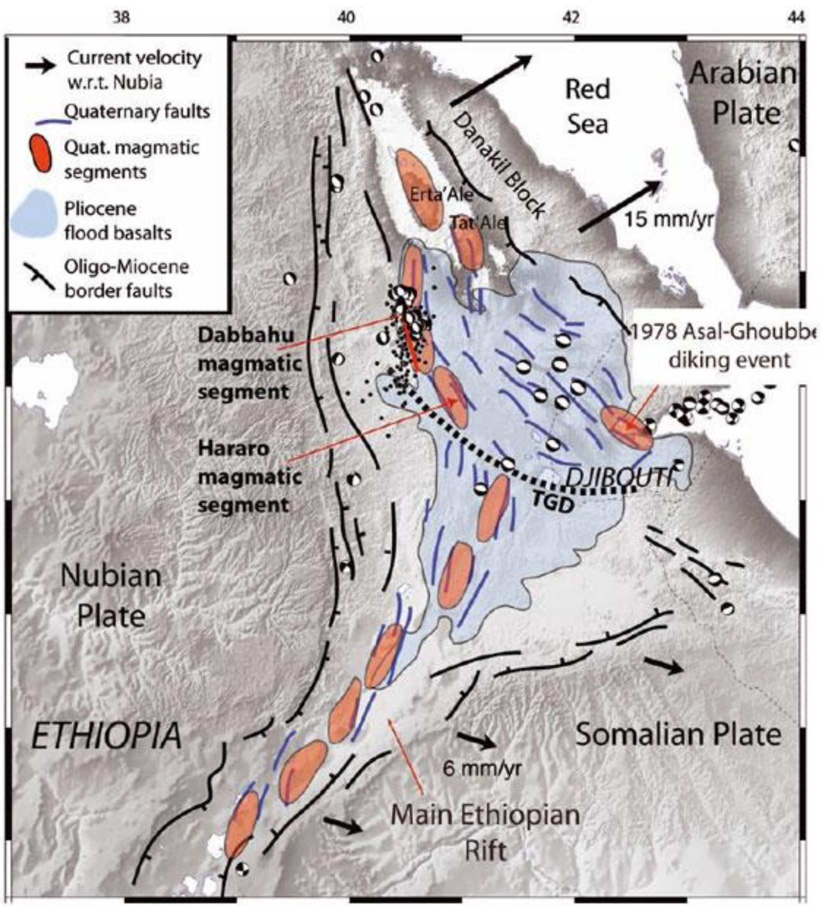

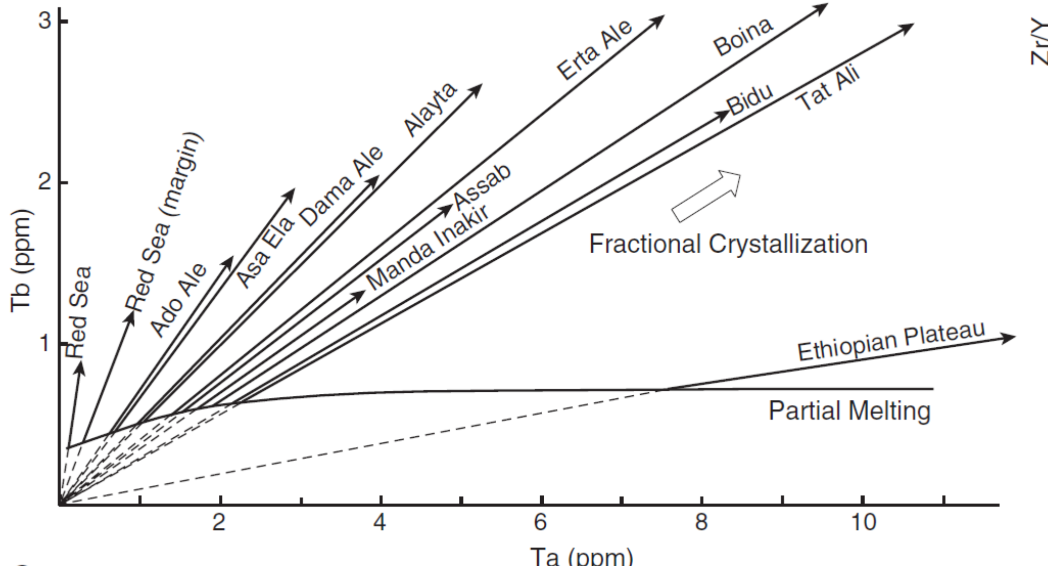

a

FIGURE 6 (a) Ta versus Tb for rocks of the Red Sea, Afar, and the Ethiopian Plateau. Rocks from a particular area show nearly constant ratios of the two excluded elements, consistent with fractional crystallization of magmas with distinct Ta/Tb ratios produced either by variable degrees of partial melting of a single source or varied sources (Treuil and Varet, 1973). Copyright © with permission from Société Géol. de France. **(b)** Zr/Y versus Zr/Nb for some East African Rift lavas showing similar constant ratios of excluded trace elements (after Kampunzu and Mohr, 1991). Copyright © with permission from Springer-Verlag.

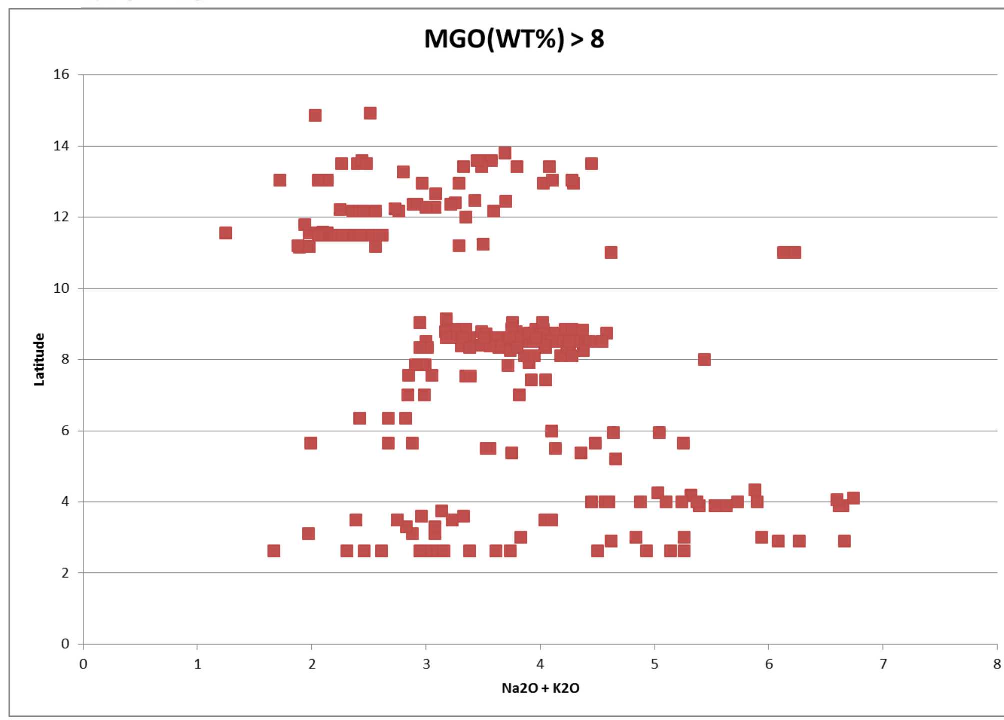

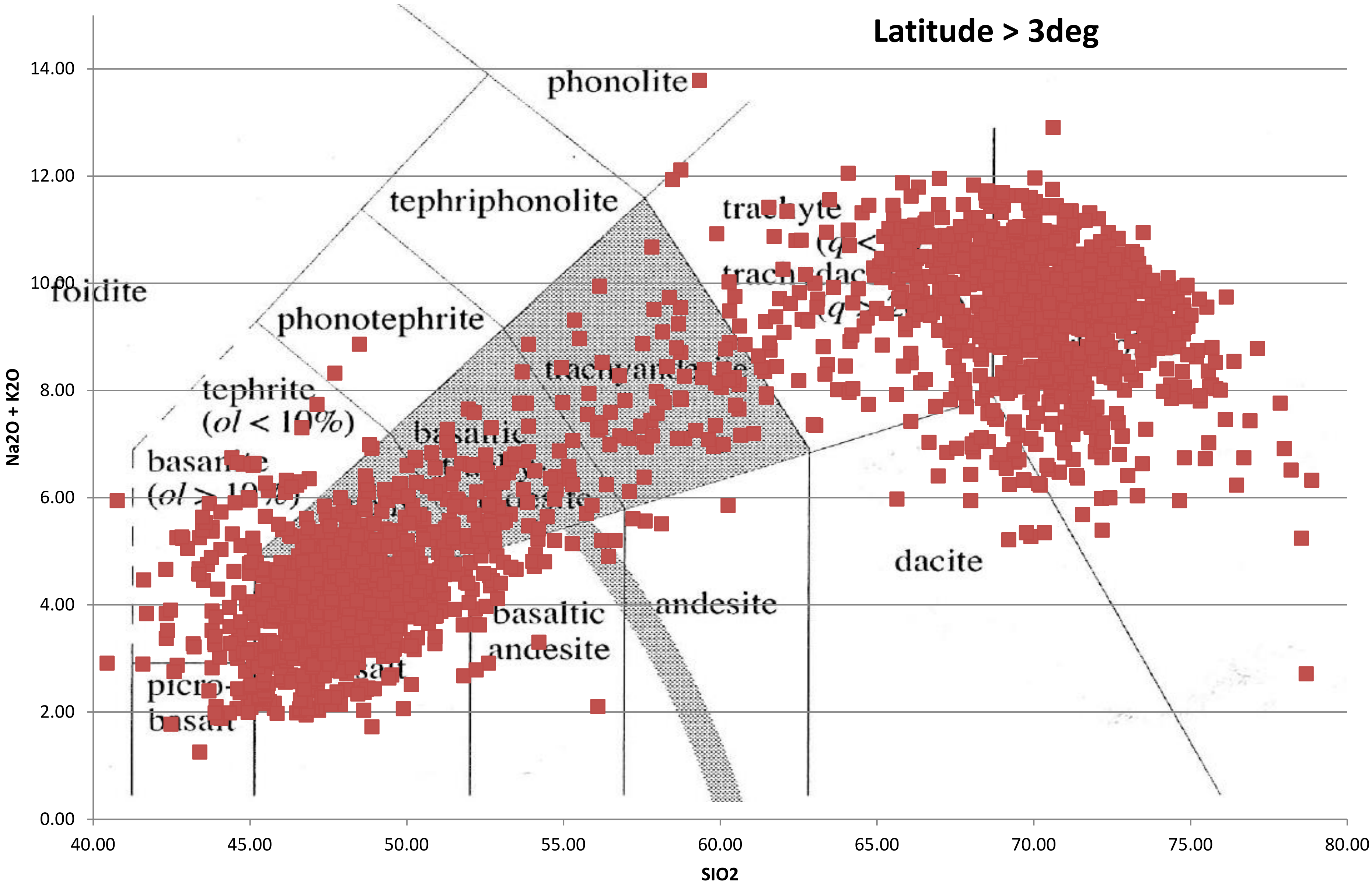

Latitude > 3deg
phonolite
tephriphonolite
foidite
phonotephrite
tephrite
(ol < 10%)
basanite
(ol > 10%)
picro-
basalt
basaltic
andesite
andesite
dacite
trachyte
trachydacite
Na2O + K2O
SIO2
14.00
12.00
10.00
8.00
6.00
4.00
2.00
0.00
40.00
45.00
50.00
55.00
60.00
65.00
70.00
75.00
80.00

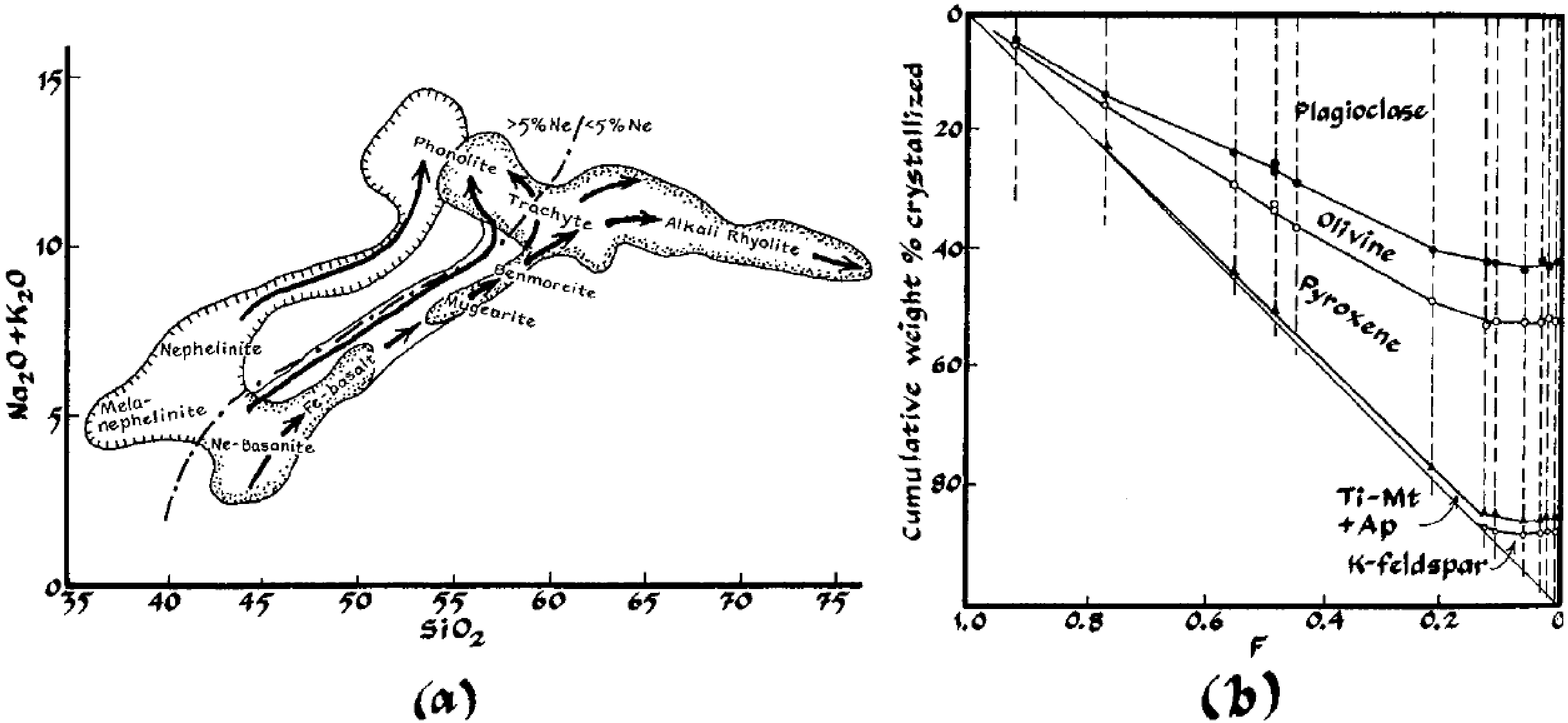

Figure 11-6 Variations of alkalies and silica in the major volcanic series of the Kenya Rift system of Figure 11-4. The heavy dashed line with dots separates rocks with greater than and less than 5-percent normative nepheline. (After B. H. Baker, 1987, Alkaline igneous rocks, *Geol. Soc. Spec. Publ.* No. 30, 293–312.) (b) Cumulative weight percentages of minerals fractionated from a parental basaltic magma to produce the various differentiated rocks of the basalt-benmoreite-trachyte series in (a). F is the fraction of liquid represented by individual rocks. Calculations are based on the method illustrated in Table 7-4. (After B. H. Baker, *et al.*, 1977, *Contr. Mineral. Petr.* 64:303–332.)

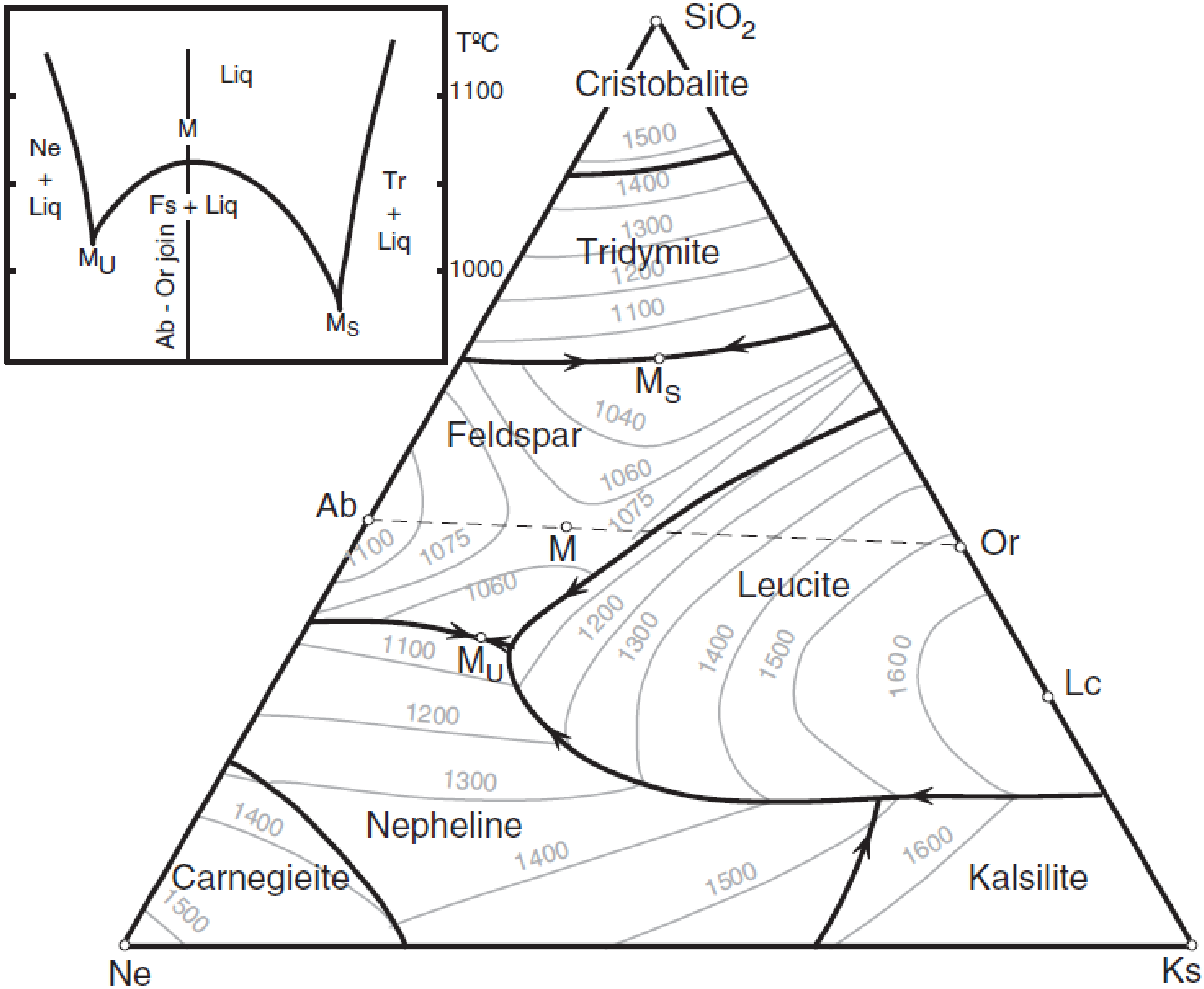

FIGURE 7 Phase diagram for the system SiO_2-$NaAlSiO_4$-$KAlSiO_4$-H_2O at 1 atm pressure. Insert shows a T-X section from the silica-undersaturated thermal minimum (M_u) to the silica-oversaturated thermal minimum (M_s) that crosses the lowest point (M) on the binary Ab-Or thermal barrier that separates the undersaturated and oversaturated zones. After Schairer and Bowen (1935 © American Geophysical Union with permission) and Schairer (1950 © the University of Chicago).

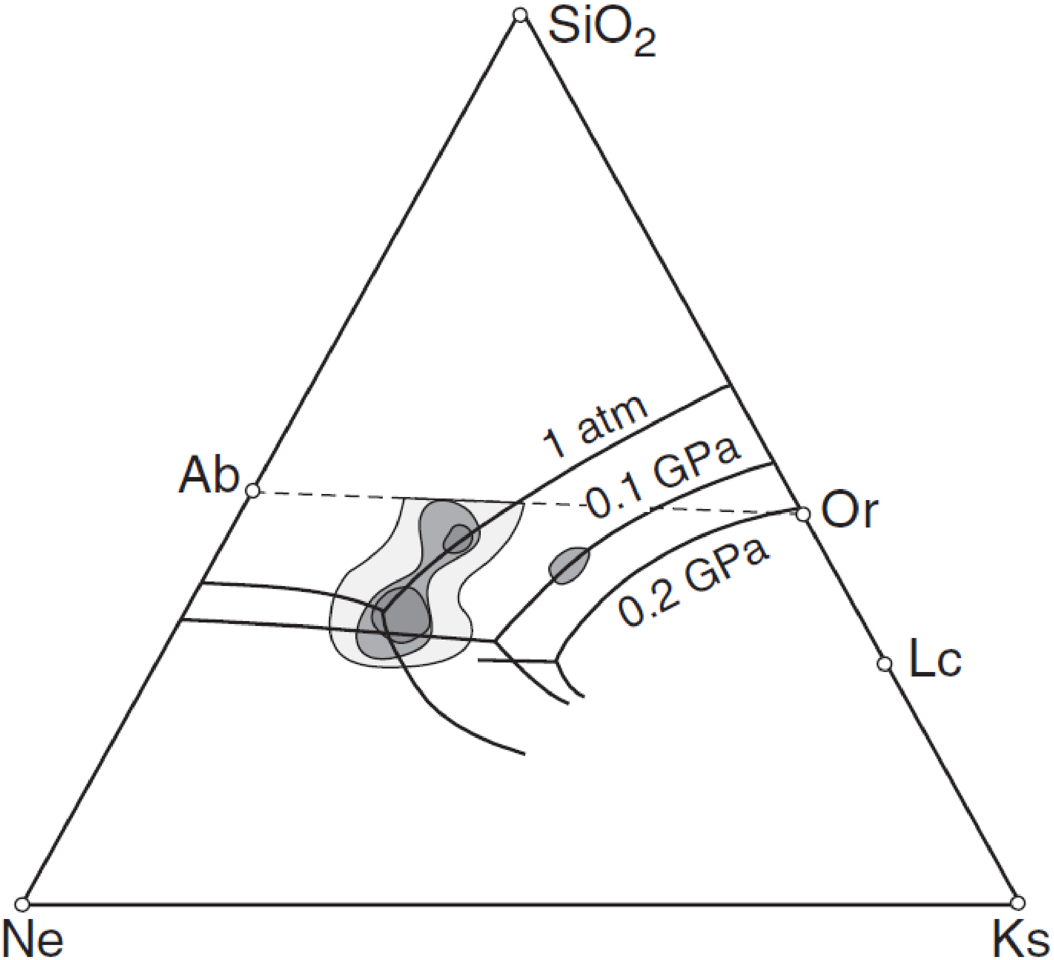

FIGURE 8 Part of the Ne-Ks-SiO_2-H_2O system at 1 atm, 0.1 GPa, and 0.2 GPa, illustrating the reduction in the leucite field with increasing p_{H_2O}. At 0.2 GPa the Lc-liquid field crosses the Ab-Or join, and the system goes from peritectic to eutectic behavior. Also shown are contours for analyses of 122 undersaturated volcanics. After Gittins (1979). Copyright © reprinted by permission of Princeton University Press.

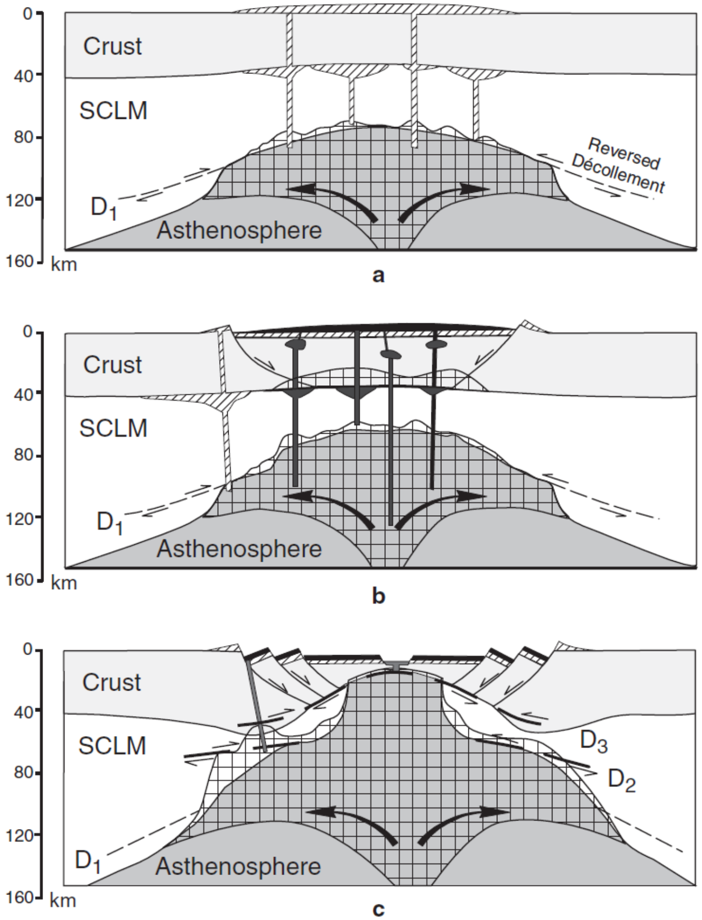

FIGURE 9 Hypothetical cross sections (same vertical and horizontal scales) showing a proposed model for the progressive development of the East African Rift System. **(a)** Pre-rift stage, in which an asthenospheric mantle diapir rises (forcefully or passively) into the lithosphere. Decompression melting (crosshatches indicate areas undergoing partial melting) produces variably alkaline melts. Some partial melting of the metasomatized subcontinental lithospheric mantle (SCLM) may also occur. Reversed décollements (D_1) provide room for the diapir. **(b)** Rift stage: development of continental rifting, eruption of alkaline magmas (black) mostly from a deep asthenospheric source. Rise of hot asthenosphere induces some crustal anatexis. Rift valleys accumulate volcanics and volcaniclastic material. **(c)** Afar stage, in which asthenospheric ascent reaches crustal levels. This is transitional to the development of oceanic crust. Successively higher reversed décollements (D_2 and D_3) accommodate space for the rising diapir. After Kampunzu and Mohr (1991) and P. Mohr (personal communication). Copyright ©

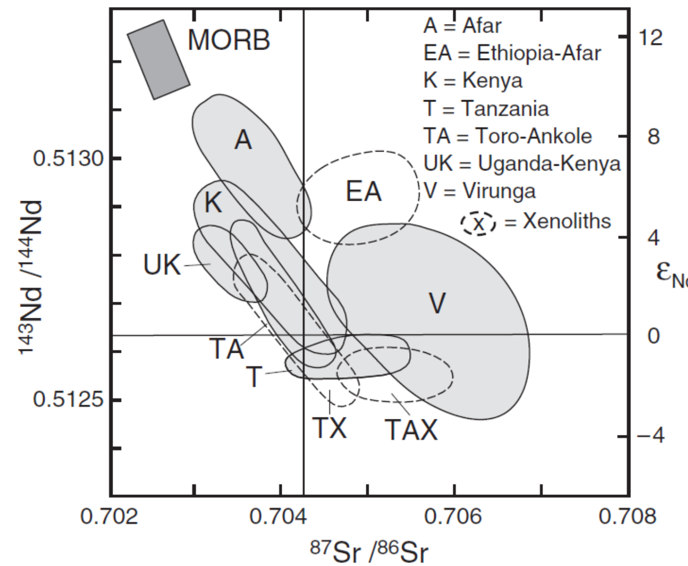

FIGURE 3 $^{143}Nd/^{144}Nd$ versus $^{87}Sr/^{86}Sr$ for East African Rift lavas (shaded) and xenoliths (unfilled dashed areas). The "crosshair" intersects at bulk Earth. After Kampunzu and Mohr (1991). Copyright © with permission from Springer-Verlag.

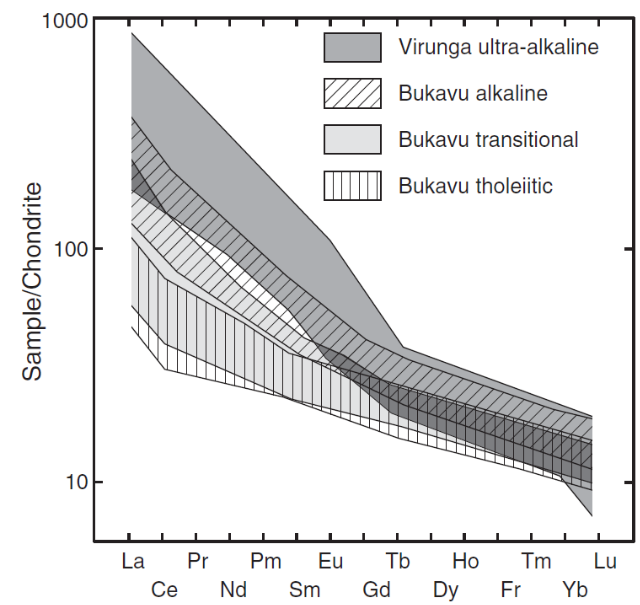

FIGURE 5 Chondrite-normalized REE variation diagram for examples of the four magmatic series of the East African Rift. After Kampunzu and Mohr (1991). Copyright © with permission